

# **Sedimentology of the Neogene Pistarda formation in the Megara Basin; Greece**

by

Steinar Polden Sæverud

Master thesis

in petroleum geoscience



Department of Earth Science

University of Bergen

June 2014



## Abstract

The Pistarda formation in the Megara Basin has not been studied in detail before. The aim of this thesis is to provide sedimentological and geochemical data, in order to increase our understanding of the depositional processes and environments of the Pistarda formation. Ten localities were found and nine of them were logged. The focus was on the vertical and lateral facies variations and trying to explain how it initiated and how it terminated.

The Pistarda formation is a half-graben with a dip towards the northeast. The localities were found higher up the dip-slope. Seven facies were identified, of which many showed evidence of *in situ* materials, indicating a shallow lacustrine environment. Some of the localities showed evidence of two units, a lower and an upper unit. When a clear difference was found between the units, the lower usually consisted of reworked material, while the upper had more *in situ* facies.

The same interpretation is made when linking this to the geochemistry. Analysis of  $\delta^{18}\text{O}$ ,  $\delta^{13}\text{C}$  and  $^{87}\text{Sr}/^{86}\text{Sr}$  ratio confirms that the formation has two units, where the lower shows evidence of being deposited by a larger and deeper lake. The opposite is found for the upper unit, showing evidence of being deposited by a smaller and shallower lake.

The structural data from the area links the development of the two units to a fault which created the accumulation space needed for the two units to form in quite a small area in the Megara basin. The development of the Pistarda formation is interpreted to be linked with shifts in the climate during the deposition, which could support the development of a lake.





## **Acknowledgements**

This thesis is a part of a master's degree in Petroleum Geoscience at the Department of Earth Science at the University of Bergen.

First I would like to thank my supervisor Rob Gawthorpe and my co-supervisor Gunnar Sælen for their guidance and helpful discussions both in the field and on my written work.

I also want to thank Rune E. Søråas for analyzing stable isotopes, Yuval Ronen for analyzing strontium isotopes and Siv Hjorth Dundas for analyzing trace elements. Furthermore, I want to thank Irina Maria Dumitru for making the thin sections and Irene Heggstad for help at the Electron Microscopy Laboratory.

Furthermore I also want to thank my fellow students at the University of Bergen for five wonderful years. A special thanks to Kristoffer Nilsen for excellent cooperation in the field and in the office. Last, but not least, thanks to Simen Auli Staff and Therese Kirkevik for proofreading my thesis.

Steinar Polden Sæverud

Bergen, 02.06.2014



# Table of Contents

<b>Abstract.....</b>	<b>I</b>
<b>Acknowledgements.....</b>	<b>III</b>
<b>1. Introduction.....</b>	<b>1</b>
1.1 Aim .....	1
1.2 Study area .....	1
1.3 Previous studies .....	2
1.4 Outline .....	3
<b>2. Geological framework.....</b>	<b>4</b>
2.1 Introduction .....	4
2.2 Regional geology and tectonic setting.....	5
2.3 Chronology and Stratigraphy of the Megara Basin .....	7
2.4 Basin structure .....	10
<b>3 Lacustrine carbonates.....</b>	<b>12</b>
3.1 Introduction - Facies models .....	12
3.1.1 Lake Margin - littoral.....	13
3.1.2 Lake Basin - pelagic.....	13
3.1.3 Bench margins with a steep gradient – low energy .....	13
3.1.4 Bench margins with steep gradient – high energy (wave dominated) .....	14
3.1.5 Ramp margins with low gradient – low energy .....	14
3.1.6 Ramp margins with low-gradient – wave influenced .....	15
3.2 Geochemistry of lacustrine carbonates.....	16
3.2.1 Isotopes .....	19
3.2.2 Strontium isotopes ( $^{87}\text{Sr}/^{86}\text{Sr}$ ) .....	19
3.2.3 Stable isotopes in lacustrine lakes, $\delta^{18}\text{O}$ and $\delta^{13}\text{C}$ .....	20
3.2.4 Element Analysis .....	21
<b>4. Methods.....</b>	<b>22</b>
4.1 Introduction .....	22
4.2 Field work.....	22
4.3 Laboratory work .....	22
4.3.1 Stable isotope analysis .....	23
4.3.2 Strontium isotope analysis .....	23
4.3.3 Trace element analysis.....	23
4.4.1 Scanning Electron Microscopy (SEM) .....	24
4.4.2 Optical microscope .....	25
4.4.3 Cathodoluminescence microscope (CL) .....	25
4.4.4 Fluorescence microscope .....	26
<b>5. Fieldwork – The Pistarda formation.....</b>	<b>27</b>
5.1 Introduction .....	27
5.2 Localities .....	27
5.3 Facies .....	29
5.3.1 Gastropods .....	31
5.3.2 Facies 1: Organic Matter.....	33
5.3.3 Facies 2: Reeds – <i>In situ</i> .....	34
5.3.4 Facies 3: Reworked Reeds by mass transport with soft sediment deformation.....	38
5.3.5 Facies 4: Reworked Reeds Turbidity .....	40

5.3.6 Facies 5: Wave reworked gastropods .....	41
5.3.7 Facies 6: Storm reworked gastropods - Coquina .....	43
5.3.8 Facies 7: Hemipelagic/Pelagic micrite.....	45
5.4 Facies association of the Pistarda formation .....	49
5.4.1 FA1 – Costal wetland, Swamp.....	49
5.4.2 FA2 – Costal wetland, Marsh .....	50
5.4.3 FA3 – Subaqueous lake center.....	51
5.4.4 FA4 – Background sedimentation .....	52
5.5 Sedimentary structures above and below the Pistarda formation.....	52
5.5.1 Below the Pistarda formation.....	53
5.5.2 Above the Pistarda formation .....	55
5.6 Depositional model for the Pistarda formation.....	57
<b>6. Geochemical studies .....</b>	<b>60</b>
6.1 Introduction .....	60
6.2 $\delta^{18}\text{O}$ , $\delta^{13}\text{C}$ and $^{87}\text{Sr}/^{86}\text{Sr}$ against the stratigraphy of locality 5.2 upper and lower unit .....	60
6.3 $^{87}\text{Sr}/^{86}\text{Sr}$ , $\delta^{18}\text{O}$ and $\delta^{13}\text{C}$ for all localities .....	62
6.4 $\delta^{18}\text{O}$ and $\delta^{13}\text{C}$ – all localities .....	64
6.5 Bacterial growth in thin section.....	65
6.6 Trace elements .....	67
<b>7. Discussion.....</b>	<b>70</b>
7.1 The Pistarda formation – lake.....	70
7.2 Facies distribution in the Pistarda formation – vertical and distribution.....	71
7.3 Lake geometry and lake depth .....	71
7.4 The formation of the Pistarda formation - Climate .....	73
7.5 Pistarda formation in the Megara Basin .....	74
7.6 Geochemistry - locality 5.2 lower unit and upper unit .....	75
7.6.1 $\delta^{13}\text{C}$ and $\delta^{18}\text{O}$ .....	75
7.6.2 $^{87}\text{Sr}/^{86}\text{Sr}$ .....	77
7.6.3 Summary .....	77
7.7 Further studies .....	78
<b>8. Summary and conclusion .....</b>	<b>79</b>
<b>9. Bibliography .....</b>	<b>81</b>
<b>Appendix I – Results of geochemistry analysis .....</b>	<b>86</b>
<b>Appendix II – Logs .....</b>	<b>93</b>
<b>Appendix III – Correlation panel.....</b>	<b>114</b>

# 1. Introduction

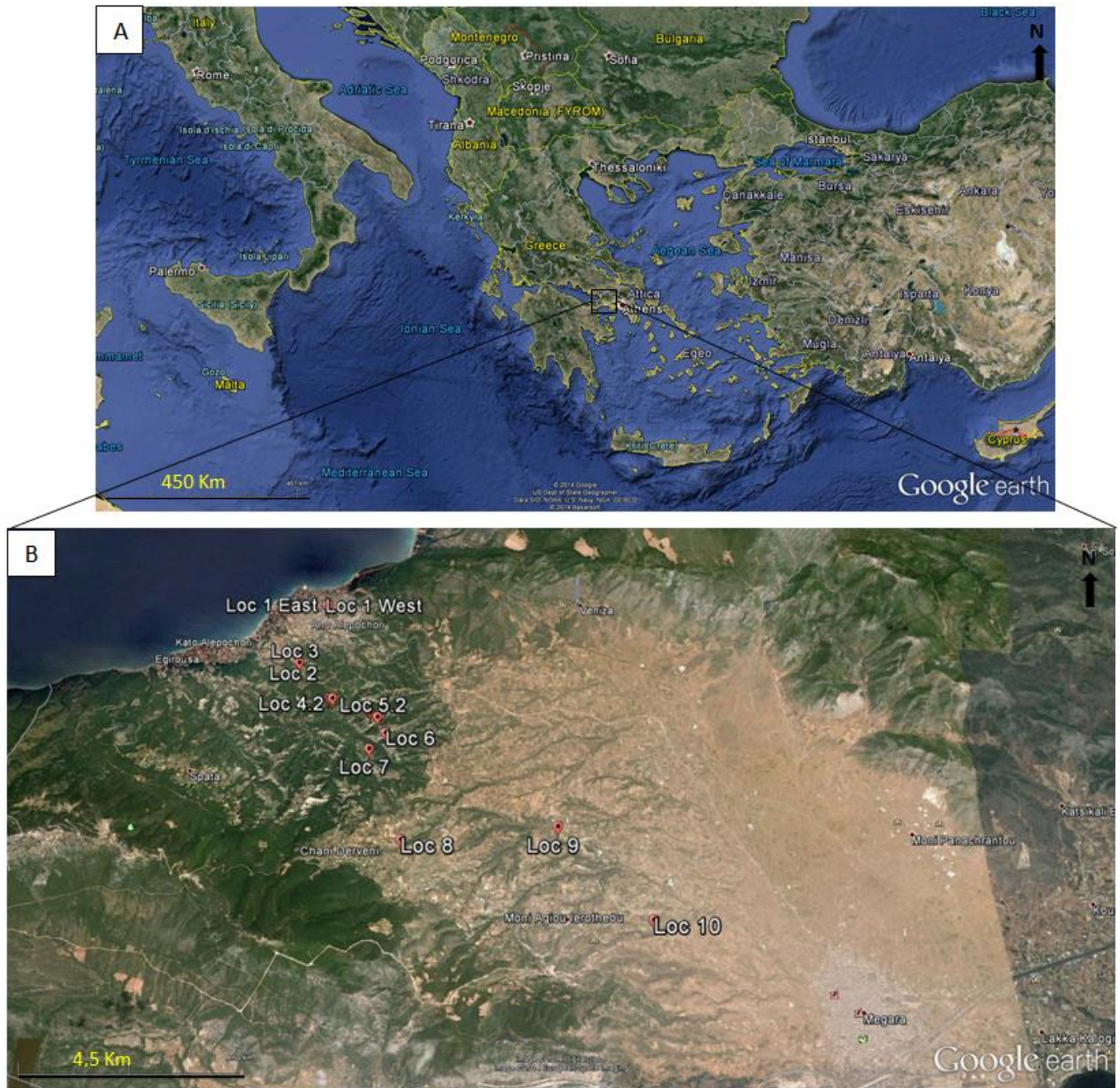
## 1.1 Aim

The aim of this project is to examine the sedimentology of the lacustrine Pistarda formation, Megara Basin, Greece. The project has a number of specific objectives:

- I. Field-based facies analysis of the Pistarda formation and the immediately adjacent stratigraphic units.
- II. Geochemical ( $^{87}\text{Sr}/^{86}\text{Sr}$ ,  $\delta^{18}\text{O}$  and  $\delta^{13}\text{C}$ ) analysis of samples from the formation.
- III. Synthesis of the above objectives with structural data from the Megara Basin and analogues from other lacustrine carbonates and rift basins to interpret the depositional environments and depositional processes operating during development of the Pistarda formation and to discuss the controlling factors (e.g. climate, tectonics)

## 1.2 Study area

The study area is located in the Megara Basin in central Greece at the margin of the Gulf of Corinth (figure 1.1). The basin is a tectonically active area and faults have created good, natural outcrops. The area is heavily forested by pine. Dirt roads give good access to the outcrops, although some of these are on steep cliffs that cannot easily be accessed. The field work was divided into two parts, the first from 22<sup>th</sup> April to 9<sup>th</sup> May 2013 and the second from 2<sup>nd</sup> October to 24<sup>th</sup> October 2013.



**Figure 1.1** – (A) Location of the study area within the Mediterranean Sea. Map (B) shows with a red marker where the localities are found in the basin. The maps are modified from Google Earth.

### 1.3 Previous studies

Bentham et al. (1991) did a large regional study over the sedimentary facies, based on fieldwork in the Megara Basin, and produced a geological map over the basin. The result from their work is the foundation for the studies described in this thesis. In Chapter 2 this will be discussed in more detail. The tectonics of the Gulf of Corinth and nearby regional plates; Anatolian Microplate,

Adriatic Microplate, African Plate and Eurasian Plate are well explored by several studies (McKenzie, 1970; Jackson and McKenzie, 1988; Bell et al., 2008; Leeder and Mack, 2009). For carbonate deposits in rift basins in a lake environment, Lake Tanganyika in Africa is a good analogue (Cohen and Thouin, 1987; Cohen et al., 1993).

## **1.4 Outline**

Followed by the introduction, chapter 2 presents a geological background of the Megara basin, focusing on regional geology and tectonic setting and the stratigraphy of the Megara Basin. In chapter 3 a facies model for lacustrine carbonates and a geochemical background for carbonate rocks in lacustrine settings will be presented. Chapter 4 presents a description of the different methods, both for fieldwork and instruments used in this study. Chapter 5 starts with an overview over the field area and facies description, facies association, sedimentary structures below and above and then a sketch of the different dispositional units along with a correlation transect for the Pistarda formation. In Chapter 6 geochemical analysis from the samples will be presented. In Chapter 7 the results are discussed with respect to geochemistry and the depositional environments of the Pistarda formation in the Megara Basin. Finally, the conclusion is given in Chapter 8.



## 2. Geological framework

### 2.1 Introduction

The study area is located west of Athens, between Athens and the Corinth channel in the Attica region (figure 2.1). The Megara basin is situated in the eastern part of the extension of the Gulf of Corinth, between the Gulf of Alkyonides and the Saronic Gulf. The basin is separated by the Gerania mountain range in the southwest and the Pateras mountain range in the northeast. The basin follows a WNW-ESE structure and it is a fault-bounded half-graben with Plio-Pleistocene sediments 1 km thick (Theodoropoulos, 1968; Bentham et al., 1991).

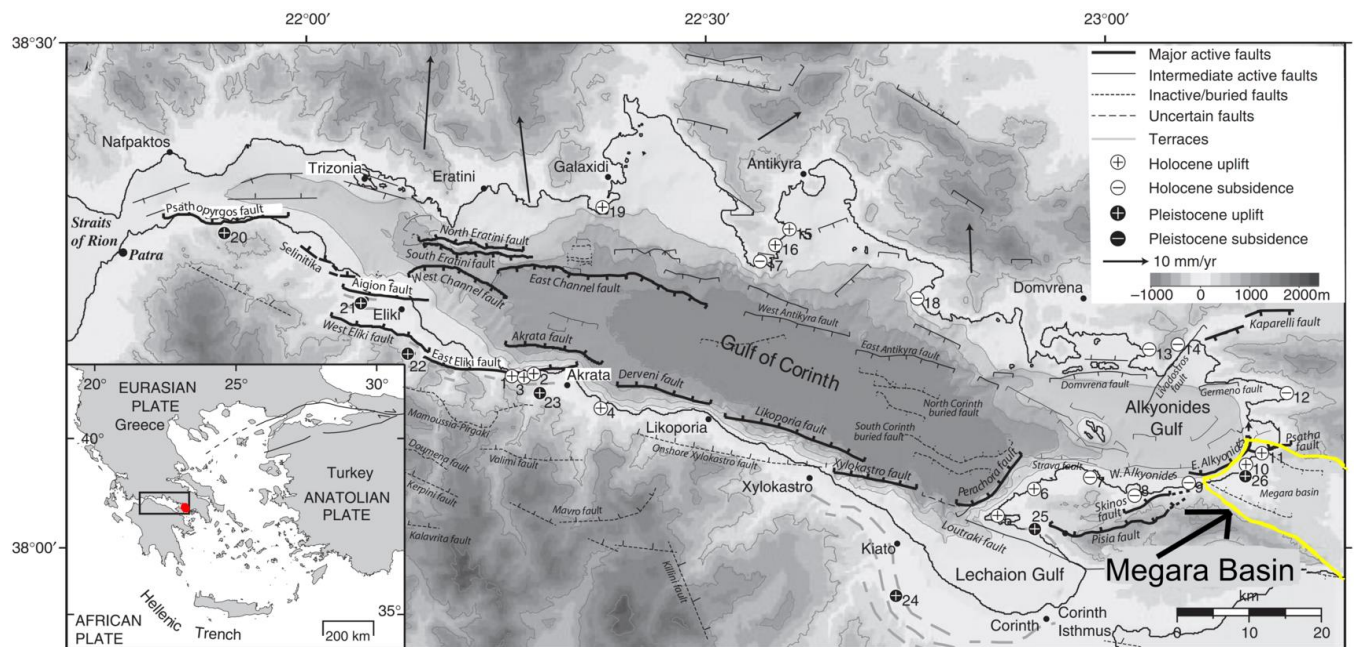


Figure 2.1 - The map shows the tectonic development in the Gulf of Corinth where the Megara Basin is a landward extension of the gulf, marked in yellow. Modified from Bell et al. (2009)

Several studies in the area suggest that the rifting started with the formation of the Gulf of Corinth, which has undergone a vast extension since the Miocene, with a maximum of 50 mm per year in the last 5 Ma, and the rifting is still active (Jackson et al., 1982; Jackson and McKenzie, 1988). This makes it an important natural laboratory to study the effects of rapid extension upon sedimentary and geomorphological processes.

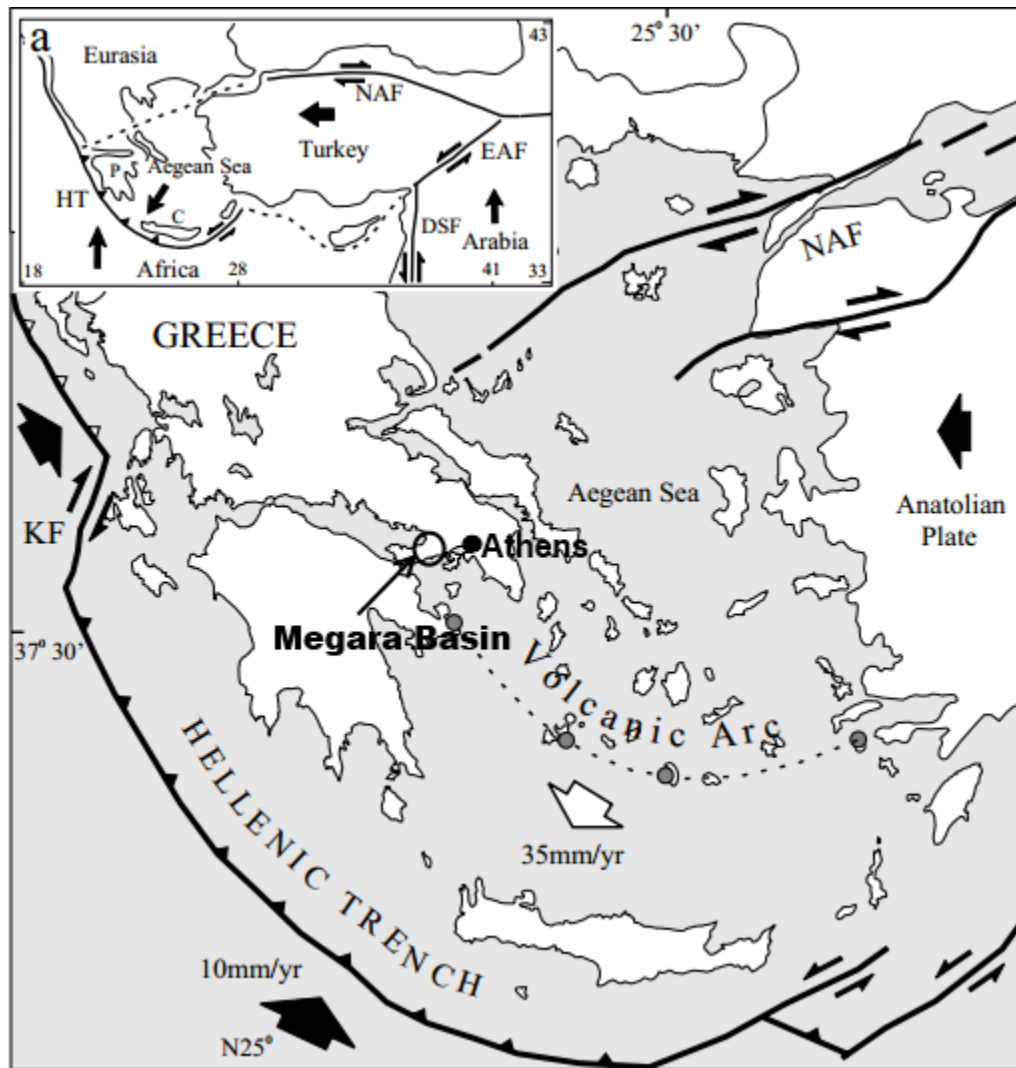
The Megara basin's boundary to the northwest is a major active normal fault, the South Alkyonides fault, and lies at the footwall of this structure. This normal fault is mostly offshore



and underwent motion during the 1981 earthquake sequence (Jackson et al., 1982). This younger fault that has led to the exposure and dissection of the thick Neogene sequence in the area (Theodoropoulos, 1968).

## **2.2 Regional geology and tectonic setting**

The tectonic development in this area is based on the interaction of the Arabian, African, and Eurasian plates and in the collision zone between the plates (figure 2.2). The main collision is between the Arabian and African plates with Eurasia (McKenzie, 1970; Jackson and McKenzie, 1984; Jackson and McKenzie, 1988). Tectonic models of global seafloor spreading, fault systems and earthquake slip vectors show that the Arabian plate is moving north-northwest relative to Eurasia at a rate of 18-25 mm/yr, averaged over about 3 Myr (DeMets et al., 1990; Jolivet et al., 1994). Similar models also indicate that the African plate is moving in a northerly direction relative to Eurasia at a rate of approximately 10 mm/yr (at 30°N, 31°E). Africa and Arabia have a differential motion between them, calculated to be 10-15 mm/yr. They mainly have a left-lateral motion along the Dead Sea transform fault which resulted in a continental collision along the Bitlis-Zagros fold and thrust belt (McClusky et al., 2000). This forced the African plate to be subducted along the Hellenic arc at a higher rate than the relative northward motion of the African plate itself. This makes the arc move southward relative to the Eurasia plate (McClusky et al., 2000). When the Aegean plate and the African plate are pressed against each other this makes the crust thicker and produces a gravitational collapse of the lithosphere behind the Hellenic arc (Jolivet, 2001). This creates a thinning of the lithosphere in the Aegean back-arc region (Papazachos and Comninakis, 1971; Doutsos et al., 1988). Since the African plate and the Eurasian plate are moving in opposite directions this creates a divergent boundary, responsible for the formation of the Gulf of Corinth. The tension from the North Anatolian fault propagation westward also creates a rotation of crustal blocks in the Hellenic thrust belt (Dewey and Sengor, 1979; Armijo et al., 1999).



**Figure 2.2 - (a)** basic map illustrating the land masses and their relative movement. The larger map shows the main structural features, summarizing the geodynamical framework. NAF = North Anatolian fault, EAF = East Anatolian Fault, DSF = Dead Sea Fault, HT = Hellenic Trench, P = Peloponnese, C = Crete, KF = Kefallonia Fault. Motion vector from Kahle et al. (1998). Modified from Doutsos and Kokkalas (2001).

The Megara basin is a landward extension of the Gulf of Corinth. The Corinth Rift in central Greece is one of the world's most active rifts and lies in a new plate boundary that is rapidly evolving (Ford et al., 2012). The rift stretches from the Ionian Sea in the west to Athens in the east, and follows an E-W to NW-SE direction. The rifting started onshore in Early Pliocene and subsequently moved north and offshore. As a result, the rift created the Gulf of Corinth with uplifting and incised basins. This provides a natural laboratory on ongoing events in early rifting and normal faulting. The gulf has a number of normal faults on both its edges. The extension is still active today and started in Pliocene (Doutsos and Kokkalas, 2001). With a 1.5 cm/y N-S

extension it is the most seismically active zone in Europe. This activity is monitored using instantaneous GPS data (Briole et al., 2000). The uplift has been measured to be 1 mm/y in the southern margin in the gulf (Rohais et al., 2007; and references therein).

### 2.3 Chronology and Stratigraphy of the Megara Basin

The extensional tectonics in the Aegean is believed to have started in the Serravalian/Tortonian boundary in late Miocene (Şengör, 1984; Meulenkamp, 1985). A sequence of volcanic rocks from the Corinth basin lie over the basin fill and are dated to be approximately 3.6-4.0 Ma. For the Megara Basin there is no data, but an age around Plio-Pleistocene is proposed for the basin. Recently an ash layer was found in one of the upper formations in the basin. Based on the  $^{40}\text{Ar}/^{39}\text{Ar}$  method the ash layer which is called the Pagae Ash Member is dated to  $2.82 \pm 0.06$  Ma. The layer occurs in the topmost part of the Louba Formation of the Alepochori Group (Leeder et al., 2008).

Bentham et al. (1991) proposed a new lithostratigraphic scheme for the sedimentary fill of the Megara Basin. The Paliochori group contains two formations - the Mylou Vrachia (c. 200 meters) and Pigaddi Dourakis formations (c. 50 meters). The Mylou Vrachia fm. forms an outcrop with angular breccias and conglomerates overlain by sandstone of the Pigaddi Dourakis fm. The Ayio Ioannou group contains the Rema Mazi formation (75-300 meters) with marls, marly siltstones and marly sandstones which pass up transitionally from the Pigaddi formation below. Above the Rema Mai formation the Kremida formation (50 meters) starts with sandstones, pebbly sandstones and fine conglomerates with minor marls and silty marls. This formation is coarsening upwards and clinoforms are well preserved within the unit. The Tombse Koukies group consists of the Toumpaniari (30-150 meters), the Pistarda (2-5 meters) and the Harbour Ridges formations (75-150 meters). The Toumpaniari formation consist of pebbly sandstones and conglomerates with one marine horizon in the lower part. The Pistarda formation overlies the Toumpaniari formation and, according to Bentham et al. (1991), it consists of travertine limestone that can be found over a large area of the basin. They suggest the formation has been formed by an unknown combination of climatic, tectonic or groundwater effects. The Harbour ridges formation is made up of pebbly sandstones, sandstones, calcareous sandstones, marls and lignites. An abundant marine fauna can be found in the marl sequence. The Alepochori group consists of the Louba

formation (90 – 320 meters) which is a series of red/brown pebbly sandstones and subordinate sandy mudrocks. Inside the Louba formation the Ayia Sofia formation (0-40 meters) is a special sequence with white breccias. Figure 2.3 shows a stratigraphic column over the sediments in Megara basin.

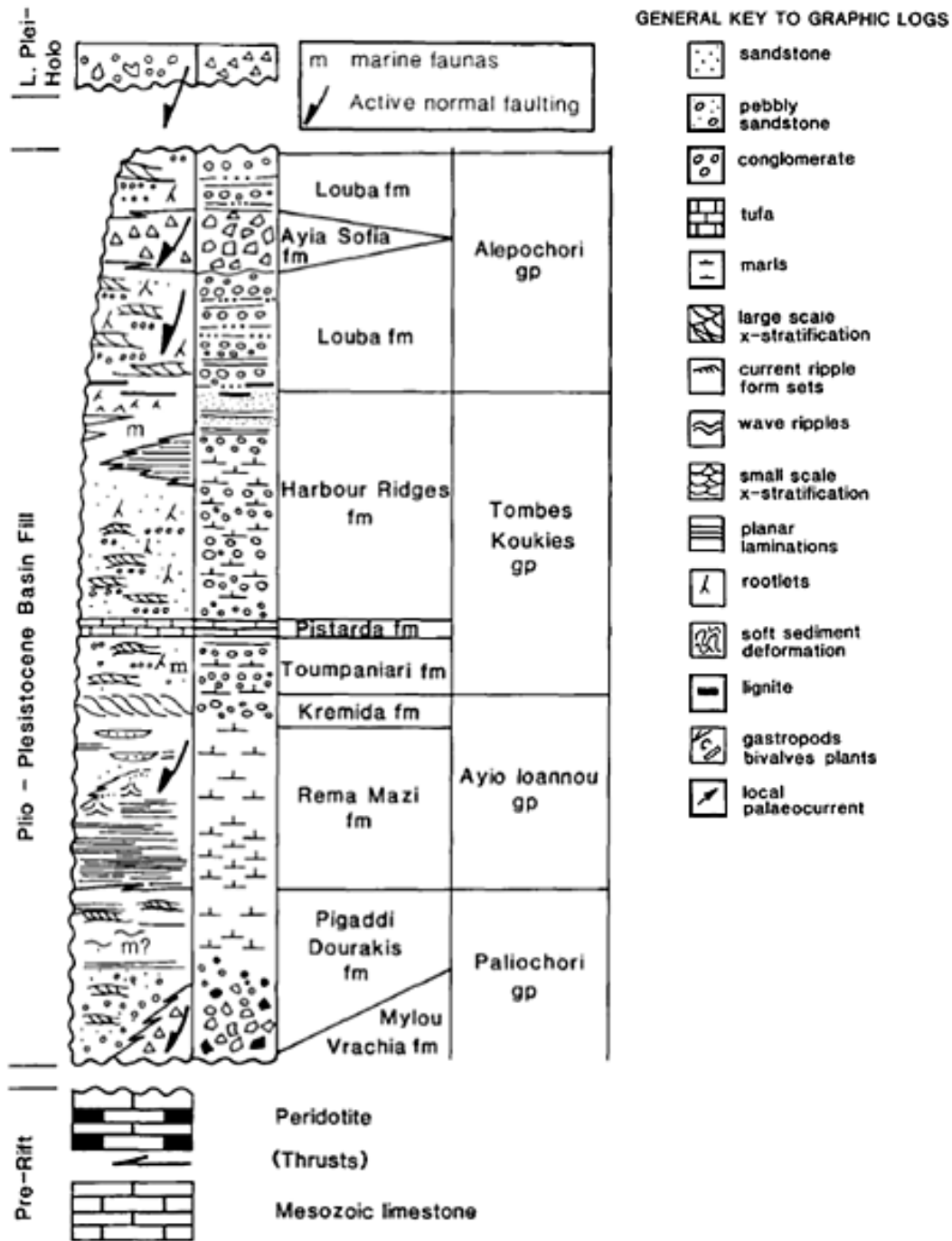
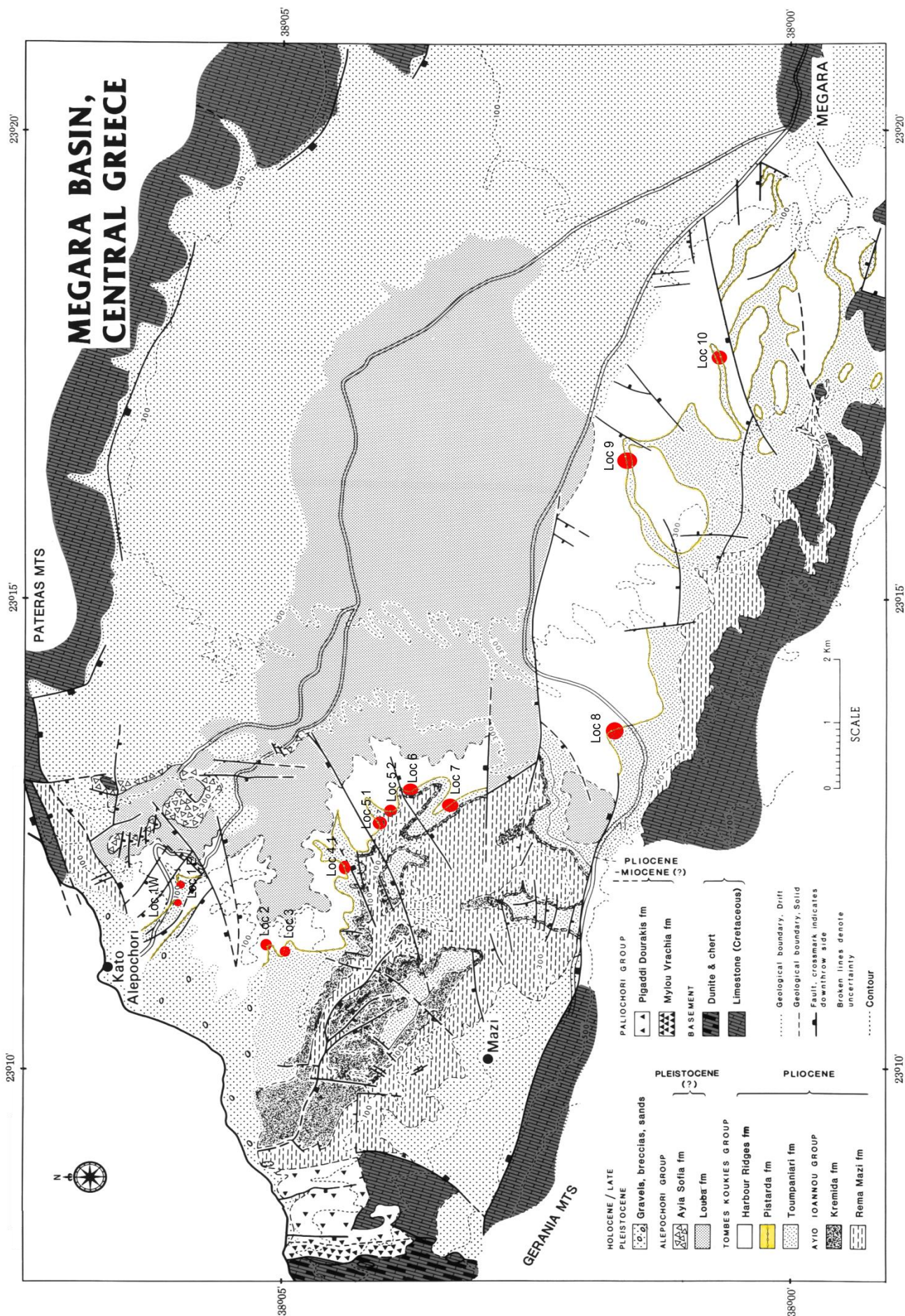


Figure 2.3 - Lithostratigraphy of the Megara basin. Modified from Bentham et al. (1991).



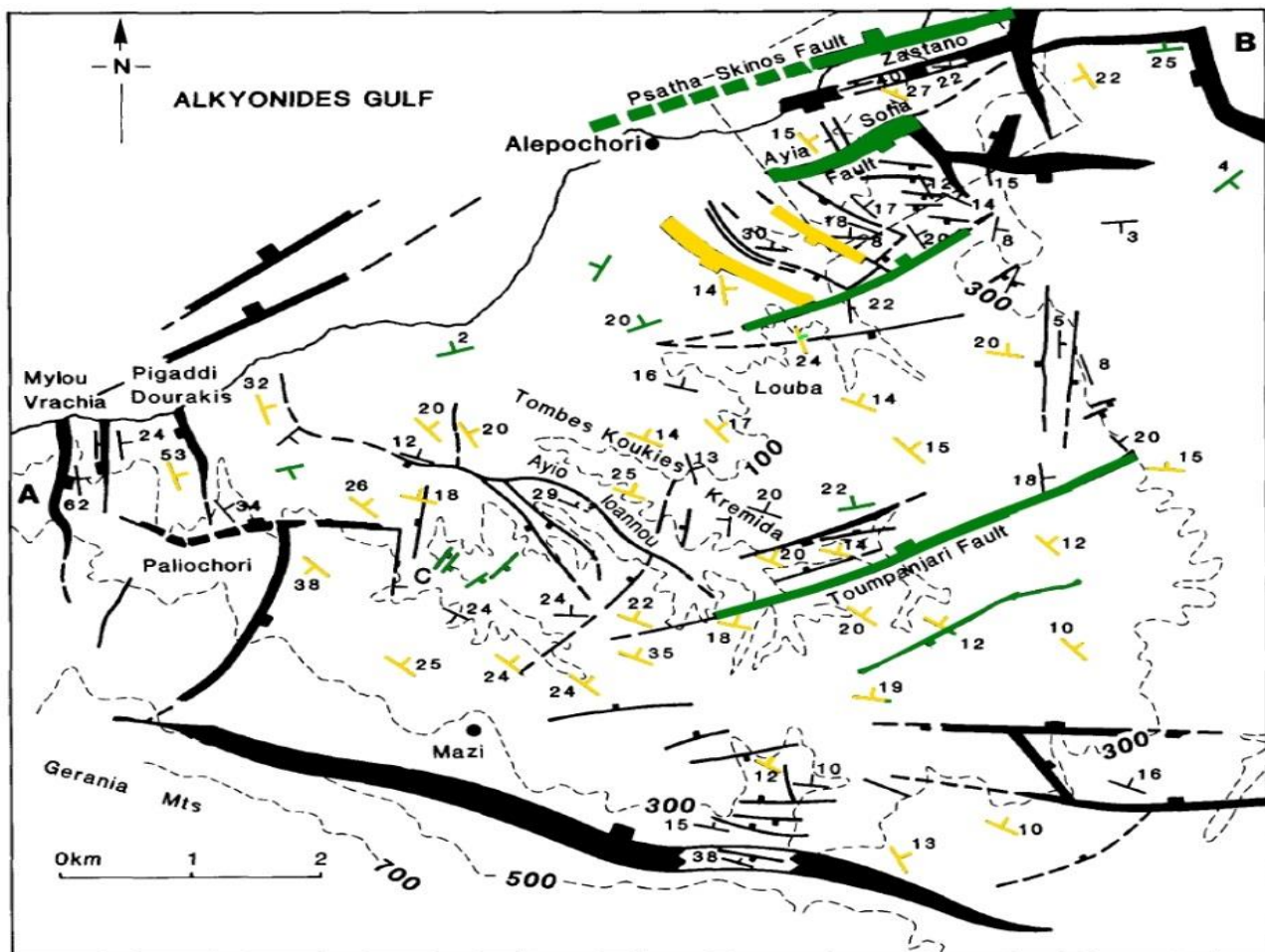


**Figure 2.4** – Map of the Megara Basin. The Pistarda formation is marked by a yellow line and the localities are shown as red dots. Modified from Bentham et al (1991).



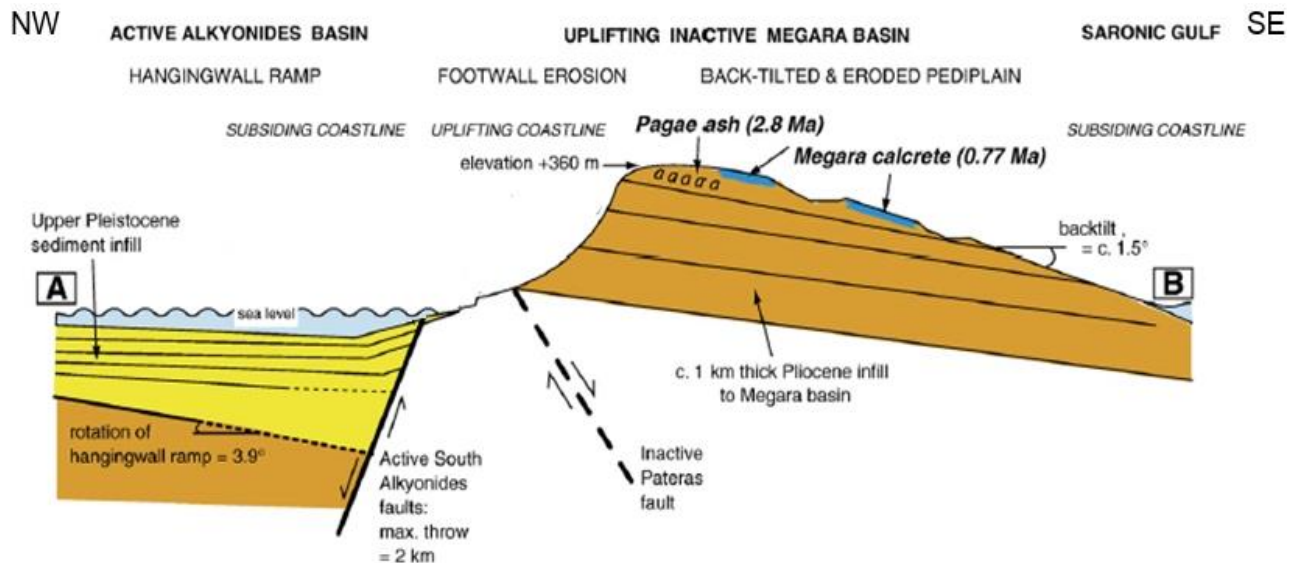
## 2.4 Basin structure

The Pistarda formation is restricted by the main faults to the southwest where the Gerania Mountains begin and to the northeast where the Pateras Mountains lie. Overall, the basin has a NNE or NE dip between 5-60°, commonly around 15-20° (Bentham et al., 1991). This causes progressively younger strata to be exposed in the northeast (figure 2.4). In the west, faults with higher dips give the basin a homoclinal form. The basin has many faults cutting through the strata with low throws of only a few decimeters to several meters, and it is suggested to be created by small adjustments in the Megara Basin when it was active (Bentham et al., 1991). In the intrabasinal structure, two primary trends of faults are seen (figure 2.5).



**Figure 2.5** – The map shows the distribution of faults in the northeastern part of the Megara Basin. The yellow faults are the first trend following NW-SE and the green faults are the second trend that follows a NE-SW to ENE-WSW direction. Modified after (Bentham et al., 1991).

The first is NW-SE (yellow) striking faults that go parallel to the basin margin faults. Some of them must have controlled the thickness of the sediments during deposition and facies boundaries when the basin developed in Neogene. The second group of faults (green) includes the Ayia Sofia and the active Psatha-Skinos fault which has a NE-SW to ENE-WSW trend. Ayia Sofia and Psatha-Skinos have a major influence on the later stages of the basin and its abandonment/uplift phase. An important fault of the Pistarda formation is the Toumpaniari fault which has an ENE-WSW trend and a normal throw to the NNW. It has a length of 5 km and is thought to have been active during the deposition of the Kremida and Toumpaniari formations and to have restrained the thickness of the Pistarda and Harbour Ridges formations (Bentham et al., 1991). Figure 2.6 illustrates a cross section of the basin, showing the uplift and back throws of the basin and the active Alkyonides fault.

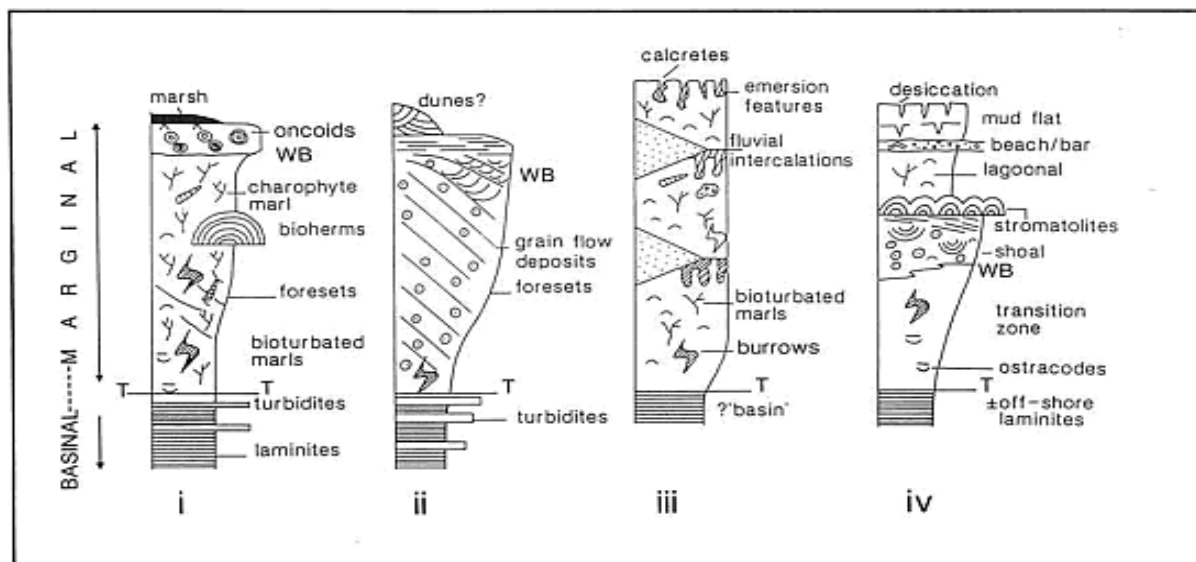


**Figure 2.6** - This figure illustrates a cross section of the stratigraphy of the basin NW-SE and the active Alkyonides fault and the inactive Pateras fault. This is only for illustration purposes. Modified from Leeder et al. (2008)

### 3 Lacustrine carbonates

#### 3.1 Introduction - Facies models

Many studies have been performed on lacustrine carbonates, for example Verrecchia (2007) and Gierlowski-Kordesch (2010). For facies models of lacustrine carbonates the literature becomes scarce, the most recent facies models are dated 20 years back (Tucker and Wright, 1990; Platt and Wright, 1991). They present a simple classification model of lacustrine carbonates. The model categorizes lakes in two main facies groups: lake margin (littoral) and lake basin (pelagic). Lakes can be further categorized based on the geometry that controls the development of the lake basin and the lake margin facies. These two types of lakes are either high-gradient bench type margins or lakes with low-gradient, ramp type margins. The first shows extensive development of lake basin facies while ramp types are more dominated by marginal lacustrine facies. The two types can be further divided into low- and high energy systems which create their own unique environments. High energy systems create cross bedding and coated grains, and low energy systems have a higher degree of bioturbated micrites. If the lakes are very shallow, they may not have a definable deep water basinal facies. See figure 3.1 for an illustration of the different logs that symbolize the different environments and showing an upwards sequence from lake basin to lake margin. The different types will be presented in the following subchapters.



**Figure 3.1** - Facies models of lacustrine carbonates showing typical shallowing upwards, progradational sequence, (i) low-energy bench margin; (ii) high-energy bench margin; (iii) low-energy ramp margin; (iv) high-energy ramp margin. T stands for thermocline; WB stands for wave base. Figure from Platt and Wright (1991)



### 3.1.1 Lake Margin - littoral

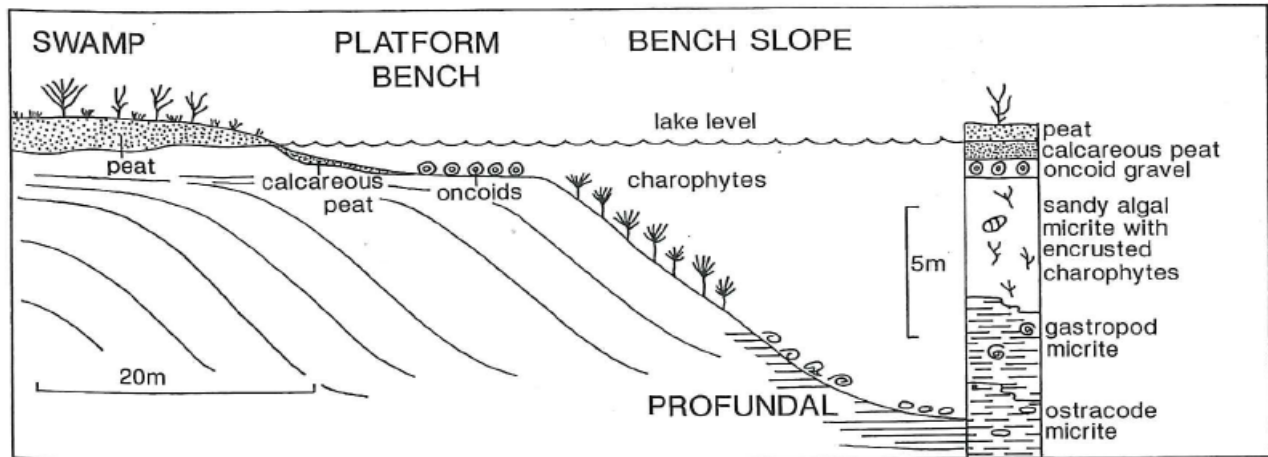
The production of carbonates mostly occurs in waters shallower than 10 m, where the bio-induced carbonate precipitation is at the highest (Thompson et al., 1997). In shallow water, inorganic carbonate precipitation can also be caused by warming, wave agitation or mixing of Ca-rich river inflow with a lake that is already rich in carbonate. In shallow lakes mudstone facies dominates and is commonly colonized by rooted aquatic plants. Reeds and charophyte algae prefer low-energy substrate and charophyte can grow up to 15 -20 m above lake level (Cohen and Thouin, 1987). High biologic production by photosynthesis increases CO<sub>2</sub> uptake and may lead to carbonate encrusting reeds and charophyte stems.

### 3.1.2 Lake Basin - pelagic

A lake basin can have a high carbonate precipitation rate bioinduced by phytoplankton and resedimentation from the lake margin zone, but will normally lack evidence of *in situ* vegetation. The content of siliciclastic is commonly higher during stable conditions and leads to development of anoxic water. Organic-rich facies may be deposited in the deeper parts. Since the deepest parts have no bioturbation, basal laminates can be developed with alternating organic-rich and carbonate-rich laminae. The lake floor gradient and local wave energy have a strong influence on which type of carbonate sediment that forms in a nearshore setting (Platt and Wright, 1991).

### 3.1.3 Bench margins with a steep gradient – low energy

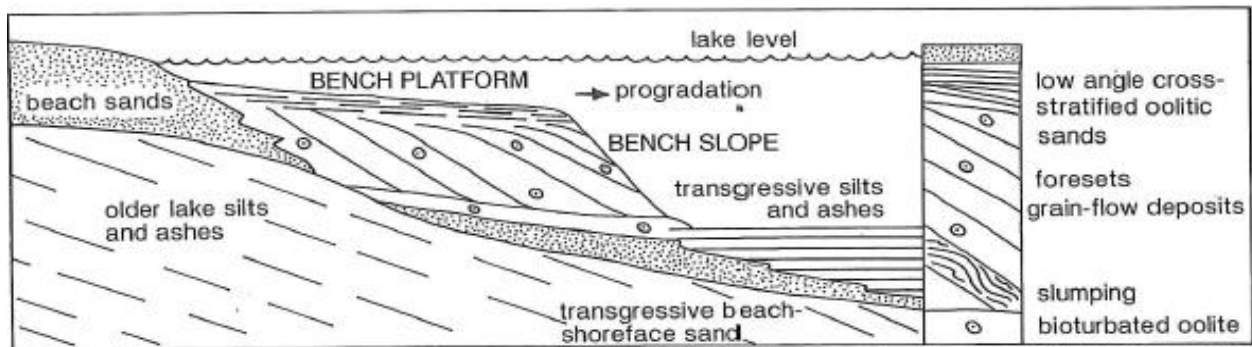
Bench margins with a steep gradient and low energy are characterized by high productivity of shallow water benthic plants in the littoral zone (figure 3.2). This creates a buildup in the shore zone which progradates into the lake. Accumulations occur from shallow playas and carbonate producing marsh and swamp (palustrine) environments. This creates similar deposits throughout the lake with only subtle facies. Stromatolites and soils indicate exposure, and in palustrine settings, charophyte, ostracode and gastropods can occur all over the lake deposit with no evidence of a deepwater basin (Platt, 1989). The ramp feature gives rise to gravity flow down the gradient and thin turbidity flow.



**Figure 3.2** - Low energy, bench-type lake margin: modern example from Lake Littlefield, Michigan, USA. Figure from Platt and Wright (1991 and reference therein).

### 3.1.4 Bench margins with steep gradient – high energy (wave dominated)

High energy bench margins with a steep gradient creates structureless lime mudstones that are bioturbated in protected low energy margins, while packstones and grainstones are found in higher energy bench settings (figure 3.3). From the high energy, carbonate ramps are formed where the rolling movement of grains creates extensive ooids, and is then redeposited on a large scale into the lake in foresets. Avalanching, slumps and normally graded laminae (turbidities) are typical near the base.



**Figure 3.3** - High energy, bench-type margin; This example is from an idealized sequence from the Pliocene Shoofly Oolite, Glens Ferry Formation, Snake River Plain, USA. Figure from Platt and Wright (1991 and reference therein).

### 3.1.5 Ramp margins with low gradient – low energy

Low gradient ramps settings in lakes are commonly shallow and lack the accumulation of facies in the stratigraphy (see figure 3.4). Ramp margin with low gradients are vulnerable to lake level shifts and a small water level reduction will expose a large area. The shallow water limestone is

rich in charophytes, including the calcified stems of algae. In the shallow water there is a low content of detrital components probably caused by baffling and trapping of clastic material in the lake marginal and marsh zones. In a regressive sequence it is common to have evidence of subaerial exposure during low lake stands. A typical regressive sequence starts with the resedimentation of pellets and intraclastic grainstones and packstones. This surface is then covered by micrite, from an open lake setting including gastropods, molluscs and charophyte stems, and gyrogonites. At the top layer, one can find pedogenic fabrics in limestones. In the sediments some sequences are incomplete and superposed because root tubules cut through several sequences.

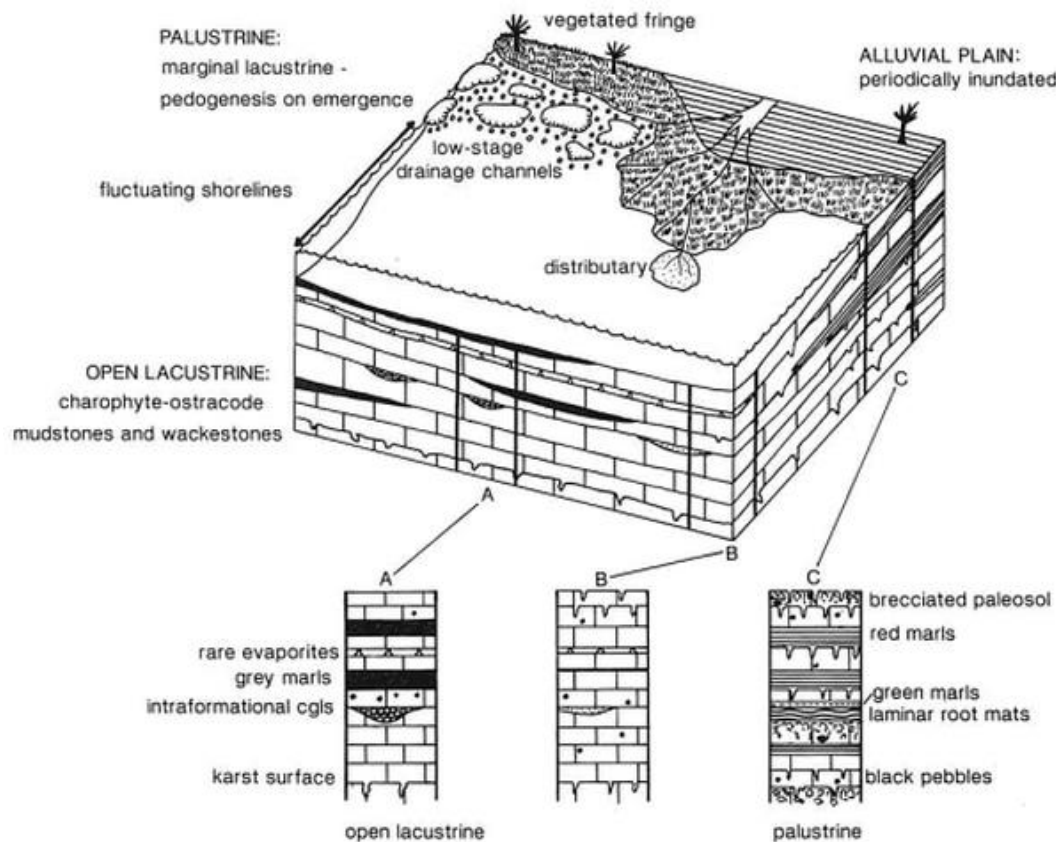


Figure 3.4 – The different facies in ramp margins with low gradient and low energy. Figure from Platt and Wright (1991).

### 3.1.6 Ramp margins with low-gradient – wave influenced

This model is based on a low gradient ramp with a strong wave influence (figure 3.5). In this environment winnowed grainstone dominates and nearshore bars can develop. The waves control the deposits and can create a lagoon, where organic matter can be deposited in an anoxic environment. In the deeper parts, stromatolites and thinly bedded laminates can be deposited,

probably under the thermocline (Donovan, 1975). Great Salt Lake of Utah is a modern example of such an environment where oolitic deposits are found along the shoreline. In the deeper part offshore bars and extensive bioherms is formed. (Eardley, 1938; Sandberg, 1975; Dean and Fouch, 1983). Shallow water carbonates from the Green River Formation is another example of a ramp margin which is wave influenced and therefore has built up barred shorelines and protected lagoons (Williamson and Picard, 1974).

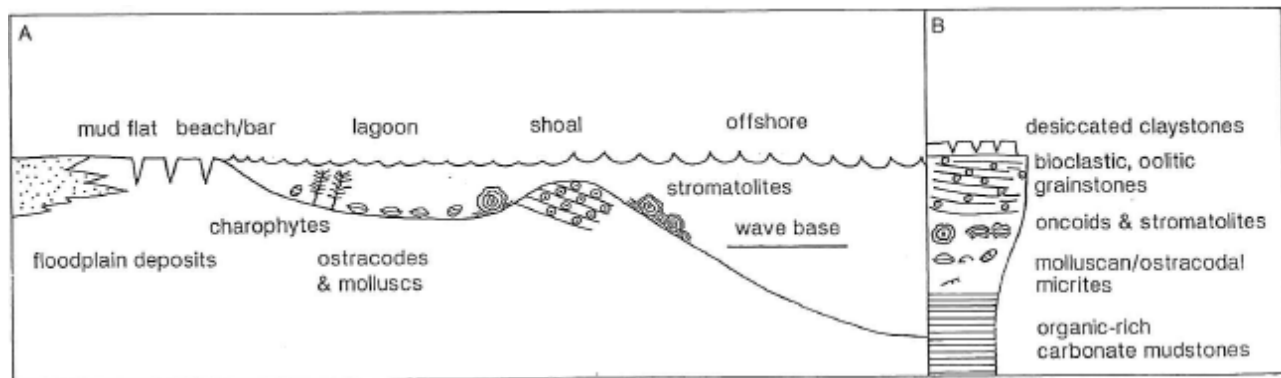


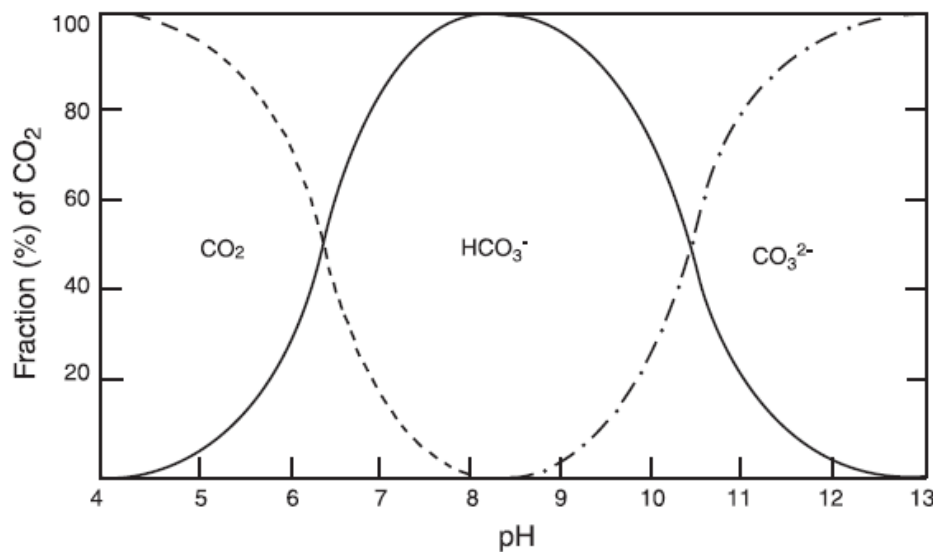
Figure 3.5 - The different facies in ramp margins with high energy. Figure from Platt and Wright (1991).

### 3.2 Geochemistry of lacustrine carbonates

The ocean has a stable chemical composition. Lakes, however, react faster to changes in the drainage area and are therefore highly variable in chemical composition and salinity. Lakes are the product of their surroundings with respect to chemical composition, biology activity and water level stability. Lakes are divided into two categories based on hydrology, closed or open. Closed lakes are lakes with annual inflow and direct precipitation lower than evaporation and annual outflow, often with no outlet. This is related to low precipitation and a dry climate, a typical example is the Dead Sea. In this type of lake it is common to create minerals like halite (NaCl), gypsum ( $\text{CaSO}_4 \cdot 2\text{H}_2\text{O}$ ) and different salts. Open lakes have annual inflow and direct precipitation equal to or greater than annual outflow and evaporation, often with an outlet. These types of lakes may have a large variation in their chemical content and pH, which is a result of erosion of the bedrock composition in the drainage area.

The pH in rain water is slightly acidic because it reacts with the carbon dioxide ( $\text{CO}_2$ ) in the air, forming carbonic acid which lowers the pH to approximately 5.7 depending on temperature and

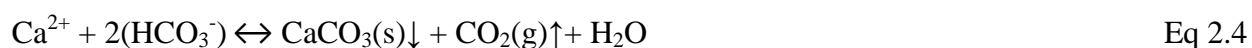
the amount of  $\text{CO}_2$  in the air. Carbonic acid is a polyprotic acid, and develops in two stages, as bicarbonate and then as carbonate (figure 3.6). In a solution this is called dissolved inorganic carbon (DIC) (Cohen, 2003). This acidification of rainwater is a major factor in dissolving carbonate rocks. Normally, the pH in lakes is controlled by biological processes rather than the equilibrium with  $\text{CO}_2$  in the atmosphere. The reaction is:



**Figure 3.6** – The  $\text{CO}_2$  and its derivatives,  $\text{HCO}_3^-$  and  $\text{CO}_3^{2-}$  and the relative proportions in relation to pH. Modified from (Wetzel, 1983).

Before the water is stored in the lake it runs through the bedrock of the drainage area, eroding and dissolving the rock in its path. This will add ions to the water and give it a chemical composition which is carried out to the lake. Groundwater takes a very long time compared to surface water, and therefore has a very large potential to dissolve a large amount of rock before it enters a lake. A typical feature in carbonate rocks is the formation of karst. It is a process created when acidic water dissolves the rock, which may create spectacular features, like caves.

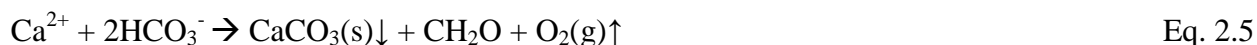
The process of dissolving rocks can also go the opposite way and precipitate calcite (Eq. 2.4). Groundwater is usually saturated with respect to calcite, with elevated partial pressures of CO<sub>2</sub> (P<sub>CO<sub>2</sub></sub>). When the groundwater enters the surface it will be exposed to the atmosphere, which can have a lower P<sub>CO<sub>2</sub></sub> than the groundwater. This will cause CO<sub>2</sub> to degas from the groundwater (Jacobson and Langmuir, 1970; Langmuir, 1971). Because of the lower CO<sub>2</sub> content in the water the capability to hold Ca-ions decreases and it becomes supersaturated. CO<sub>2</sub> can be removed by inorganic (degassing) and organic (photosynthesis) processes (Eq. 2.5), thus inducing carbonate precipitation. For the inorganic degassing process:



Two factors control the reaction: heating and turbulence. Elevated temperatures affect the solubility of CO<sub>2</sub>, increasing its fugacity which in turn decreases the level of CO<sub>2</sub> in the solution (Stumm and Morgan, 1981, pp.204-207; cited in Heimann and Sass, (1989)). This is most important in lagoons and shallow waters with high evaporation and with a low degree of exchange with other water bodies. To create turbulence in the water, rapids and falls have an enormous effect on the turbulence. This will enhance the CO<sub>2</sub> degassing (Lorah and Herman, 1988). Supersaturation of calcite is not enough to force precipitation. Studies by Lorah and Herman (1988) showed that the water was supersaturated up to 9 times, along the Falling Spring Creek, which runs for 1120 meters before the crest of the falls. This forced the water to become turbulent and gave a massive drop in Ca<sup>2+</sup> and HCO<sub>3</sub><sup>-</sup> which indicates that calcite precipitation begins in the vicinity of the waterfalls. This is possible because of the outgassing of CO<sub>2</sub> that allows the kinetic inhibition on calcite crystallization to be overcome. It is also proven by (Nielsen, 1964; Berner, 1980) that in order to precipitate crystals directly from a solution, an increase in free energy is needed. Therefore, a certain critical degree of supersaturation has to be achieved in order to pass this nucleation barrier (Heimann and Sass, 1989).

An important CO<sub>2</sub> remover is simply photosynthesis (Eq. 2.5). Both micro- and macrophytes use CO<sub>2</sub> in the process of photosynthesis, by producing carbohydrates (Heimann and Sass, 1989 and reference therein). This is a very effective mechanism to increase precipitation of carbonate. This can occur all over the lake, but also in small micro zones around the plants, especially if they

grow densely packed in an environment where Charophyta thrives (Królikowska, 1997). Growth season and seasonal variations make it possible to deposit varve or seasonal precipitation rates. The chemical reaction can be simplified as this (note that some plants use  $\text{CO}_2$  rather than  $\text{HCO}_3^-$ ):



### 3.2.1 Isotopes

When measuring two isotopes from the same element it is difficult to measure an absolute amount of the less common isotope (such as  $^{18}\text{O}$  and  $^{13}\text{C}$ ). Therefore it is best to use an amount that is quantitative, and is compared with a known external standard. This  $\delta$ -value is defined as:

$$\delta = \frac{R_{\text{Sample}} - R_{\text{Std}}}{R_{\text{Std}}} \times 1000 \quad \text{Eq.2.6}$$

Where  $R_{\text{sample}}$  is the sample value and  $R_{\text{std}}$  is the standard value from the reference sample. The  $\delta$ -value is an expression of the heavy and light isotope relative to a common standard ( $R_{\text{std}}$ ) presented in per mille (‰). A negative  $\delta$  value indicates enrichment in the light isotopes, relative to the standard, and the opposite for a positive  $\delta$  value. The standard for carbonates is VPDB (Vienna Pee Dee Belemnite) and for water it is common to use SMOW (standard mean ocean water).

### 3.2.2 Strontium isotopes ( $^{87}\text{Sr}/^{86}\text{Sr}$ )

The ratio between the two isotopes  $^{87}\text{Sr}$  and  $^{86}\text{Sr}$  is an important number that is used in dating and strontium isotope stratigraphy (SIS). The only source of  $^{87}\text{Sr}$  is from radioactive decay of rubidium-87 which has a long half-life,  $4.92 \times 10^{10}$  yr, and will therefore have only a small effect (Elderfield, 1986). The effect only happens where rubidium can occur, which it can't in carbonate minerals. This is because rubidium has a different size and charge and it does not fit in the carbonate lattice. Strontium on the other hand has the same positive charge ( $^{2+}$ ) and similar size as Ca, and therefore it can substitute for all carbonate minerals. Both  $^{87}\text{Sr}$  and  $^{86}\text{Sr}$  are stable isotopes, so they do not change over time and are preserved in the carbonate mineral. Therefore,

carbonate minerals incorporate the strontium ratio at the time of creation and keeps the ratio stable. Because of this, the ratio can be correlated to a specific time of deposition, see McArthur et al. (2001) for a list of ratios correlated to geological time. This is also possible because sea water has a relatively short mixing time compared to the residence time for the isotope, which makes for a homogenous ratio both between the stable isotope and their pervasiveness in the ocean.

All of this makes strontium a good tool to use in dating fossils and carbonate rocks, because the  $^{87}\text{Sr}/^{86}\text{Sr}$  ratio in carbonates is the same as the ambient seawater. When working with freshwater carbonates there are some differences. Lake water only gets an input of strontium by erosion of the bedrock composition in the drainage area. Therefore the ratio can vary from very low to very high values. If the drainage pattern changes during deposition of sediments in the lake, this will also change the ratio according to the new bed rock composition. Rhodes et al. (2002) used this for the Eocene Green River Formation, Wyoming, to determine if the lake had two sources of drainage. The drainage that normally was filling the lake had a specific strontium ratio, which is the product of the bedrock composition. Sometimes a nearby river which usually had a different path and did not enter the lake, would shift direction during a flooding event and go into the lake. The new direction of the river was over a different type of bedrock, volcanics, which had a lower strontium ratio. In this case it was possible to use strontium isotope stratigraphy to determine that the flooding happened four times in the Arco Washakie Basin, in the Eocene Green River (Rhodes et al., 2002).

### 3.2.3 Stable isotopes in lacustrine lakes, $\delta^{18}\text{O}$ and $\delta^{13}\text{C}$

Oxygen isotopes occur in three different stable isotopes,  $^{16}\text{O}$ ,  $^{17}\text{O}$  and  $^{18}\text{O}$ . The rate at which they occur is 99,763 %, 0,0375 % and 0,1995 % respectively (Garlick, 1969).  $^{17}\text{O}$  occurs in such small values that it is not being used in oxygen isotope studies. Therefore, the ratio between  $^{18}\text{O}$  and  $^{16}\text{O}$  is used.  $\delta^{18}\text{O}$  is a product of different hydrological processes and is an important number that relates to evaporation in lakes. It can also tell if the lakes were open or closed. This is because when water evaporates the lighter  $^{16}\text{O}$  is removed first, leaving the heavier  $^{18}\text{O}$  in the lake (Boggs, 1995). This process is called isotopic fractionation and leads to the water vapor



being depleted of  $^{18}\text{O}$  (Merlivat and Jouzel, 1979). In closed lakes the  $\delta^{18}\text{O}$  value will therefore be positive because of high evaporation and the opposite for open lakes.

Carbon occurs in two stable isotopes,  $^{12}\text{C}$  and  $^{13}\text{C}$ , at a rate of 98,89 % and 1,11 % respectively (O'Leary, 1988). Carbon can exist either in oxidized form, as an element (graphite or diamond) or in reduced form (methane or organic matter). The heavy isotope  $^{13}\text{C}$  is often more abundant in oxidized form, as  $\text{CO}_2$ ,  $\text{HCO}_3^{2-}$  and as carbonate minerals. The lighter isotope  $^{12}\text{C}$  contributes to a higher amount of organic material, because it is easier to use the lighter carbon  $^{12}\text{C}$  (Craig, 1954). This is related to a slight difference in the chemical and physical properties of  $^{12}\text{C}$  and  $^{13}\text{C}$ . High biological activity makes the lake richer in  $^{13}\text{C}$ . On the other hand, high precipitation of carbonate minerals can reduce the DIC (dissolved inorganic carbon) amount of  $^{13}\text{C}$  in the lake. The lakes have two categories that will influence the DIC value in the lake:

1. Photosynthesis preferentially extracts  $^{12}\text{C}$  from  $\text{CO}_2$ , leading to DIC subsequently enriched in  $^{13}\text{C}$  (Arthur et al., 1983). (i.e. primary production will result in lower  $\delta^{13}\text{C}$  in the organic matter of phytoplankton. The use of  $\text{CO}_2$  will increase the possibility of precipitation of inorganic carbon which then must be the “left over” heavier DIC (i.e. enriched in  $^{13}\text{C}$ )).
2. Larger plants in lake margins, for example reeds, use photosynthesis to lower the  $\delta^{13}\text{C}$  of phytoplankton. This gives a higher value  $\delta^{13}\text{C}$  of inorganic carbon that precipitates as a result of increased primary production.

### 3.2.4 Element Analysis

The purpose of element analysis is to measure the amount of trace elements in order to check what type of calcite carbonate is dominating, low magnesium calcite (LMC), high magnesium calcite (HMC) or aragonite. This is also linked to what kind of carbonate that is stable under precipitation. To determine diagenetic indicators, it is also useful to use strontium and manganese, which have divergent partition coefficients (i.e. they don't want to be mixed) (Brand and Veizer, 1980). Both of them can exist within the carbonate lattice, and because of the large composition difference in marine and meteoric water they can be used as diagenetic indicators (Kinsman, 1969).

## **4. Methods**

### **4.1 Introduction**

To understand the Pistarda formation, a variety of different methods were used to gain as much information as possible. In this chapter the different methods in geochemistry and microscopy will be presented.

### **4.2 Field work**

Together with my fellow student Kristoffer Nilsen and in cooperation with my supervisors, Rob Gawthorpe and Gunnar Sælen, the fieldwork was completed over the course of two separate trips of approximately 3 weeks each. The first trip was from 22<sup>th</sup> April to 9<sup>th</sup> May 2013 and the second trip was from 2<sup>nd</sup> to 24<sup>th</sup> October 2013. The equipment used in the field was standard field equipment and a laser rangefinder (TruPulse 360 series), GPS and a digital camera. The purpose of the fieldwork was to map the Pistarda formation over the Megara basin and create lithostratigraphic logs. A geological map over the Megara basin made by Bentham et al. (1991), was used to find areas of possible exposure of the Pistarda formation. Samples were brought back for analyses for geochemical purposes and to make thin sections. Carbonates in the field were classified after the Dunham (1962) classification scheme, modified by (Embry and Klovan, 1971).

### **4.3 Laboratory work**

The first laboratory work was performed on the samples brought back from the first trip, with samples from localities 1, 4 and 5.2. Samples from localities 1 and 5.2 were selected as a starting point in getting a good distribution of geological data from the basin. From each rock, three holes were carefully selected and drilled out using a dentist drill. After the second trip, samples from the new localities were chosen. The powder from the samples was used for analysis of strontium, stable isotopes and trace elements. Thin sections were made by Irina Dumitru at the University of Bergen.

### 4.3.1 Stable isotope analysis

62 analyses were carried out on the stable isotopes  $\delta^{13}\text{C}$  and  $\delta^{18}\text{O}$ . Rune Søråas did the analysis using the Finnegan Mat 251 mass spectrometer at the GMS-Laboratory at the Bjerknes Centre for Climate Research and Department of Earth Science at the University of Bergen. The analysis was carried out using approximately 50  $\mu\text{g}$  of powder from the samples and using conventional methods. Results are reported as per mille (‰) deviation from the Vienna Pee-Dee Belemnite (VPDB) standard. The procedure is in accordance with Shackleton and Opdyke (1973). The calibration is done after the reference material NBS-19 and NBS-18. An overview of the results is displayed in appendix (Table 8.1).

### 4.3.2 Strontium isotope analysis

Strontium analysis was conducted on 36 samples. 50-100  $\mu\text{g}$  of sample material was analyzed with a mass spectrometer at the laboratory of the Department of Earth Science at the University of Bergen, by laboratory technician Yuval Ronen. The strontium ratio ( $^{87}\text{Sr}/^{86}\text{Sr}$ ) was measured by a Finnegan MAT 262 Mass spectrometer. After the powder was drilled out from the sample it was collected in acid washed (nitric acid ( $\text{HNO}_3$ )) Eppendorf tubes. The chemical processes were performed in an ultra-clean room with HEPA filter and overpressure. The powder was rinsed with deionized water before it was dissolved with 0.75 ml 3.0 M  $\text{HNO}_3$  in prewashed centrifuge tubes. The extract was then used to separate the strontium isotopes from the other elements using the specific extraction chromatographic method described by Pin et al. (1994). Then the extract was placed in a double filament and analyzed in static mode. The standard deviation ( $\sigma$ ) is a measurement of analytic precision and the probability of the  $^{87}\text{Sr}/^{86}\text{Sr}$  relationship is plotted as  $1\sigma$  and  $2\sigma$ , 68% and 95% respectively. All of the results were normalized to SRM 987=0.710240 (former NBS 987). An overview of the results is displayed in the appendix (Table 8.1).

### 4.3.3 Trace element analysis

A total of 6 samples were used for trace element analysis and all of them are from locality 5.2. The trace element analysis was performed by Siv Dundas at the ICP-laboratory of the Bergen Geoanalytical Facility at the University of Bergen. The samples were weighted to approximately 15  $\mu\text{g}$  and stored in acid washed Eppendorf tubes. 100  $\mu\text{l}$  of concentrated  $\text{HNO}_3$  was added to

dissolve the carbonate, and then 900 µl of H<sub>2</sub>O was added. The samples were mixed by a whirlimixer. When needed, the samples were diluted using 2% w/v of HNO<sub>3</sub>. Similar methods are shown in Jenner et al. (1990) and Eggins et al. (1997). Magnesium (<sup>24</sup>Mg), manganese (<sup>55</sup>Mn), iron (<sup>57</sup>Fe), strontium (<sup>88</sup>Sr) and indium (<sup>115</sup>In) was analyzed with a High Resolution Inductively Coupled Plasma Mass Spectrometry (HR-ICPMS) using a Thermo Finnigan Element 2. All samples were analyzed in medium resolution. Because of the high amount of calcium (Ca) an Inductively Coupled Plasma Atomic Emission Spectroscopy (ICP-AES), Iris Intrepid, Thermo Elemental was used instead. The spectral lines that were used were 317.8 nm for Ca and 361.3 nm for scandium (Sc). A solution of 2 µg/l In was added to all samples when using ICP-MS. When operating the ICP-AES, the samples were added 1 mg/l Sc. Quantization was done using external standard curves.

Ca concentration is given in percent (%), whereas Mg-, Mn-, Fe- and Sr concentration is given in milligrams per kilo (mg/kg). Trace element data is presented in table 8.1 in the appendix. The internal uncertainty (RSD = “Relative standard deviation”) in the instrumental measurements are calculated from repeated measurements by instrumental analysis of the various isotopes. %RSD is indicated by SD /mean \*100. The internal uncertainty is presented in table 8.4 in the appendix.

#### **4.4.1 Scanning Electron Microscopy (SEM)**

A SEM was used to photograph four samples of the matrix, two samples from the inner and outer edge of the calcification from a plant stem, two gastropods, two samples from a laminated layer, and two thin sections (figure 4.1). The samples were covered in gold (Au)/Palladium (Pd) using a Polaron SC502 Sputter Coater and the thin sections were covered in carbon using an Agar Turbo Carbon Coater. The purpose of covering the samples with these elements is to establish good conductivity on the surface of the sample. After the preparation they were studied by a ZEISS Supra 55VP scanning electron microscope, with a magnification up to 1.5 million times. An energy-dispersive x-ray spectroscopy (EDS) was also connected to the microscope to do an element analysis based on the element’s unique set of peaks on the X-ray spectrum.

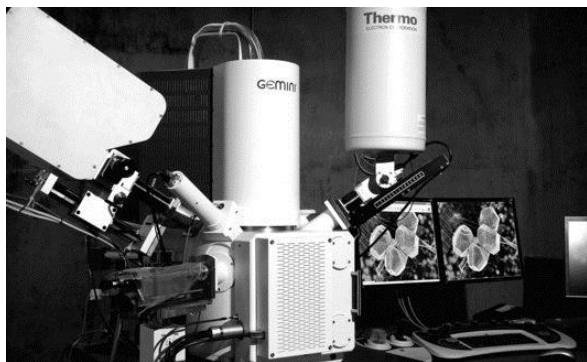


Figure 4.1 - ZEISS Supra 55VP scanning electron microscopy. Photo by Irene Heggstad.

#### 4.4.2 Optical microscope

A Nikon Alphaphat 2 YS2 microscope was used to view the thin sections under ordinary light. The microscope had three levels of magnification, 4X, 10X and 40X. This was used to check mineralogy, texture and diagenetic features.

#### 4.4.3 Cathodoluminescence microscope (CL)

Some of the thin sections were also checked using cathodoluminescence microscopy, in order to see if diagenetic processes had affected the studied samples (e.g. Tucker and Wright (1990)). A Technosyn LTD8200 instrument with a SPOT3 digital camera and included software was used. Operating conditions were approximately 15 kV accelerating voltage, with a 150  $\mu$ A gun current. The concept of cathodoluminescence is to send electrons against the thin section and to see what kind of light that is emitted from the sample. Luminescence in calcite is mainly controlled by the concentration of  $\text{Mn}^{2+}$  and  $\text{Fe}^{2+}$  in the calcite lattice (Meyers, 1974) where  $\text{Mn}^{2+}$  behaves as an activator and  $\text{Fe}^{2+}$  as an inhibitor, see also (Pierson, 1981; Fairchild, 1983). The color and the intensity of the luminescence is more related to the ratio between Fe and Mn than the concentration of these two elements (Tucker and Wright, 1990). Diagenetic calcite can contain large amounts of these elements (McArthur, 1994; Veizer et al., 1999). Reducing environments are the only places  $\text{Mn}^{2+}$  and  $\text{Fe}^{2+}$  can exist, because in oxidizing environments the ions will not be found as dissolved compounds and can't go into the calcite lattice. In the upper sedimentary layer it is most common to have an oxidizing environment and it continues down to where the dissolved  $\text{O}_2$  is gone. This environment is characterized by no luminescence (James and Choquette, 1984).

#### **4.4.4 Fluorescence microscope**

Fluorescence is a type of luminescence which is transmitted by materials that emit light when exposed to visible or ultraviolet light. The sample was examined using incident-light fluorescence with a blue-light excitation filter (400 - 440 nanometers). Modern types of ooids and molluscs are naturally brightly fluorescent, due to the abundant presence of organic matter (Ferguson and Ibe, 1982). Therefore, if there is a signal it indicates that remnants of organic matter are still present in and between the calcite crystals. When carbonate minerals are exposed to freshwater diagenesis, organic matter is destroyed by oxidation when the recrystallizing of stable low-magnesium calcite occurs. This will destroy the natural fluorescence, so fluorescence microscopy can be used to check if diagenesis has occurred or not (Dravis and Yurewicz, 1985).

## **5. Fieldwork – The Pistarda formation**

### **5.1 Introduction**

The localities visited during the fieldwork are spread out over a large geographic area and the outcrop quality and thickness varies very much. Figure 5.1 displays one of the best outcrops, located in the middle of the Megara Basin. This locality is used as the main locality regarding establishing facies and geochemistry analysis. The facies is divided on the basis of composition, biological content, sedimentary structures, texture and color. The main characteristics that divide them are fossils, plant stems, microbial encrustations and gastropods which are major biogenic components. Further analysis with thin sections and SEM gives a more complete picture of their fossil context and types of minerals.

### **5.2 Localities**

The localities have been divided into 10 main localities, further subdivided when they were opposite each other in a gorge. The localities are successively numbered from 1 to 10, starting in the northwest with locality 1, following along a southeasterly line (table 4.1). The distance between localities 1 and 10 is more than 12 km. The topography of the area is mostly the results of the latest uplift in the Megara Basin, which created two drainage systems. The drainage system in the northwest contains localities 1-7. The drainage system in the southeast contains localities 8-10.

The quality of the different localities varies greatly with respect to exposure and accessibility. Some of the localities are very thin, around 1 meter, and do not give a complete section through the formation. Because of this, locality 5.2 was selected as the main locality, as it gives a good and a complete section through the Pistarda formation.

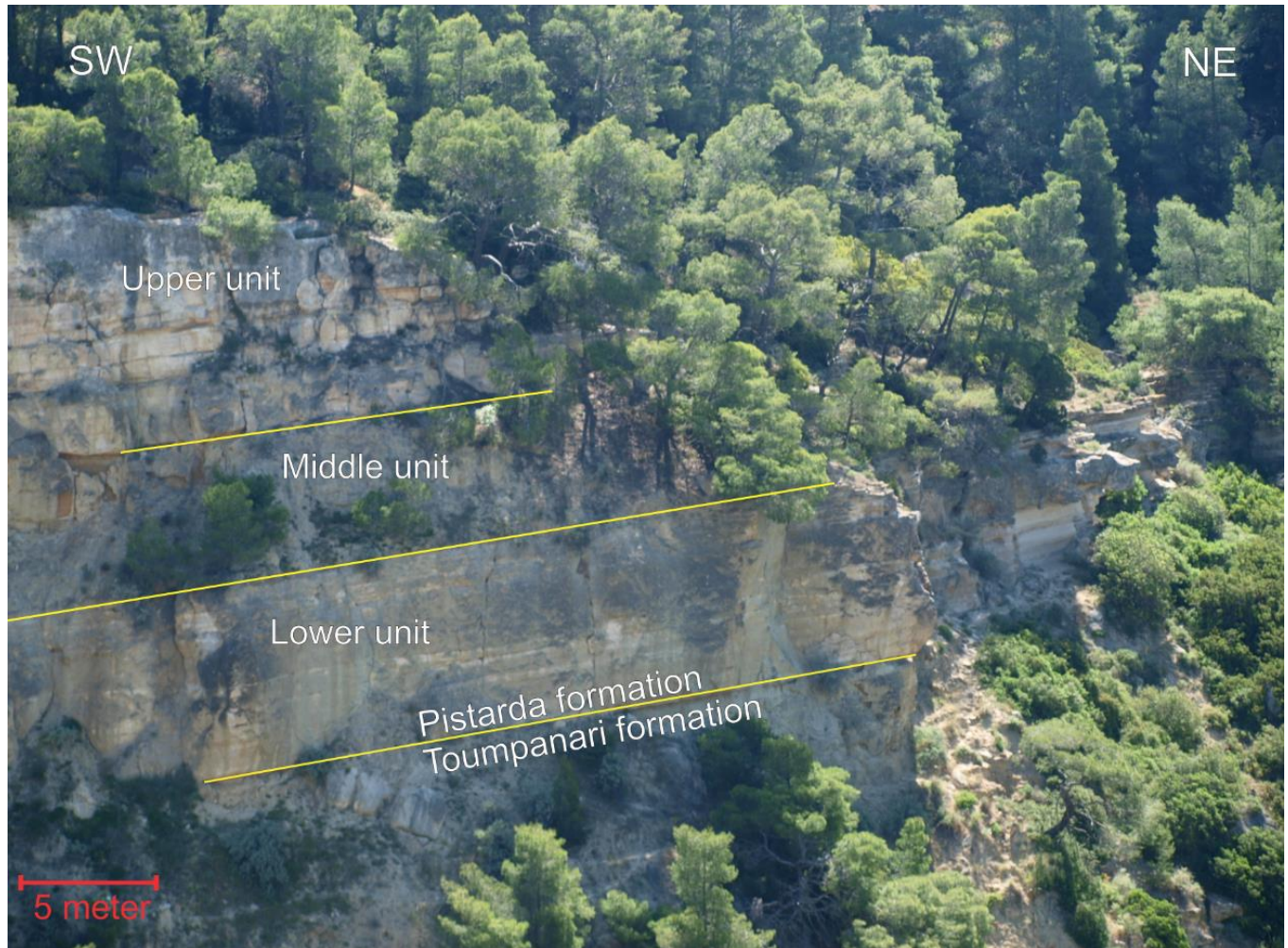
Table 5.1 - Table of localities and their coordinates

<b>Locality</b>	<b>Coordinate</b>
<b>1 East</b>	N38° 04.852' E023° 11.680'
<b>2</b>	N38° 04.049' E023° 11.292'
<b>3</b>	N38° 03.947' E023° 11.343'
<b>4.1</b>	N38° 03.398' E023° 11.958'
<b>4.2</b>	N38° 03.391' E023° 12.026'
<b>5.1</b>	N38° 03.194' E023° 12.701'
<b>5.2</b>	N38° 03.123' E023° 12.834'
<b>6</b>	N38° 02.904' E023° 12.999'
<b>7</b>	N38° 02.646' E023° 12.774'
<b>8</b>	N38° 01.376' E023° 13.491'
<b>9</b>	N38° 01.675' E023° 15.929'
<b>10</b>	N38° 00.517' E023° 17.459'

At some of the localities it was possible to see that the Pistarda formation consists of two units, the lower unit and the upper unit (figure 5.1(Locality 5.2)). In between these two units there is a middle unit which was not possible to work on, as it was inaccessible. The middle unit is covered with debris and landslide material from the upper unit and the formation above. The thickness is 11,3 meters for the upper unit, 7,0 meters for the middle unit and 6,8 meters for the lower unit .

The two units, upper and lower, are only found in localities 4, 5 and 6, with 6 being too steep to work on. In other localities no clear difference is found to distinguish between the two units.














**Figure 5.1** – Locality 5.2. The work was done on the right side of the picture. The three units, upper (11,3 meters), middle (7,0 meters) and lower (6,8 meters) units marked by line and name. Scale in the lower left hand corner. See figure 2.4 for a map of the localities in the Megara Basin.

### 5.3 Facies

The facies are based on their components and they are classified after the (Dunham, 1962) classification scheme, modified by Embry and Klovan (1971) (figure 5.2). The carbonate classification scheme was used to visually describe the outcrop and it gives a good idea of how the outcrop appears with the respective bioclasts instead of using grain size. The thin section is used as a supplement to the facies and will be included in the descriptions of the facies if they are available. The thin sections gave some information of what fossils (e.g. reeds, gastropods and ostracode) that are found in the formation, but they consist almost entirely of micrite. The best classification to use on the thin section was also Embry and Klovan (1971), because by using for

example (Folk, 1959; Folk, 1962) all of the thin sections would be classified as biomicrite since some fragments of bioclasts are found to some degree in all of the thin sections.

Original components not organically bound together during deposition						Boundstones: original components organically bound during deposition		
Contains lime mud			Lacks mud and is grain-supported	> 10 % grains > 2 mm		Organisms act as baffles	Organisms encrust and bind	Organisms build a rigid 3D framework
Mud-supported		Grain-supported with muddy matrix		Matrix-supported	Supported by > 2 mm component			
< 10 % grains	> 10 % grains							
Mudstone	Wackestone	Packstone	Grainstone	Floatstone	Rudstone	Bafflestone	Bindstone	Framestone
								

**Figure 5.2** - Classification system of carbonate rocks established by (Dunham, 1962) and later modified by (Embry and Klovan, 1971). This figure is from (Embry and Klovan, 1971).

An overview of the different facies is presented in table 5.2

**Table 5.2** – Facies and their respective properties.

<b>Facies</b>	<b>Description</b>	<b>Thickness</b>	<b>Boundary</b>	<b>Depositional process</b>	<b>Interpretation</b>
<b>1</b>	Dark grey to black in color	A few cm up to 10 cm	Above Sharp Below: Sharp	Organic material/paleosol formed on land	Paleosol and organic material
<b>2</b>	Vertical orientated plant stems or sub-vertical orientated	Typically from 30 cm up to 2 meter, but can be thicker	Above: Gradational/sharp Below: Gradational /Sharp	Buried reeds <i>in situ</i>	Reeds - In situ
<b>3</b>	Water escape structures	Around one meter, also thinner.	Above: Sharp/Erosive Below: Sharp	Mass transport sedimentation	Slump and load structures
<b>4</b>	Chaotic reeds with fining upwards structures	Around one meter	Above: Sharp/Erosive Below: Sharp	Mass transport sedimentation	Turbidity - Reworked reeds

5	Thinly bedded layers in a larger strata with gastropods	Around 50 cm	Above: Gradational/Sharp Below: Gradational/sharp	Deposition of whole gastropods under low energy orbital velocity	Reworked gastropods
6	Thinly bedded layer with broken gastropods	Thin layer around 1-10 cm	Above: Gradational Below: Erosive	Redeposition of more broken gastropods during high energy orbital velocity	Reworked gastropods, coquina
7	Micrite mud with no structures with or without gastropods. Can also be laminated	Up to a few meters	Above: Sharp Below: Sharp	Microbial induced precipitation or from increased photosynthesis during phytoplankton blooms	Hemipelagic/Pelagic micritic

### 5.3.1 Gastropods

There are two types of gastropods found in the Pistarda formation. The first manifests with a smooth surface and a brownish color. The second is the one that is most abundant in the formation, found all over the basin and in all facies. It has grooves and a white color (figure 5.3).

The white gastropods are interpreted to be *Melanopsis gorceixi*, similar to what Willmann (1985) found in the island of Kos, Greece (figure 5.4(B)). It was first described by Tournouër in 1875. Willmann (1985) found many different species of *Melanopsis gorceixi* in the sequence he studied. Based on the number of ribs around the gastropods it was possible to distinguish between the different *Melanopsis gorceixi*. The *Melanopsis gorceixi* has changed a lot over time due to adaptation to the environment. The number of ribs per whorl can indicate which type it is. Two types of *Melanopsis gorceixi* are found: The first has 10 ribs per whorl and is therefore a *Melanopsis gorceixi aegaea*; the second has 15 and is therefore a *Melanopsis gorceixi proteus* (figure 5.4(A)).



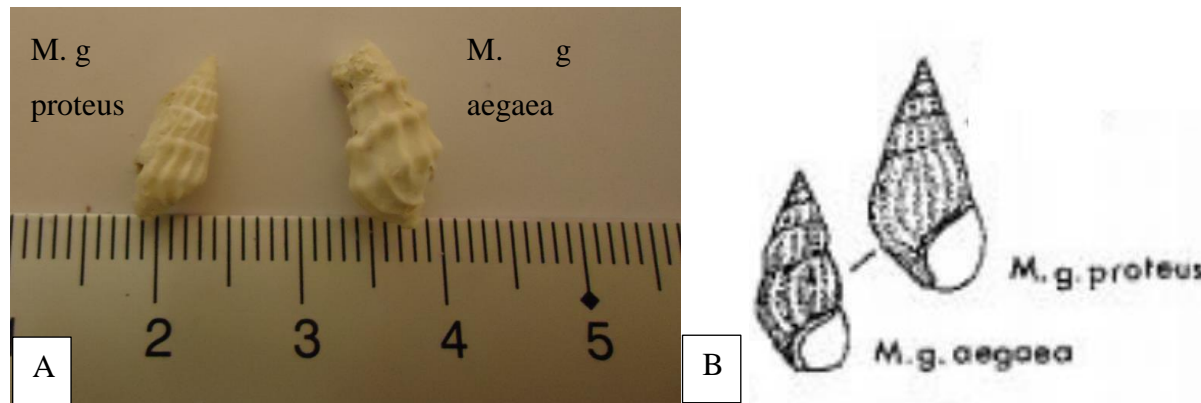


**Figure 5.3** - Locality 1 East. The width of the hammer is around 3 cm. The red box to the left of the hammer is a *Melanopsis gorceixi* Tournouër, 1875, and the box to the right is interpreted as species *Viviparus viviparus* under the family Viviparidae, a type of river snail.

The round and smooth gastropods in figure 5.3 are interpreted to be *viviparus viviparus*, in the family Viviparidae. This is classified based on what Bentham et al. (1991) found in another formation in the Megara Basin. It is a river snail which thrives in running water in the middle or the lower part of the river, and it is therefore interpreted to be transported into the Pistarda formation by rivers. They are only found in locality 1, 2 and 3. Therefore, these localities are thought to have had an influx of river water where *viviparus viviparus* has been transported into the lake.

The *Melanopsis gorceixi* is found everywhere in the lake and in large amounts. Gastropods are considered a good indicator of the paleoenvironment, because the diversity of species and they strives to specialize and adapt to different environments. What kind of environment the *Melanopsis gorceixi* thrives and reproduces in is unknown, but it is known to be a freshwater snail. It was found in calcareous marls with freshwater fauna deposited in Plio-Pleistocene, which are environments similar to the Pistarda formation. From the SEM figure it was possible to

identify that the gastropods are composed of aragonite. This is interpreted to be a genetic feature rather than having a geochemical cause.



**Figure 5.4** – (A) The two different kinds of *Melanopsis gorceixi*. Note that *M. g. proteus* has more ribs per whorl than *M. g. aegaea*. (B) A sketch of the same gastropods, published in (Willmann, 1985).

### 5.3.2 Facies 1: Organic Matter

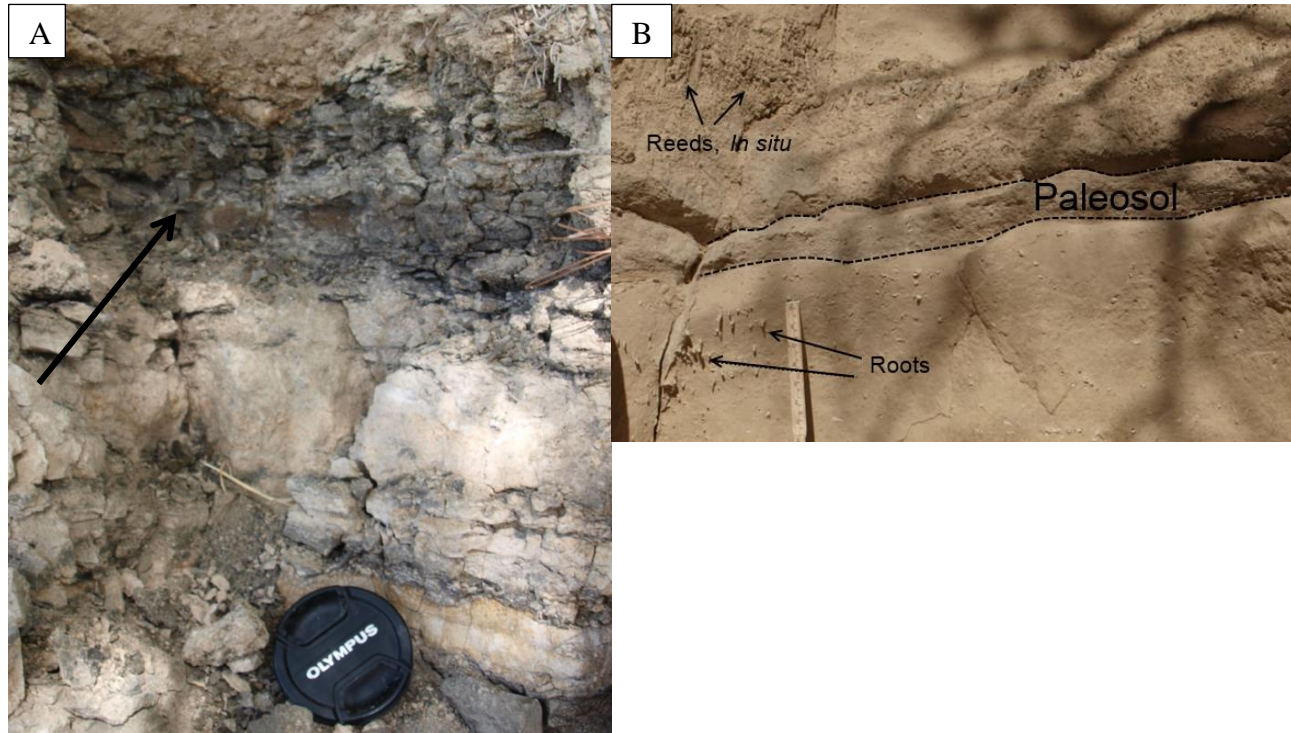
#### *Observations:*

A thin layer of grey or dark grey material is found at some localities in the Pistarda formation basin, namely in localities 1, 3, 4.1, 5.2 and 10. The layer has sharp boundaries below and above. The layer is relatively thin, around a few cm up to 10 cm, but never larger. The layer is homogeneous with no roots or other fragments. In locality 5.2, a thin horizon is found in the upper unit with yellowish color, with a thicker unit of micrite below containing gastropods and roots.

#### *Interpretation:*

Based on the color and appearance this is interpreted to be organic material. Organic material has three principal sources: terrestrial vegetation, marginal macrophytes swamps and phytoplankton (Reading, 2009). To create an organic layer in a lake, the lake needs to have anoxic conditions at the bottom or the organic material will be decomposed. Since the layer exists only locally and with a sharp base, it is not thought to be formed by phytoplankton, which requires the lake to be anoxic. The other cause could be an influx into the lake from terrestrial vegetation. During flooding, eroded sediments from nearby swamps enters the lake and settles new layers and the

organic material is not decomposed before it is covered by new sediments. In this case it is interpreted to have been formed by terrestrial vegetation, which also created the paleosol. The paleosol units have a leaching zone beneath them where roots are found in the upper parts.



**Figure 5.5** – (A) Locality 3. The arrow indicates the dark grey layer that is interpreted to be an organic layer. Lens cover as scale. (B) Locality 5.2 upper. The arrow indicates the roots that are found in the leaching zone to the paleosol. Reeds *in situ* are found directly above the paleosol. The folding ruler is 20 centimeters.

### 5.3.3 Facies 2: Reeds – *In situ*

#### *Observations:*

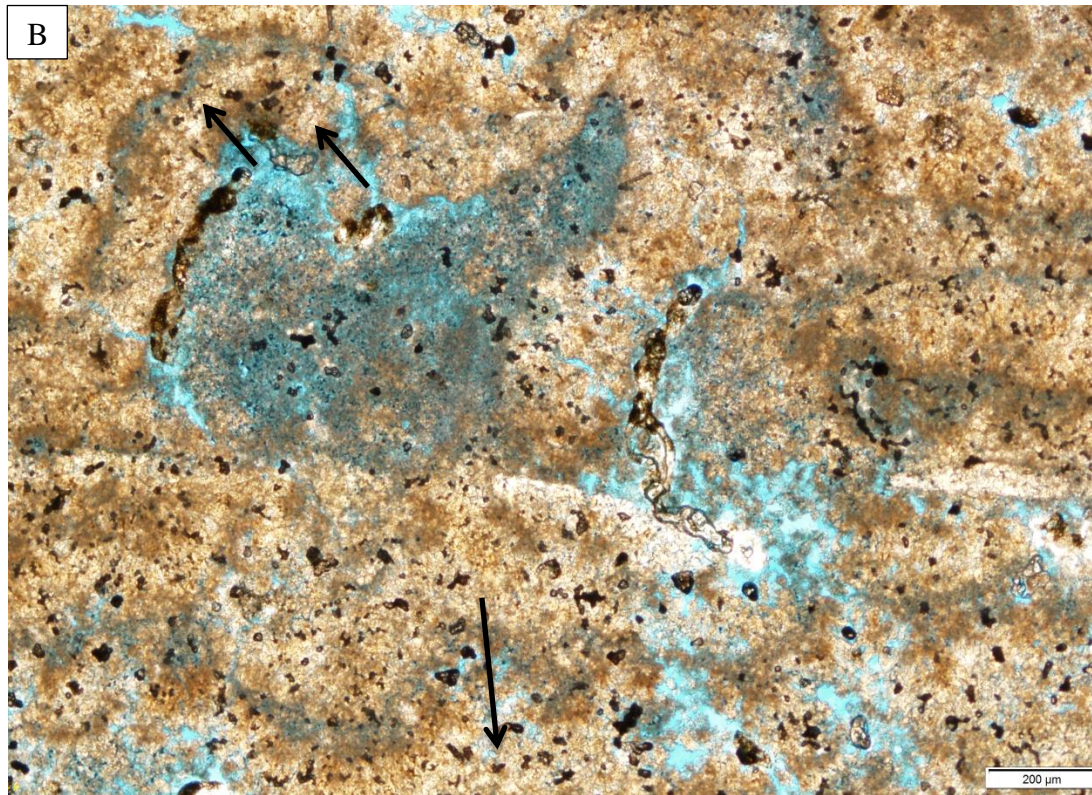
This facies is found all over the basin and the following observation is done on outcrops at locality 5.2 (figure 5.5(A)). This facies often has a sharp base with a more gradational transition zone at the top and is not always laterally extensive. It occurs in most of the upper part of the Pistarda formation. The facies is around 70 centimeters thick, but can be much smaller, around 30-40 centimeters. The consolidation varies greatly and can be rather poor. The color is grayish to yellow. The main characteristic of this facies is large plant stems, averaging around 5-7 cm in length. The majority of the plant stems are oriented perpendicular to the layer orientation. Most of them lie to one side, imbricated, or are vertical. The matrix between the plant stems ranges in



grain size between mud and very fine sand and comprises of micritic mud. Evidence of gastropods is only found in a few places. Figure 5.6(B) is a thin section of this facies where the crusts from the reeds are visible, marked with black arrows.







**Figure 5.6** – (A) Locality 7. Interpretation of these plant stems are reeds *in situ*. The length of the folding ruler is 20 cm. (B) Thin section from the same facies, and shows reeds crustation marked with black arrows. Thin section is interpreted to be wackestone due to the higher concentration of crust fragments that exceed 10%. The scale bar is 200  $\mu\text{m}$ .

### *Interpretation:*

The plant stems are interpreted to be a type of reed (e.g. *Phragmites australis*). Based on their arrangement within beds they are thought to be *in situ*. The patterns are created when dead reeds fall over to one side or stand subvertical if they have been densely packed and acts as a bafflestone, trapping sediments between the reeds. Based on this, the facies is interpreted as being in the shallow parts of a lake. Reeds can manage to grow in shallow water as well as on land close to the lake/shoreline. The same type of facies is also found in the Antalya Tufa (Glover and Robertson, 2003).

The reeds are completely coated with  $\text{CaCO}_3$ . This calcification is due to water supersaturated with calcium ions,  $\text{Ca}^{2+}$ . During photosynthesis the plants use  $\text{CO}_2$  which accelerates the reaction, and calcium carbonate is precipitated out of the water. Not only does the water need to be supersaturated, but the minerals need something to precipitate onto. The reeds provide a nucleation



surface. This only happens to the part of the reed that is submerged in water. That is why some of the outcrops have different lengths of reed stems. It could also be that some deposits consists of a different type of reeds or they are not fully grown. The thickness of the calcium crust gives an indication of how long the reed was exposed to the water. The thin section figure 5.6(B) has a high content of crusts ( $>10\%$ ) and is therefore classified as a wackstone.

Gastropods are only found in a few places in this facies, indicating that the gastropods do not thrive and reproduce in the same area as this type of reed does. Figure 5.7 is taken of reeds that grow in a submerged area by a small river in Psatha, not far from the Megara Basin. The area is relatively flat, and is perhaps only a few meters above sea level. Note the trees growing behind the reeds, indicating a lower watertable.

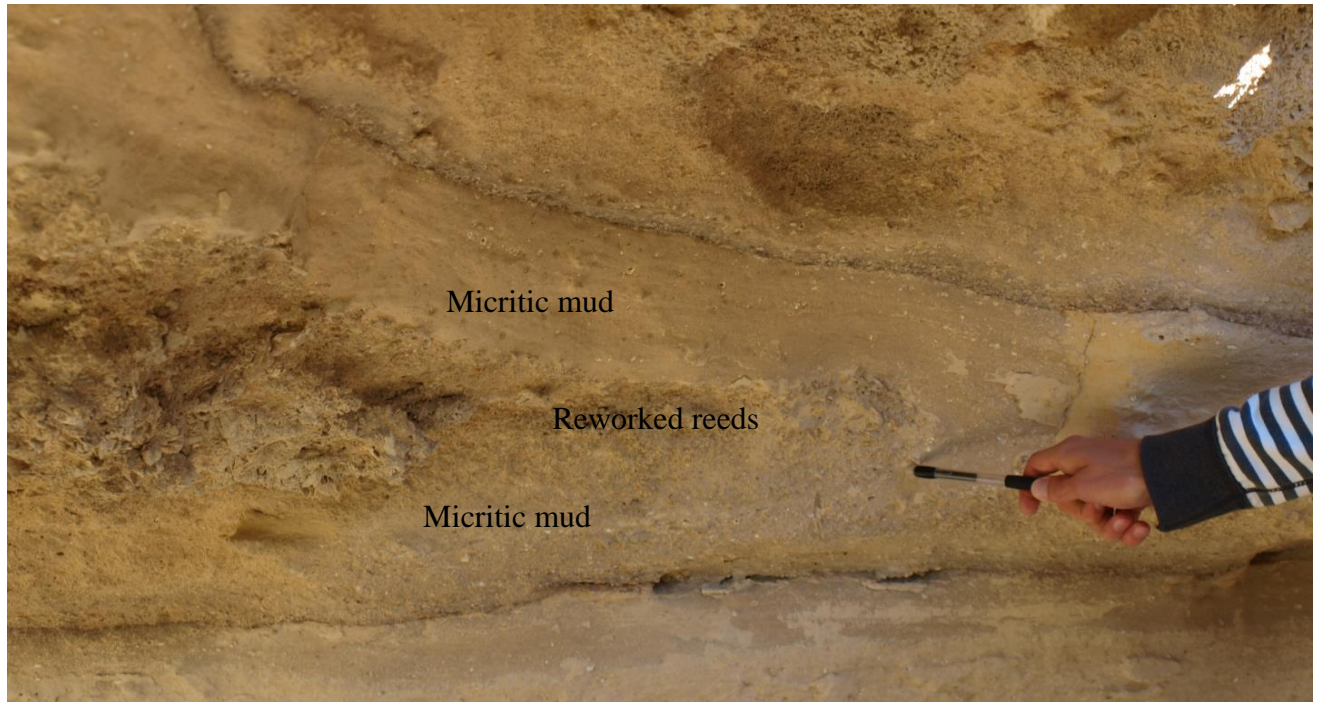


**Figure 5.7** – Living reeds *in situ*. Notice that the reeds are quite high. In the nearby area reeds dominate completely. The area is flat and submerged, with a river that comes down from the mountain in the background. The river settles before it meets the ocean, which is 50 meters to the left of this picture. Also note the vegetation growing in the background. Nissan Micra for scale.

### 5.3.4 Facies 3: Reworked Reeds by mass transport with soft sediment deformation

#### *Observations:*

At locality 5.2 in the lower unit there is different type of layer. This layer contains micritic mud with a core of reeds with chaotic texture (figure 5.8). The micritic mud seems to be a local feature. It has a sharp boundary both below and above the micritic mud. The layer is protruding out of the rest of the outcrop and is not laterally extensive. This means that it is thicker towards the outside of the outcrop, and its thickness decreases inward until the layer terminates. Where it terminates it has something that looks like a turning point where the layer is turning around, as seen in figure 5.8. Outside the view of figure 5.8 the layer continues around a corner, as seen in figure 5.9. The top is the reed layer with an undulating surface. The bottom is micritic mud.



**Figure 5.8** – Locality 5.2 lower unit. Kristoffer is pointing out where the turning point is. Pen as scale.



**Figure 5.9** – Locality 5.2 lower unit. This is around the corner from the slump above and the reeds in the top of this figure are from the slump. The dashed line is indicating where the reeds begin and the micritic mud ends. A soft sediment deformation is visible below the dashed line, where the heavier reeds layer is sinking into the micritic layer with lower density. The folding ruler is 60 cm.

### *Interpretation:*

The reed layer with the micritic layers are interpreted to be caused by mass transport (slumping). Slumps are deposited by down-slope movements of under-consolidated sediments, activated by gravitational forces working on a coherent mass (Mills, 1983). The movement is characterized by sliding along a concave-upward or planar surface. Typical slumps occur when a detached landmass moves along a planar surface. The turning point is formed by a rotational point due to a concave-upward slip surface with rotation about an axis parallel to the slope. The layer has no internal deformation and the reed stems are deposited in a chaotic pattern. The processes that can trigger slumping are overburdening by under-consolidated sediments in an oversteepened slope. Oversteepening can be due to a top depositional or tectonic response. Often a trigger is necessary to start the process of liquefaction. A typical trigger can be earthquake shocks, wetting, storms and other similar processes (Morgenstern, 1967 in (Mills, 1983)). The inclinations do not need to be high to be identified by slope deposits, as they have been recorded down to  $1^{\circ}$  (Shepard, 1955). Boggs (1995 p. 32) defined slumps as *"Shear failure among discrete shear planes with little internal deformation or rotation."*

Figure 5.9 is interpreted to be the base of the slumps which shows signs of soft sedimentation deformation of the undulating surface. This is where the reed layer has sunk into the micritic layer due to the lower density of the latter. Different mechanisms can create soft-sediment

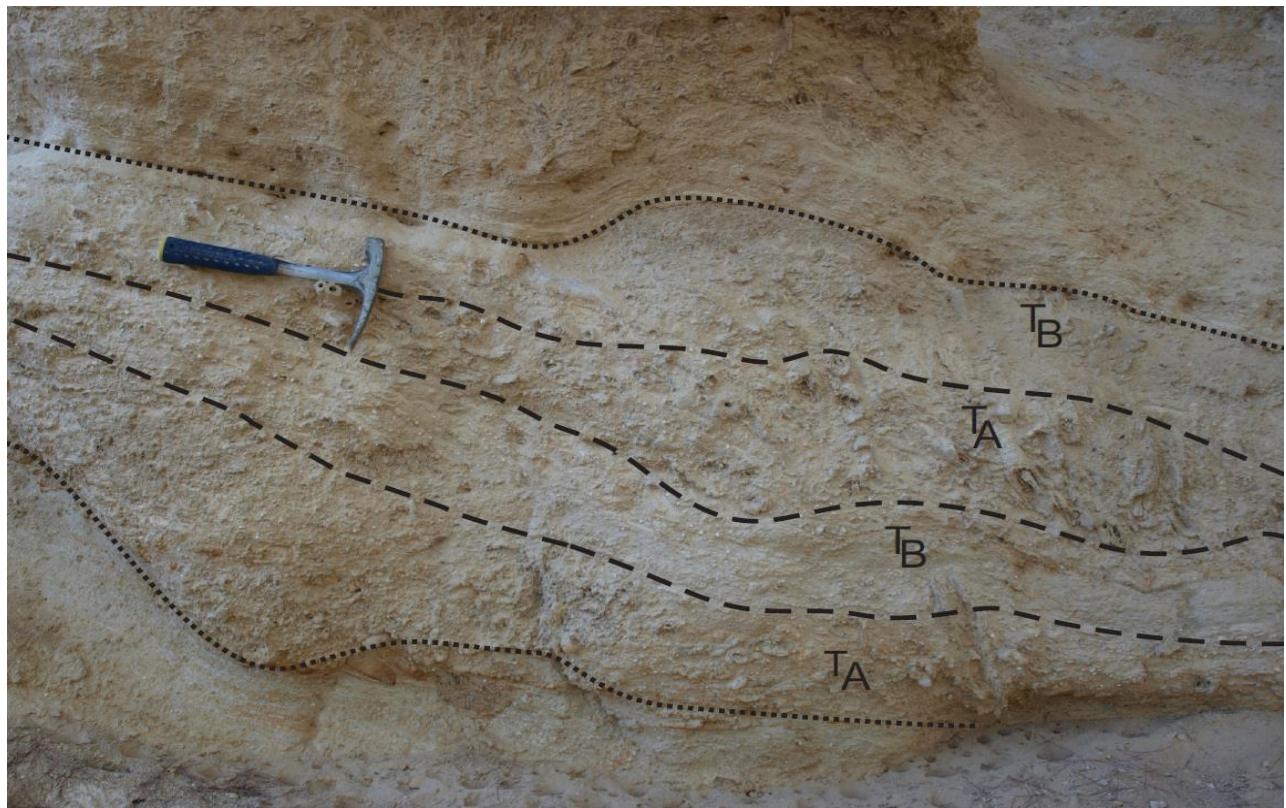


structures, such as (1) liquefaction or fluidization; (2) reverse density gradation; (3) slope failure or slumping and (4) shear stress (Blatt et al., 1980). This is thought to be a result of the slumping which also created the soft deformation.

### 5.3.5 Facies 4: Reworked Reeds Turbidity

#### *Observations:*

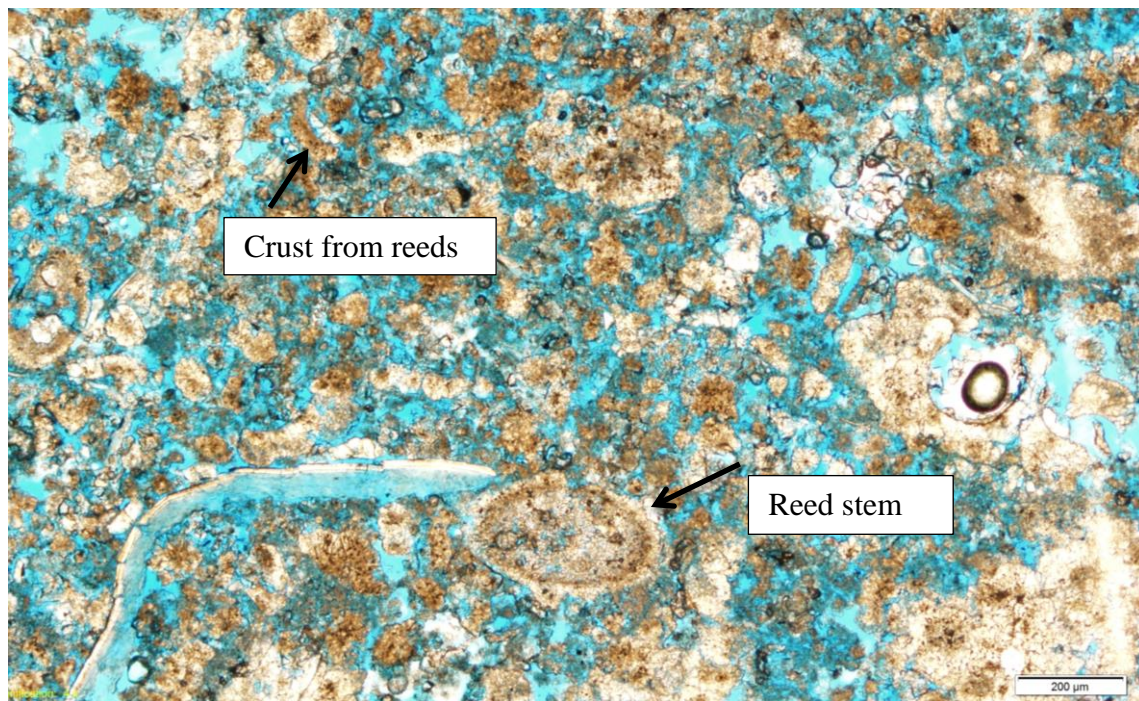
This facies is found in locality 4.1 in the upper unit (figure 5.10). It is around 1 meter thick and consists of reed stems and gastropods, observed in thin section (figure 5.11). The base is erosive and the top is sharp. Inside the layer it is possible to distinguish two packages that occur twice. The first starts at the base and is around 15 cm thick and contains chaotic reeds. It gradually grades into a more laminated texture containing fewer reeds. It appears to have a fining upward trend for these two packages,  $T_A$  and  $T_B$ . Above this the same happens again and the next package is almost the same size as the first. The layer has an indication of redeposition because of the chaotic pattern.



**Figure 5.10** – Locality 4.1. The dotted lines mark the top and base of the turbidity current where  $T_A$  and  $T_B$  are visible. The dashed lines indicate the base and the top of the layer. Hammer for scale.

*Interpretation:*

The sediments are interpreted to be deposited by mass-transportation (turbidities), which is indicated by the erosive base. The massive and graded layer correlates with layer A; whereas the planar laminated layer can be correlated with layer B in relation to the well-established Bouma sequence (Bouma et al., 1962). The source of these sediments is from slumping in the marginal zone and then develops into turbidity current. As mentioned, a shock is often needed to start the events that trigger the overburdening of sediments. See Lowe (1982) and Kneller and Buckee (2000) for reviews of turbidity currents. The thin section is interpreted to be a wackestone with crusts from reeds and reeds stems visible in a micritic mud (figure 5.11).



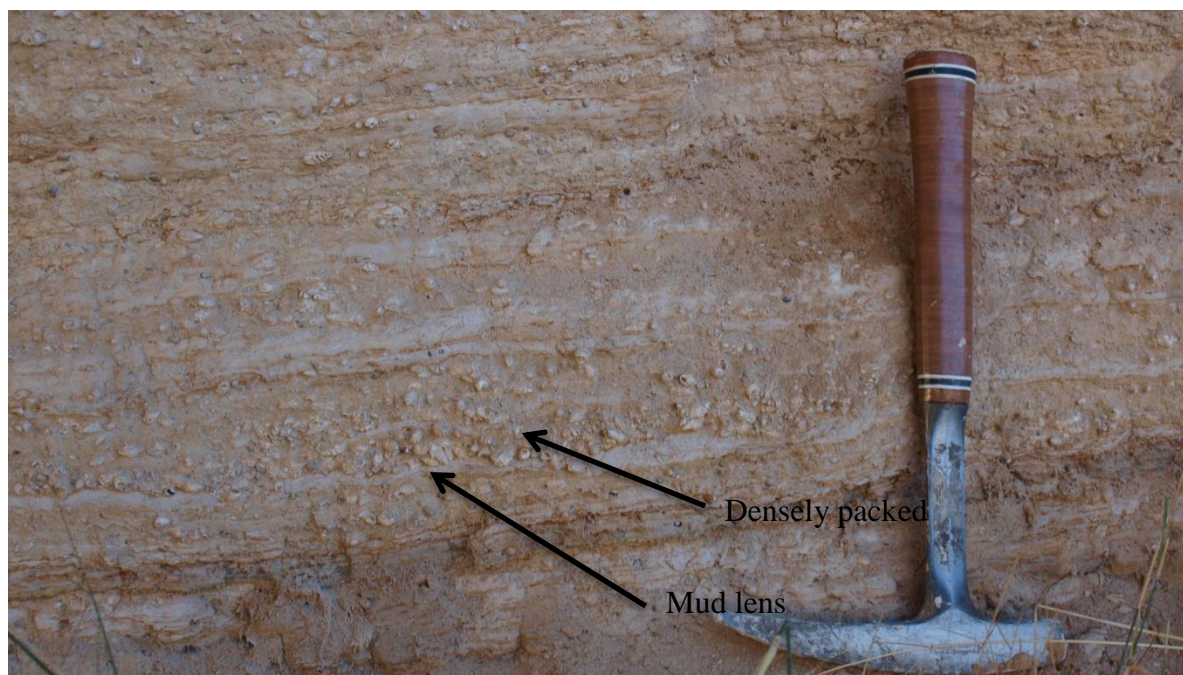
**Figure 5.11** – Thin section from the same place as figure 4.10. A much higher porosity around the grains is interpreted as being from reworked material. Plant stems and crustification is seen, black arrows. The scale bar is 200 µm.

### 5.3.6 Facies 5: Wave reworked gastropods

*Observations:*

These observations are made only in locality 10 (figure 5.12). The layer is composed of micritic mud and whole gastropods (figure 5.13). The boundary is sharp both above and below. The layer is laterally extensive, where the gastropods follow a planer line. Apparently, gastropods are deposited together as separate layers, with thin layer of mud lens.

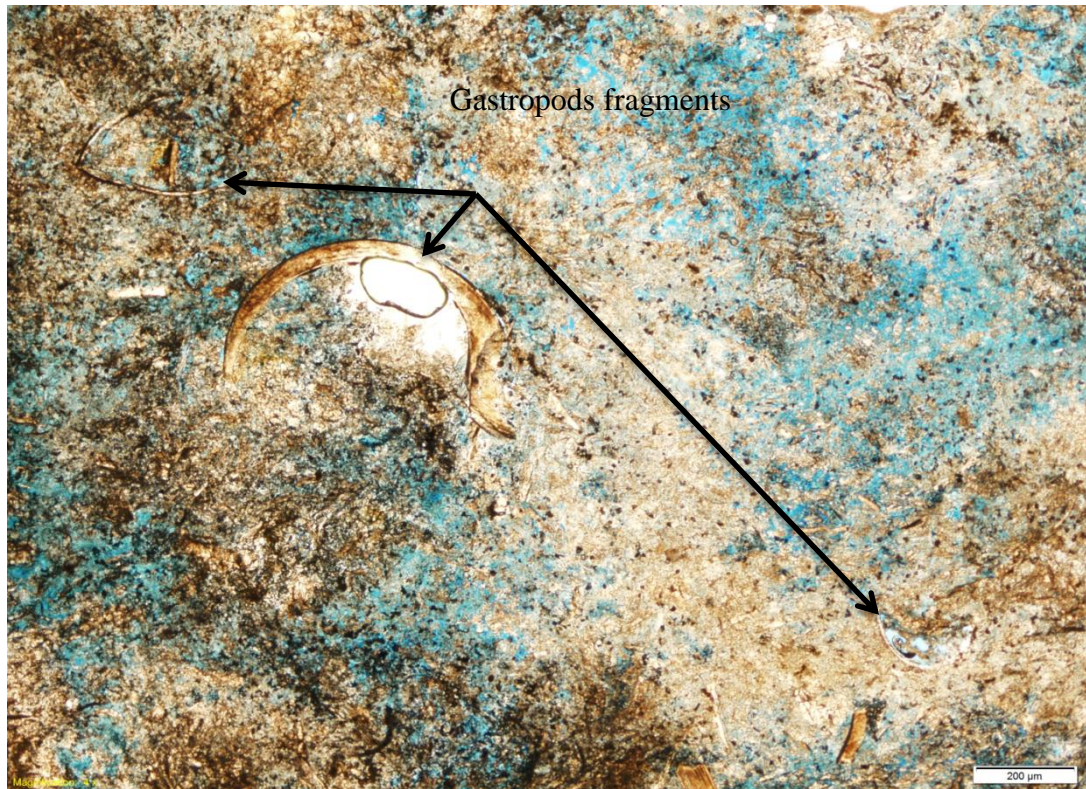




**Figure 5.12** – Locality 10. Gastropods reworked by energy from waves. Hammer for scale.

*Interpretation:*

This is interpreted to be reworked gastropods because they are densely packed, showing evidence of reworking. This is interpreted to be wave action with low to medium energy above the wave base. The mud lens is interpreted to be formed during calmer water by hemipelagic/pelagic mud settling out from the water column.



**Figure 5.13** – Micritic mud with fragments of gastropods. Because it has less than 10% grains it is interpreted to be a mudstone. The scale is 200  $\mu\text{m}$ .

### 5.3.7 Facies 6: Storm reworked gastropods - Coquina

#### *Observations:*

This facies is found in localities 9 and 5.2. The facies is composed of a thin blanket of gastropods that can have more broken material than facies 5 (figure 5.14). The layer is no more than a few centimeters thick, but is laterally persistent. Such layers can often be found as layers within massive micritic layers. The coquina in location 5.2 has a clear erosive boundary, which is not as clear in locality 9.





**Figure 5.14** – Locality 9. Thinly bedded shell deposits that are interpreted as coquina, formed by storms. Hammer for scale.

*Interpretation:*

This bed is interpreted as coquina, a thin shell bed layer defined as “clastic or detrital limestone that contains a high proportion of coarse shell debris cemented by calcium carbonate” (Allaby and Allaby, 2008). This is interpreted to be a medium to high energy environment, above the storm wave base. The wave erodes the lake bottom and settles the gastropods together in a thin layer on the scour surface. Similar beds are found in Lake Tanganyika (Cohen and Thouin, 1987). This kind of bed was found at depths of between 15 to 70 m, extending up to 40 km long and 4 km wide. The layers occur on flat or gently dipping platforms. Cohen and Thouin (1987) suggest that the layer is formed by a combination of mud-winnowing due to changes in lake level, or current activity with subsequent biological reworking. Coquina is often found in shallow-marine water throughout the Phanerozoic and is interpreted to be a product from episodic storms. Storms rework sediments that are rich in fossils. This normally happens below fairweather wave base (Eyles and Lagoë, 1989 and referenc therein). A fall in sea/lake level can also give rise to in situ bottom-dwelling communities (Müller and Milliman, 1973; Kidwell, 1986). The degradation of organic matter in their shells can produce gas in their coil, which also has another effect. De Deckker (1988) found that when they float they can accumulate in huge numbers upon the lake shores and form beds that are similar to coquina. Since they are found in



the lower unit at locality 5.1 and in locality 9 they are interpreted to be formed over the storm base because the other facies around the coquina layer are interpreted to be formed under relatively deep water.

### **5.3.8 Facies 7: Hemipelagic/Pelagic micrite**

#### *Observations:*

This is the most common facies and it occurs in every locality. It has very fine grained material and is massive. It occurs either as loosely packed material (figure 5.16) or as a hard distinctive layer which is protruding (figure 5.16). Gastropods are common within the unconsolidated layers, but are found without them as well. The hard layers are regularly found with only the imprint of gastropods, lacking any visible remains. They are typically only a few centimeters. A very distinctive feature is that these layers are very solid and not easily broken by a hammer. Figure 5.17 shows a typical thin section from the facies, with abundant micrite with or without gastropods.

#### *Interpretation:*

The loosely packed layers and the hard layers are both interpreted to be from hemipelagic or pelagic marl which has settled out of the water column. To get this type of sediment it is necessary that to have phytoplankton or similar substrates where the crustal formation can commence (Galat and Jacobsen, 1985; Stabel, 1986). This also applies to lakes where the water is supersaturated with all the common carbonate minerals. When the process begins the concentration can quickly get so high that the water becomes cloudy, known as *whitings* (Robbins and Blackwelder, 1992).

The gastropods are interpreted to be living in the environment this facies is deposited in. For facies 3 and 4 it is interpreted that they incorporated the gastropods during the mass transport and carried them further out into the lake. There is also another process that causes the gastropods to spread around in the formation. When gastropods die they tend to float, as their decaying body tissue creates gas inside the upper coils of the shell (Boyer, 1982). Because of this they can be

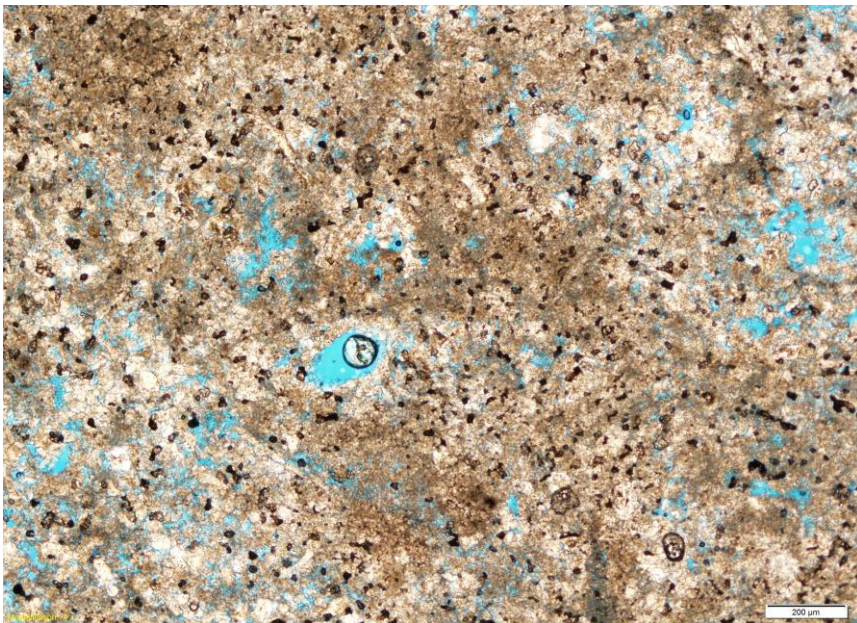
transported to deeper water, sinking to the bottom when the gas escapes and can be spread all over the lake.



**Figure 5.15-** Locality 9, hard protruding layers.



**Figure 5.16 -** Locality 7, soft micritic mud.



**Figure 5.17 –** Thin section taken from the location in figure 5.16. It shows abundant micritic mud. It is seen in other thin sections from this facies with ostracodes. The black material is microbial shub and will be interpreted under chapter 6.5. The round bubble is an artifact from the process of making the thin section. The scale bar is 200  $\mu\text{m}$ .

The hard protruding layers are interpreted to be the result of as diagenetic processes where the dissolution of gastropods is cementing the layer. This makes them more lithified than the layers below and above. The hard layers have a higher content of gastropods than the softer layers. One can assume that the softer layers do not have enough gastropods in them to make the diagenetic process occur.

### Laminated limestone

#### *Observations:*

Localities 5.1 and 4.1 are the only places in the basin where plane parallel lamination is found (figure 5.18). At locality 5.1 the facies is 14 cm thick and at 4.1 it is around 3 meters thick. The layering in the outcrop is horizontal, with gastropods at 5.1, but not at 4.1. At locality 4.1 tiny fragments of plant clasts are observed. In both places the lamination are easily recognized in the field. In the SEM picture from locality 4.1, small rectangular pellets are seen (figure 5.19).



**Figure 5.18** – Locality 5.1. The base has reeds *in situ*, followed by micrite and reworked gastropods. The reeds layer marks a flooding event. Pencil as scale.

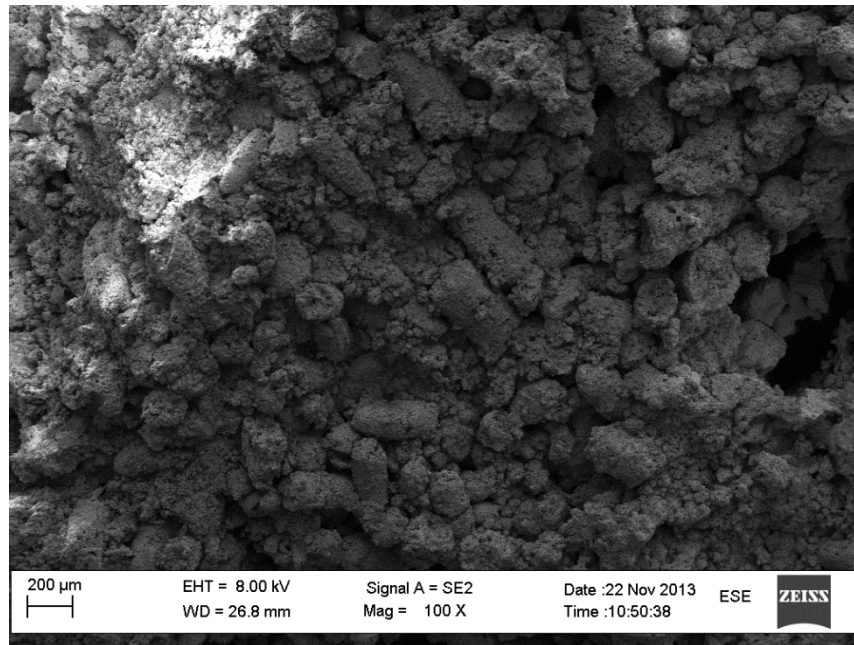


Figure 5.19 – SEM picture of the laminated layer in figure 5.18. The scale is 200  $\mu\text{m}$  and magnification is 100X.

### *Interpretation:*

Lamination can occur in three situations: low activity of bioturbation, anoxic water or high sedimentation where the sediment was buried before bioturbation could occur (Reading, 2009). Because no observation indicates that the lake was anoxic, a high sedimentation rate is the best suggestion. There is no good explanation for the reeds at locality 4.1, but most probably it is reworked material. For locality 5.1 the gastropods are thought to be driven by the formation of gas in their coil which escapes, making them settle out from the water column. From the same locality a SEM picture was taken of the laminated facies (figure 5.19). The rectangular clasts are interpreted to be either some kind of fecal pellets that are similar in shape, or it can be cyanobacteria, like *Rivularia sp.* or *Cladophorites sp.* (Tucker and Wright, 1990).

Cyanobacteria and other aquatic macrophytes have the ability to metabolize  $\text{HCO}_3^-$ , which in alkaline waters is present in relatively much greater concentrations than  $\text{CO}_2$ . This can give them an advantage over species that are unable to utilize  $\text{HCO}_3^-$ . Therefore, it is most likely that the laminated layers are of some kind of cyanobacteria settling in quiet water and building up layers during seasonal sedimentation, also called varve. Therefore, it is interpreted that the gastropods were not living there, because they could have destroyed the lamination.



### 5.4 Facies association of the Pistarda formation

Facies association is done in order to distinguish the observed facies from depositional environments. Each facies association represents a particular sedimentary environment, table 5.3.

Table 5.3 – Facies association and their characteristics

<b>Facies association</b>	<b>Lithofacies</b>	<b>Interpretation</b>
<b>FA1 Costal wetland - swamp</b>	F1	Forming of organic matter on land
<b>FA2 Costal wetland - marsh</b>	F2	Shoreline - water level $\pm$ 1 meter
<b>FA3 Subaquatic mass transport</b>	F3, F4, F5, F6	Reworked material
<b>FA4 Hemipelagic/pelagic environment</b>	F7	Hemipelagic/pelagic sedimentation

#### 5.4.1 FA1 – Costal wetland, Swamp

##### *Observations:*

The facies association is solely composed of lithofacies F1, and is found a few places on some localities. FA1 is typically found in the middle of the outcrop, but also at the base. The thickness is rarely more than 10 cm, with no fossils or other bio-fragments. This indicates a stable environment with an accumulation of organic matter over time. At locality 5.2 it is only found in the upper unit where a paleosol layer is found as well.

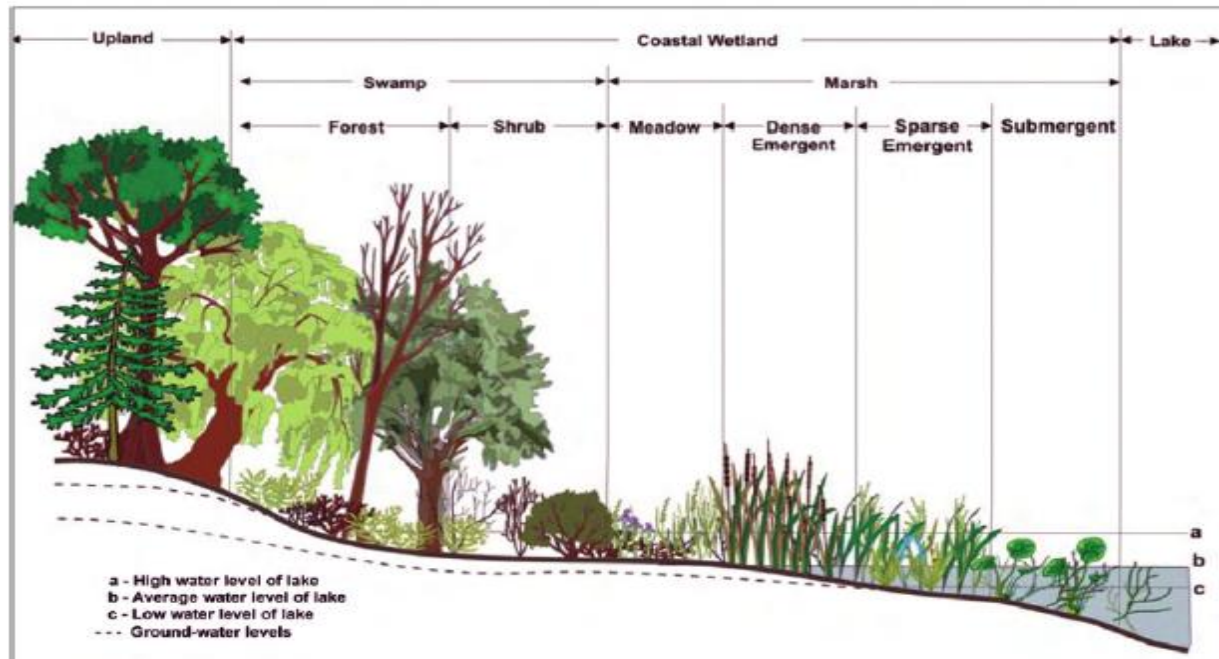


Figure 5.20 – Figure showing the difference in the coastal wetland between swamp and marsh. Where marsh is flooded and swamp is not flooded, but with a high water table. Figure from Wilcox et al. (2007).

#### *Interpretation:*

This facies association is interpreted to be terrestrial deposit in swamp where decomposition of organic matter is lower than the accumulation rate because no evidence of plant remains is found. This environment is close to the lake shore, and a high water table could maintain an anoxic condition preventing the decomposition of organic matter. The paleosol indicates that this is on land since it cannot be formed in water, therefore it is a swamp (figure 5.20). This facies association occurs only with FA2 and FA4, indicating a normal fluctuation between shallow waters up to swamp.

#### **5.4.2 FA2 – Costal wetland, Marsh**

##### *Observations:*

This facies association consists of facies 2(Reeds *in situ*) and is widespread in the formation, occurring in most of the localities. It is mostly found in combination with FA4, where they alternate.

##### *Interpretation*

Reed grows 1 meter below- and above the water table. It is interpreted that the Pistarda formation had dense communities of reeds growing at the shoreline. Very few gastropods are found in this facies association and they are therefore unlikely to have lived in these areas. Since little other animal and plant remains are found in the deposit and only the calcification around the reeds remains, this indicates water rich in oxygen. As mentioned, the reed facies association occurs with FA1, FA3 and FA4, which are interpreted to mean that the reed facies is between the swamp and lake environment.

### **5.4.3 FA3 – Subaqueous lake center**

#### *Observations*

This facies association consists of facies F3, F4, F5 and F6, which denote reworked material. F5 and F6 are reworked material consisting only of gastropods, indicative of a calmer environment than F3 and F4. The latter are found in some localities, especially the lower unit at locality 5.2. In this facies association F3 and F4 are the most dominant processes and the reworking of gastropods are of less importance to the environment and to the Pistarda formation.

#### *Interpretation*

This type of deposition environment is interpreted to be from reworked material deposited into the deeper part of the lake. Facies 3 and 4 are interpreted to be mass transport sedimentation which may have started in the coastal area and was transporting materials out into the deeper parts of the basin. The reeds found in these facies are interpreted as having been deposited in FA2 first. Facies 5 and 6 are interpreted to be deposited from wave agitation in the lake, thus depositing materials in a more shallow area. The gastropods in facies 3 and 4 also have a reworked pattern, indicating that the facies picked up the gastropods when passing through an area where the gastropods lived. This is also the reason why the gastropods are not always present. This facies association occurs very sporadically, but is often found with FA2 or FA4.

#### **5.4.4 FA4 – Background sedimentation**

##### *Observations:*

Facies association 4 consists only of facies 7, which is one of the most common facies in the formation as it is found in every outcrop. The facies association denotes a calm environment where accumulation of sediments happened relatively fast, without interference from other processes.

##### *Interpretation*

High production of carbonate minerals in calm waters results in hemipelagic/pelagic settling. This is interpreted to have happened all over the lake, especially in areas with high levels of photosynthesis, the major factor in CO<sub>2</sub> removal. This type of sediment makes a soft layer of micritic mud. As mentioned, the gastropods are thought to have been living in this sediment, eating for example cyanobacteria or other microorganisms at the bottom. Facies association 4 is often found in combination with FA2 and FA3, occurring only in the water, as expected.

#### **5.5 Sedimentary structures above and below the Pistarda formation.**

To understand the development of the Pistarda formation it is necessary to identify what lies beneath and above the formation. All localities were examined to find out where the transition is, though many of the localities were impossible to investigate in detail due to very steep slopes or that no sediments were found. The Pistarda formation is often found as the top layer of cliffs where a dirt road goes. The inward side of the road is regularly composed of debris material and good exposure is hardly ever found. In the following sections this will be explained, beginning with what is found below and then what is found above. Since this is of minor importance they are not categorized into facies associations. However, the transition zone may be very important to understand the formation of the Pistarda.



### 5.5.1 Below the Pistarda formation

#### Toumpaniari formation, flood plain

##### *Observations:*

Below the Pistarda formation in locality 1 (figure 5.21), the typical plant stems in the marl disappear and is replaced by layers of mud and very fine sand with gastropods. The mud and very fine sand layers are alternating back and forth throughout the visible part of the outcrop.



**Figure 5.21** - Above the dashed line is the Pistarda formation, while below is the Toumpaniari formation. The Toumpaniari formation is interpreted to be a fluvial environment, which most likely had shallow, multi-channel stream depositions. Hammer for scale (marked by the red box).

##### *Interpretation:*

The observation is interpreted to be a floodplain environment, where these very fine grained layers most likely originated from a large fluvial system consisting of multi-channel streams. Bentham et al. (1991) found this kind of sediment in both the Louba formation of the Alepochori group and the Toumpaniari formation in the Tombes Koukies group. Since this is found below the Pistarda formation it is interpreted to be the Toumpaniari formation that is visible here.

**Kremida formation, pebbly sandstone***Observations:*

Around 7 meters below the lower unit of locality 4.1, a layer of possible sandstone is visible. This layer is poorly exposed before a clearer second layer of pebbly sandstone with red chert is exposed.

*Interpretation:*

The sandstone layer is possibly the Toumpaniari formation overlying a thicker sequence of the Kremida formation. The latter is one of the few formations with the red chert in it.

**Toumpaniari formation, lateral accretion packages (LAP)***Observations:*

The layers below the Pistarda formation at locality 5.2 start with a coarse sand packages (>1 meter thick) and pebbly sandstone at the base, where the layers inside the bed have S-shaped curves. At locality 7 similar sediments were found, but it was impossible to get close enough to verify this.

*Interpretation:*

It is interpreted to be of some kind of fluvial deposit. Bentham et al. (1991) interpreted this as lateral accretion packages based on the sigmoidal form of the deposits, making it a part of the Toumpaniari formation. This type of sediment is interpreted to be from a shallow river with many channel stream deposits, where sand and gravel is transported in longitudinal bars and in curved-crested dunes, building up of a hierarchy of channels.

### 5.5.2 Above the Pistarda formation

#### **Harbour Ridges formation, conglomerate**

##### *Observations:*

At locality 4.2 an outcrop is visible, situated on the other side of the road that lies on top of the Pistarda. The outcrop is in bad shape and looks like a landslide debris field; however it gives a good indication of what lies above the Pistarda formation. The outcrop consists of conglomerate with clasts size ranging from 0,4 cm to 1,2 cm, with a typical average of 0,5 cm. The conglomerate consists of clasts supported with medium sand as matrix.

##### *Interpretation:*

Bentham et al. (1991) recognized this as the Harbour Ridges formation, which consists of conglomerate and pebbly sandstone. This is also expected since it stratigraphically overlying the Pistarda formation.

#### **Harbour Ridges formation, pebbly sandstone**

##### *Observations:*

This observation is done at an outcrop not far from locality 5.1. It lies a few meters above the main outcrop with the Pistarda formation. The outcrop is in poor condition and is covered by a lot of debris from small landslides down the steep cliff. It consists of fine to medium sand as matrix and clasts ranging from 1 to 3 mm.

##### *Interpretation:*

The poor state of the outcrop makes interpretation difficult. The red/brown chert on the ground indicated that the overlying formation is the Louba formation. Therefore this outcrop should also be from the Harbour Ridges formation, before going into the Louba formation.

**Harbour Ridges with *Cardium sp.****Observations:*

This outcrop is above locality 10 on the other side of the gorge, where it is possible to follow the Pistarda formation going up to the formation above. In figure 4.22, we can see that the Pistarda formation stops below the person and the next formation is seen above. It consists of fine sand without fossils, stratigraphically overlain by medium sand with abundant fossils of gastropods and bivalves. The transition zone between the two formations is unclear.



**Figure 4.22** - The outcrop below the person is the top of the Pistarda formation. The picture is taken from the main outcrop, locality 10 across the gorge. Person for scale.

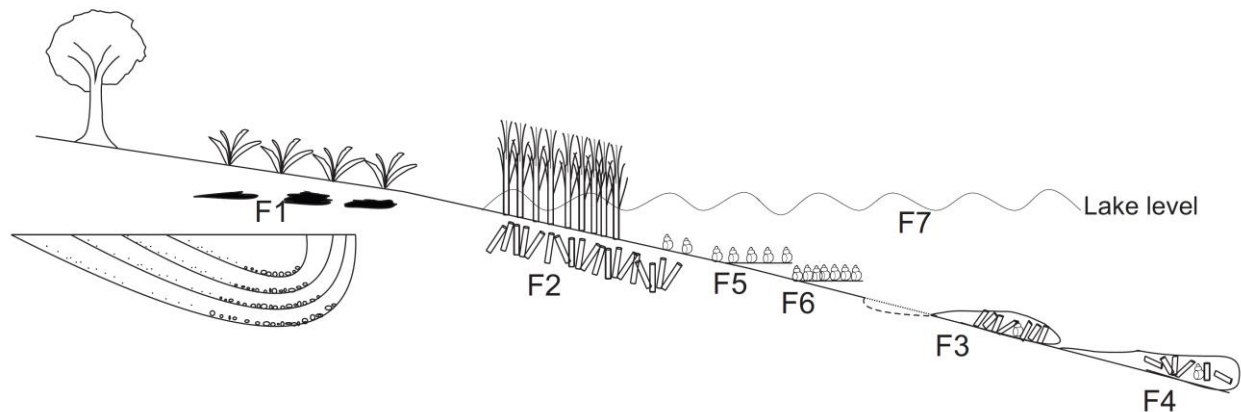
*Interpretation:*

The bivalve found in the sediments is interpreted to be a type of cockle with the scientific name *Cardium sp.* This is a marine bivalve and is very common in shallow marine environments. Bentham et al. (1991) found one marine horizon with *Cardium sp.* in the Tombes Koukies group in the Harbour Ridges formation, which is overlying the Pistarda formation.



## 5.6 Depositional model for the Pistarda formation

To summarize how the facies are distributed, a simple sketch is made, see figure 4.23. Below the trees an old fluvial system is drawn in, symbolizing the underlying formation. Facies 1 is organic matter that is buried below in a swamp zone. Facies 2 is illustrated where the reeds grow. Next to it are facies 5 and 6. Facies 5 is gastropods reworked by waves and facies 6 is interpreted to be formed by storms because of their erosive base. Facies 3 and facies 4 are formed by an overburdening of sediments that are moving from a density current to a slump and to turbidity with increasingly higher turbulence in the sediment. This is the reason why the turbidity shows evidence of a fining upwards pattern and why the reeds are dropping out before the micrite settles. Facies 7 appears all over the lake and is interpreted to be from the extraction of CO<sub>2</sub> by phytoplankton and plants (reeds) by photosynthesis, forcing the supersaturated water to precipitate carbonate, CaCO<sub>3</sub>.



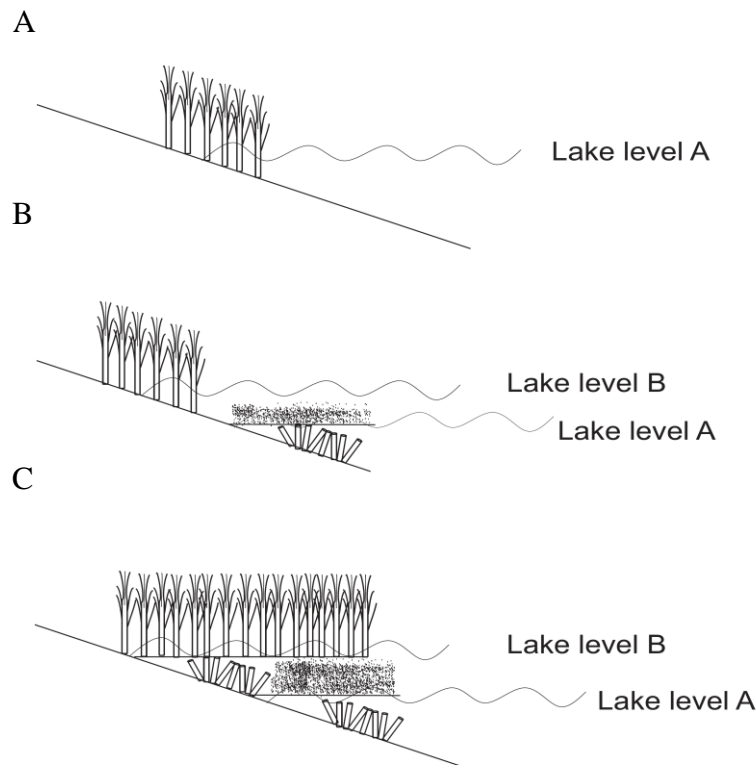
**Figure 5.23-** Illustration of how the different facies are distributed in the lake. F1= Organic matter; F2 = Reeds *in situ*; F3 = Density current, slumping; F4 = Turbidity current; F5 = Reworked gastropods; F6 = Whole/Broken gastropods in a coquina layer; F7 = Hemipelagic/pelagic mud induced by the extraction of CO<sub>2</sub> from the water by photosynthesis. The river channel on the left illustrates the formation below.

Based on this simple model the facies stacking pattern and key surface can be recognized. A complete log would start with a fluvial system at the base, depositing the deepest facies 4 and 3. After that facies 6 and 5 would be expected, but they are not so common. Facies 2 will give rise to large reed beds and at the top organic matter will be deposited above the lake level. Facies 7 is

found between every layer, independently of lake depth and gradient. Above the Pistarda formation a new sequence of fluvial deposits will occur.

The correlation transect illustrates how the facies is distributed in the logs. The information interpreted from the logs is that considerable amounts of landward facies are found, in which facies 7 and facies 2 are by far the most common, indicating a shallow lacustrine environment. The lower unit of locality 5.2 is the only place where major components from reworked materials are found. This indicates that the lower unit was formed in deeper water. At localities 4.1, 8, 9 and 10 some reworked material is also found.

Locality 1 consists of facies 2 and 7, alternating. This happens from the top to the base, where the last two layers are from the Toumpaniari formation. This is interpreted to be formed by a fluctuation in the shoreline, where the hemipelagic/pelagic mud represents a flooding surface over the old crustation from the reeds. This is illustrated in figure 4.24.



**Figure 4.24** – (A) Reeds are thriving in the shoreline and are deposited. (B) An increasing lake level forces the reeds to move higher up, and the old crust from the reeds is flooded and is covered by micritic mud which settles out of the water column. (C) Then with a stable shoreline the reeds will grow over the micritic mud.

Reeds grow in the shoreline zone where calcified crusts are deposited. When the lake level rises, micritic mud will be deposited upon the old reeds stems. This will build up to the water level and then the reeds can grow over again. This is believed to be how the fluctuation in water level gives rise to the change between facies 2 and facies 7 and gives rise to a depositional cycle.

A correlation panel (Appendix III) is created by using the logs made from the field work (Appendix II). This is made for illustration purposes to show how the thickness variation changes across the logs. All facies are colored based on their facies association. The facies association has tried to be correlated, but there is a great uncertainty about the true top and base of some of the logs. As well as almost none key surfaces are found in the logs to base the correlation on.

## 6. Geochemical studies

### 6.1 Introduction

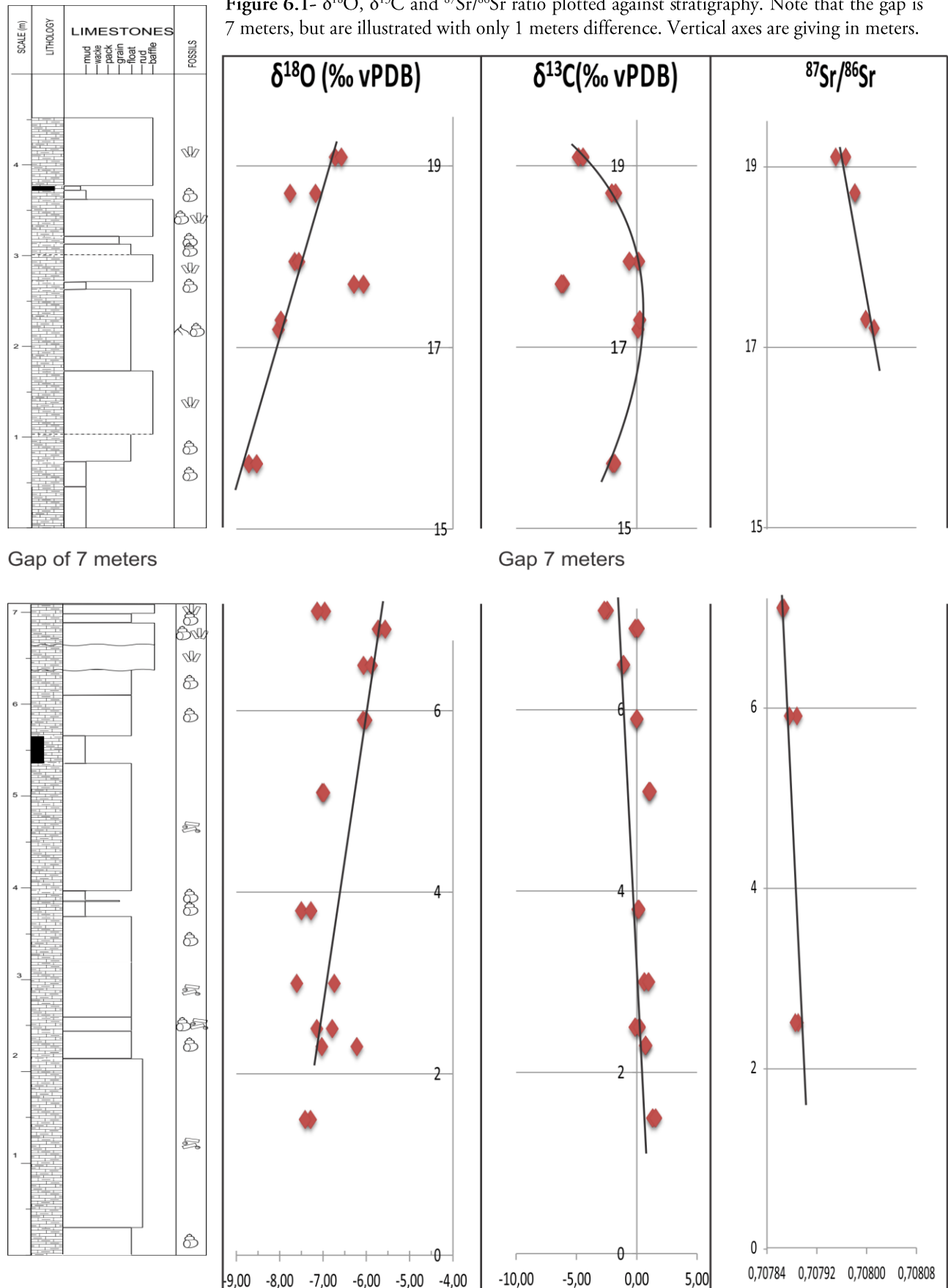
To better understand the Pistarda formation, a geochemical analysis was conducted. The purpose was to better understand how the Pistarda formation was formed. It is particularly interesting to see if there are any differences between the two units in the formation. Strontium isotopes are used to see any changes in drainage area. Lakes are prone to changes in water level which in turn changes the water chemistry. Stratigraphic variations in the lithofacies are therefore also expected to be recorded in the chemical signatures.  $\delta^{18}\text{O}$  and  $\delta^{13}\text{C}$  are used as indicators of climate, and to see if biological production was higher or lower through the stratigraphy and in the two units. A complete list of all the geochemistry analysis can be found in appendix I.

### 6.2 $\delta^{18}\text{O}$ , $\delta^{13}\text{C}$ and $^{87}\text{Sr}/^{86}\text{Sr}$ against the stratigraphy of locality 5.2 upper and lower unit

The values of  $\delta^{18}\text{O}$ ,  $\delta^{13}\text{C}$  and the  $^{87}\text{Sr}/^{86}\text{Sr}$  ratio are plotted against the stratigraphy to see how it changes from the base to the top. Figure 6.1 shows both the lower and upper units from locality 5.2. The difference between the units is 7 meters, but it has been plotted with only a 1 meter difference for illustration purposes.



**Figure 6.1-**  $\delta^{18}\text{O}$ ,  $\delta^{13}\text{C}$  and  $^{87}\text{Sr}/^{86}\text{Sr}$  ratio plotted against stratigraphy. Note that the gap is 7 meters, but are illustrated with only 1 meters difference. Vertical axes are giving in meters.



**Lower unit**

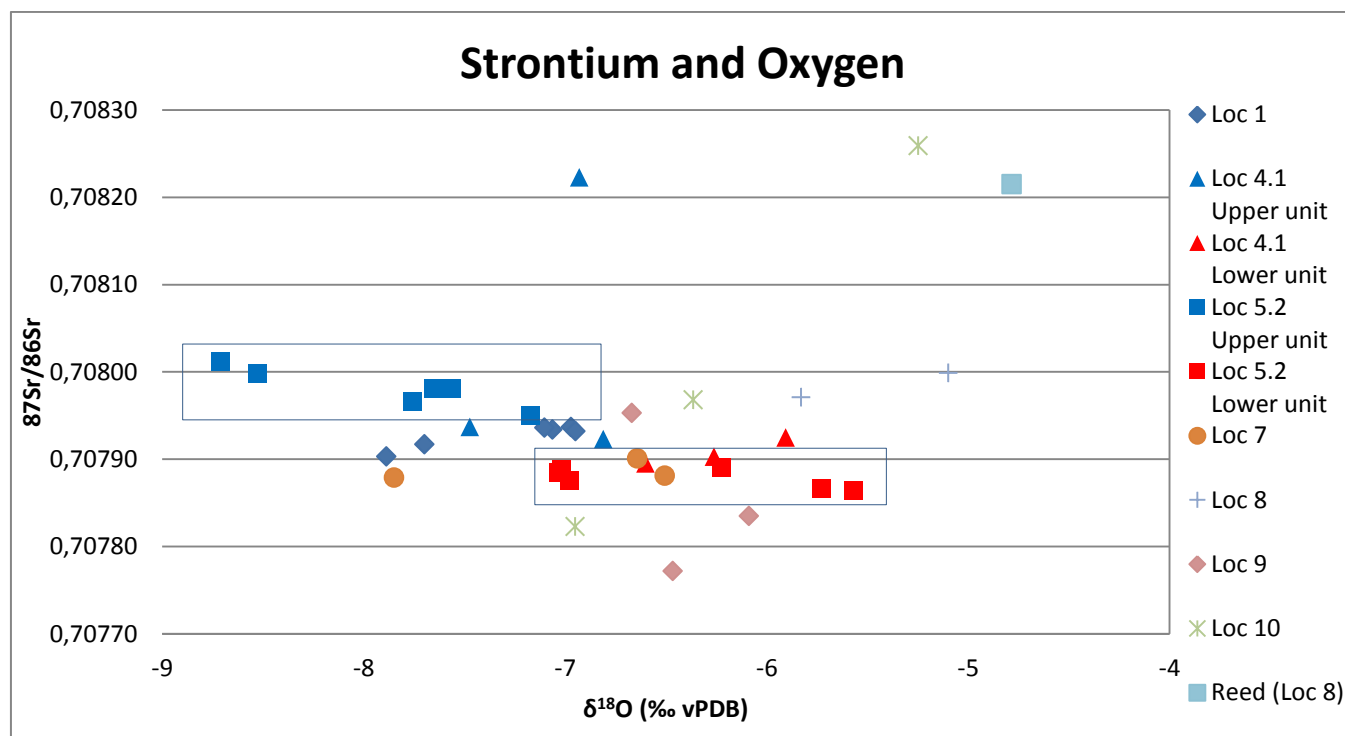
$\delta^{18}\text{O}$  has an increasing trend upward from -7 to -5, indicating an enrichment through the stratigraphy.  $\delta^{13}\text{C}$  is positive for the lower part and is decreasing upwards, from +2 down to zero. It has an almost straight trend, but in comparison with the upper unit, it has a more positive value. The  $^{87}\text{Sr}/^{86}\text{Sr}$  ratio has a decreasing trend downwards from 0,70789 to 0,707865. An important point is that this value is much lower compared to the upper unit, and therefore it must have had a different drainage area than the upper unit.

**Upper unit**

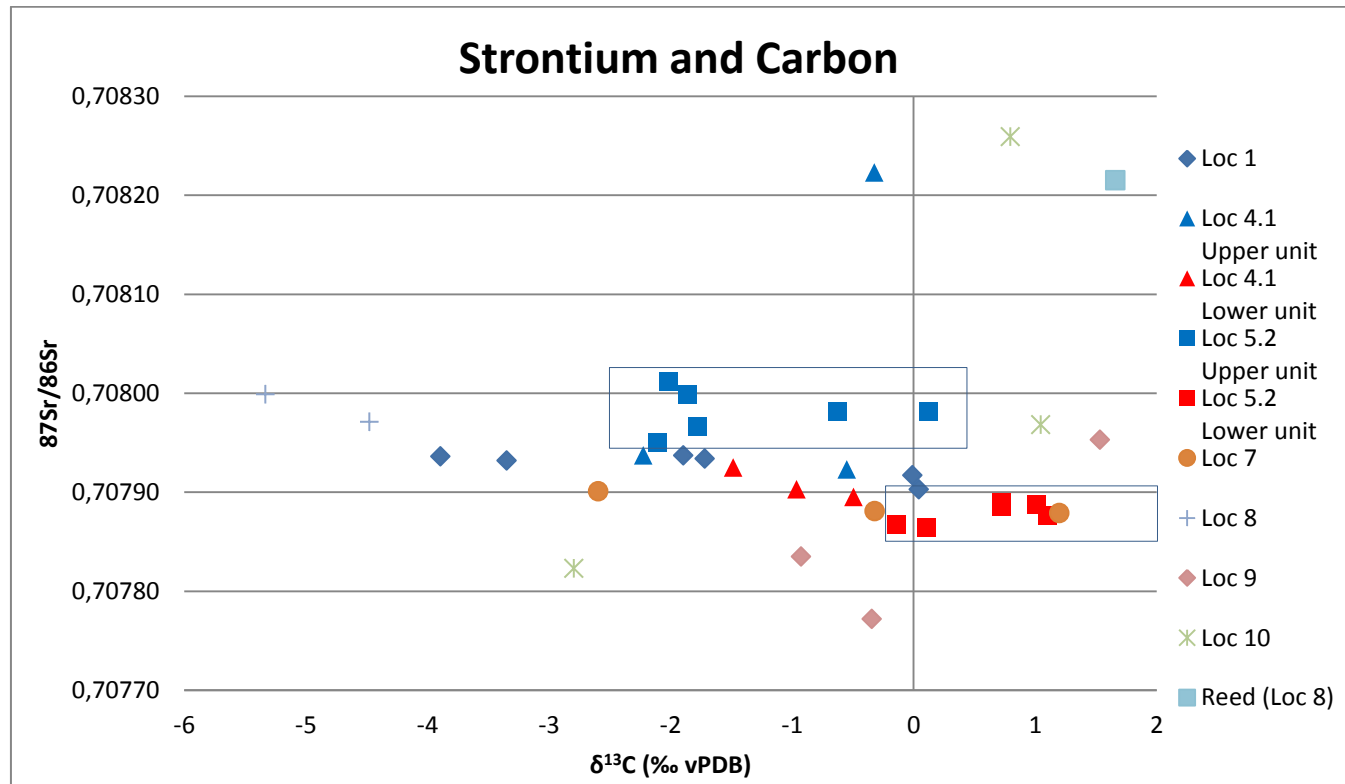
$\delta^{18}\text{O}$  has a more positive trend from the base and up to the top, showing a trend of increasingly more positive values. This indicates enrichment in heavier isotopes.  $\delta^{13}\text{C}$  starts from a value of -2 at the base with a more positive trend, showing an enrichment in heavier isotopes, before returning to a more negative trend around -4. This indicates a shifting in the lake. The strontium ratio has a decreasing trend from around 0,70800 to 0,70795. These values will be presented and interpreted in the discussion chapter, and then compared with the sedimentology of the Pistarda formation.

**6.3  $^{87}\text{Sr}/^{86}\text{Sr}$ ,  $\delta^{18}\text{O}$  and  $\delta^{13}\text{C}$  for all localities**

To better see how the values change, two scatter plots are made. Firstly,  $^{87}\text{Sr}/^{86}\text{Sr}$  ratio against  $\delta^{18}\text{O}$  (figure 6.2). Secondly,  $^{87}\text{Sr}/^{86}\text{Sr}$  ratio against  $\delta^{13}\text{C}$  (figure 6.3). All values from all of the localities are presented in these plots.



**Figure 6.2** – Scatter plot of  $^{87}\text{Sr}/^{86}\text{Sr}$  and  $\delta^{18}\text{O}$ . Note that locality 5.2, upper and lower has a clear difference in the  $\delta^{18}\text{O}$  value.



**Figure 6.3** – Scatter plot of  $^{87}\text{Sr}/^{86}\text{Sr}$  and  $\delta^{13}\text{C}$ . Note that locality 5.2, upper and lower has a clear difference in the  $\delta^{13}\text{C}$  value.

Both plots show a difference in the strontium ratio between locality 5.2 upper (blue square) and locality 5.2 lower (red square), where the upper has the higher value. For  $\delta^{18}\text{O}$  the upper unit is more negative, meaning it is enriched in  $^{16}\text{O}$  than  $^{18}\text{O}$ . Regarding  $\delta^{13}\text{C}$ , the same can be extracted from the plots. Note that locality 1 fits in between the upper and lower units of locality 5.2. The same can be said for the upper and lower units of locality 4.1. The uncertainty is that locality 4 upper and lower units only has a tiny difference between  $^{87}\text{Sr}/^{86}\text{Sr}$  ratio,  $\delta^{18}\text{O}$  and  $\delta^{13}\text{C}$  values that are not as clearly differentiated as the locality 5.1. The rest of the localities give no clear answer as to where they fit in, some with lower values of  $^{87}\text{Sr}/^{86}\text{Sr}$  and others have a much higher ratio.

Both scatter plots show 3 plots with a significantly higher  $^{87}\text{Sr}/^{86}\text{Sr}$  ratio compared to the rest. One of them is a sample taken directly from a reed stem (locality 8). Locality 4.1 upper is also from a heavily dense reed layer, but at locality 10 the sample is taken from a micritic layer. The difference in strontium ratio between the upper and lower unit at locality 5.2 is interpreted to be the result of a difference in drainage area. This will be discussed in the next chapter.

#### 6.4 $\delta^{18}\text{O}$ and $\delta^{13}\text{C}$ – all localities

Here  $\delta^{18}\text{O}$  and  $\delta^{13}\text{C}$  is plotted against each other in a scatter plot (figure 6.4).

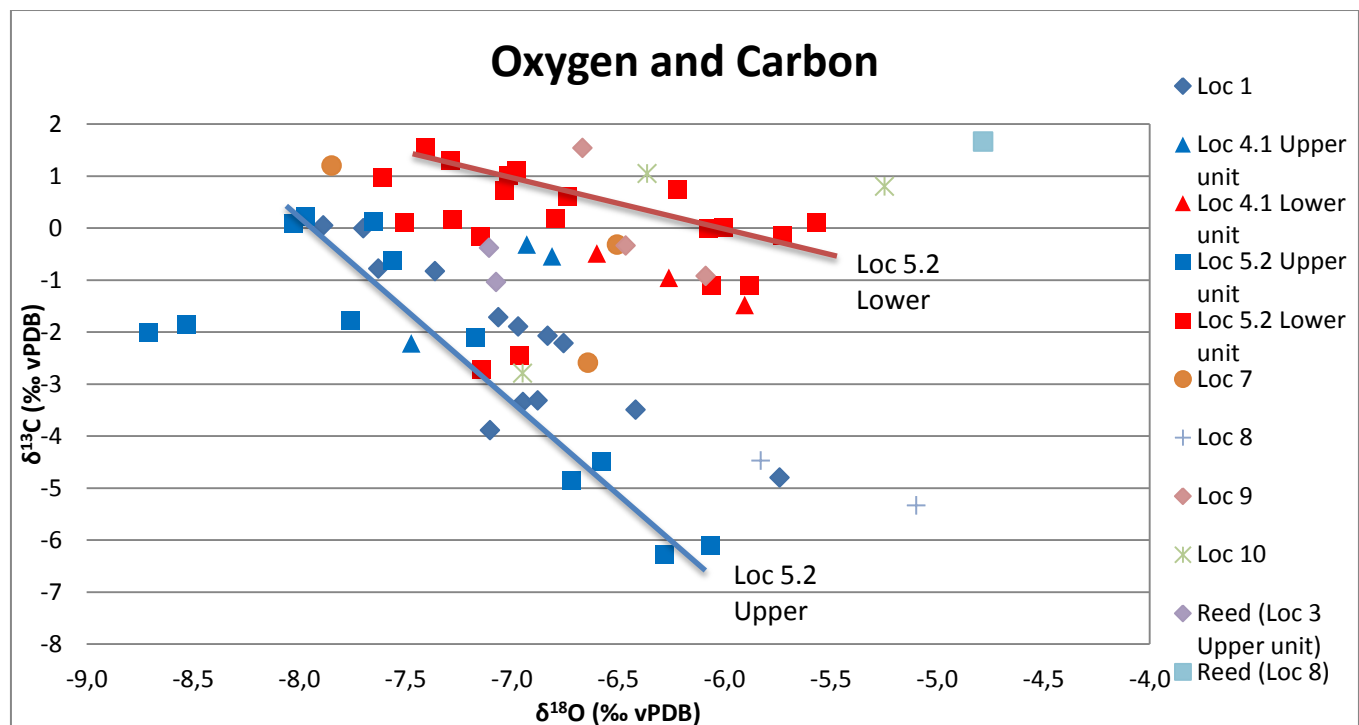


Figure 6.4 -  $\delta^{18}\text{O}$  and  $\delta^{13}\text{C}$  – two trends between the lower and upper unit

This scatter plot illustrates that locality 5.2 upper (blue square) follows a trend line plotted beneath mostly all of the other values, shown with a blue line. For the locality 5.2 lower unit (red square) a much higher value of  $\delta^{13}\text{C}$ , shown with a red line. This indicates that the lower and upper units at locality 5.2 are formed under two different environments. Locality 1 also has a similar trend as the lower value, and this could indicate that it is formed under similar conditions as the upper unit. As for locality 4.1 upper and lower, a similar trend is seen, but it needs more values to confirm that there is a trend.

The difference between the two trends will be discussed in the next chapter connecting the geochemically analyses with sedimentology of the Pistarda formation.

### 6.5 Bacterial growth in thin section

When examining the thin sections, it becomes clear that many of them have had extensive bacterial shrubs growing in the samples (Chafetz and Guidry, 1999). To see if this had any impact on the geochemical values, a visual examination of the bacterial growth on the thin sections was plotted against  $\delta^{18}\text{O}$  and  $\delta^{13}\text{C}$  (figure 6.5)

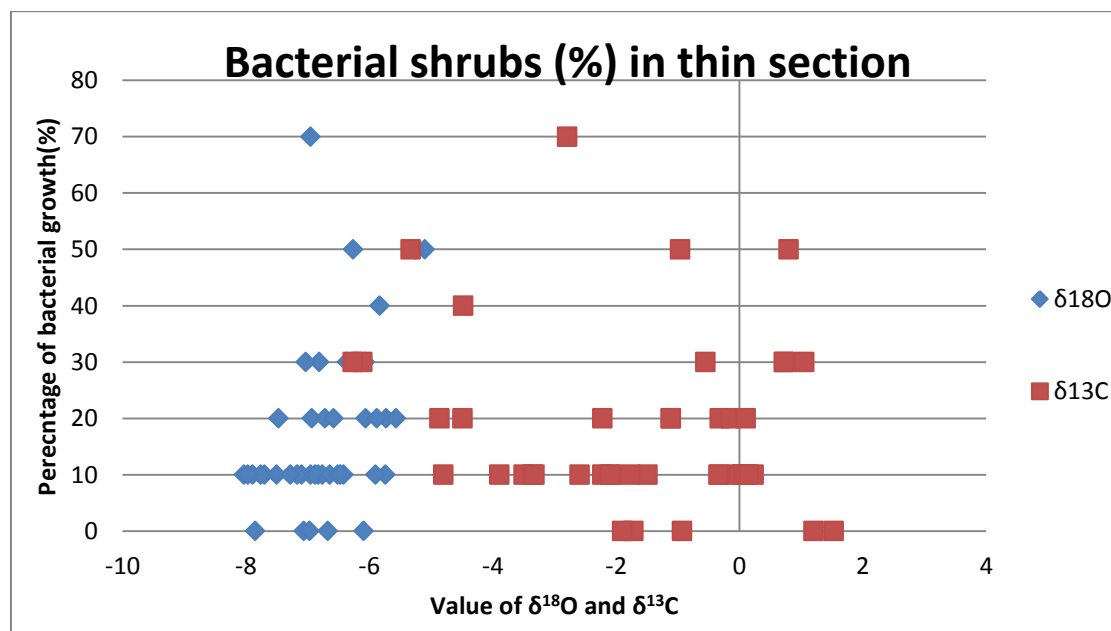
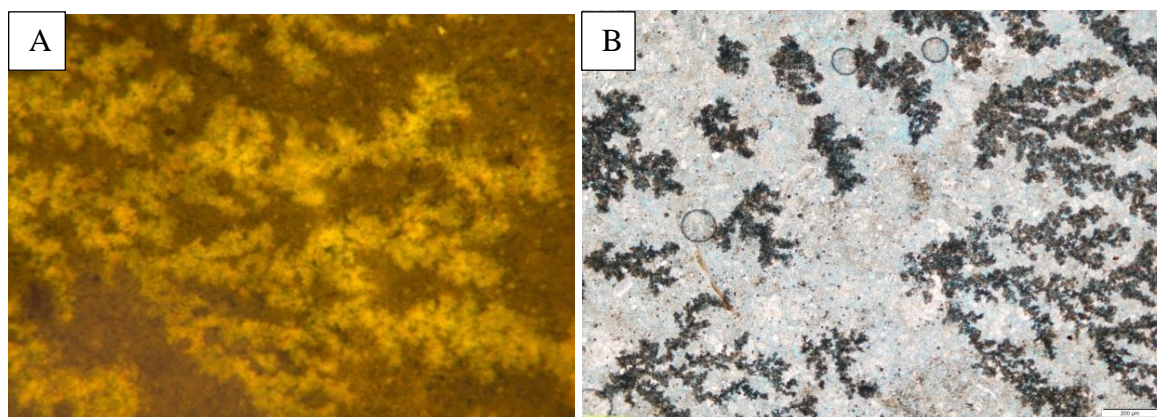
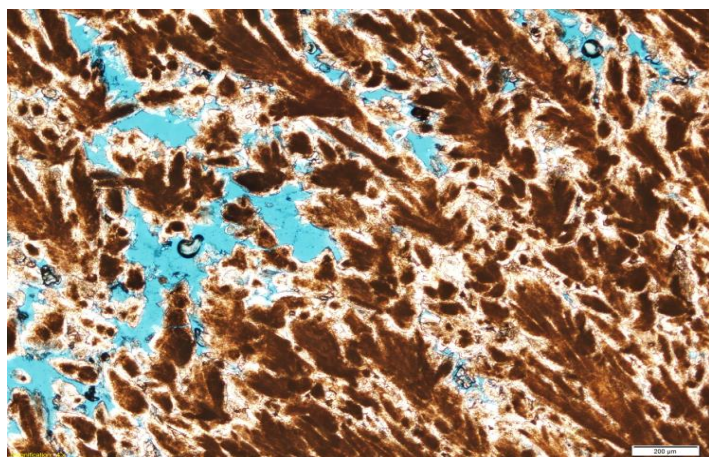


Figure 6.6 shows no significant difference in  $\delta^{18}\text{O}$  or  $\delta^{13}\text{C}$  values in the thin sections that contains bacterial growth. This means that the bacterial growth has no effect on the values of  $\delta^{18}\text{O}$  and  $\delta^{13}\text{C}$ . Cathodelumination of the thin sections showed that they had no luminescence. This indicates that primary carbonate is still present in the samples, therefore it is possible to use the geochemical signal as an indicator of the paleoenvironment. By using a microscope with blue fluorescent light, it was shown that the microbial bacteria and the oncoids are still fluorescent. This means that the organic material is still present intercrystal and/or intracrystal.



**Figure 6.6** – (A) Thin section from sample 5.2-2.2 in blue light showing that primary organic material is present. (B) The same thin section in ordinary light where the bacterial shrubs are seen. The CL picture was taken in the lower right corner. The scale bar is 200 micrometer.

Figure 6.7 is from a thin section taken from a quarry a few miles up in the mountains, not far from the city of Xylokastro. Comparing it with the figure 6.6(B) it is clear that the Pistarda formation does not have the same amount of bacterial shrubs in them.



**Figure 6.7** - Thin section from a quarry a few miles up in the mountains, not far from the city of Xylokastro, Peloponnese, Greece. Example of crystal shrubs which are interpreted as tufa deposits. The scale bar is 200  $\mu\text{m}$

## 6.6 Trace elements

Six samples are analyzed to check for trace elements of calcium, magnesium, manganese, iron and strontium. Also, some of the elements are plotted against each other to give a ratio between them. This is presented in table 5.1.

**Table 6.1** - Table over trace element analyses and ratio between of some of the elements

		ICP- AES		ICP-MS				
		Ca	Mg	Mn	Fe	Sr	Mg/Ca	Sr/Ca
		%	mg/kg	mg/kg	mg/kg	mg/kg	mmol/mol	mmol/mol
Locality 5.2 Upper	5.2-1.2a	35,1	6357	16,7	106	987,1	29,87	1,2864
	5.2-1.3a	32,5	6976	19,6	64,7	530,5	35,40	0,7466
	5.2-1.6a	34,4	8290	30,4	66,6	528,7	39,74	0,7030
Locality 5.2 Lower	5.2-2.2a	35,4	7159	154,6	255,3	995,5	33,35	1,2863
	5.2-2.7a	40,8	7998	21,5	63,3	581,5	32,33	0,6519
	5.2-2.11a	37,2	5702	14,1	45,5	668,1	25,28	0,8215

The values of table 6.1 are also plotted against the stratigraphy of locality 5.2, upper and lower units. None of the trace elements have a significant difference in the value between them and no particular trend is visible. There is a relatively higher level of magnesium than expected. Therefore, not only low magnesium calcite (LMC), but also high magnesium calcite (HMC) or aragonite can be present in the sediments. The average Mg/Ca ratio is 32, which is a high ratio. Typically, HMC will occur around a Mg/Ca ratio of 2-12 and aragonite must have greater ratio than 12 (Tucker and Wright, 1990). But in an open lacustrine setting the most common mineral in a low salinities lake is LMC, and it is also the only stable mineral. The amount of calcium is a common value for carbonate minerals. To check for any trends between the Mg/Ca ratio against the Sr/Ca ratio, they are plotted in figure 6.8.

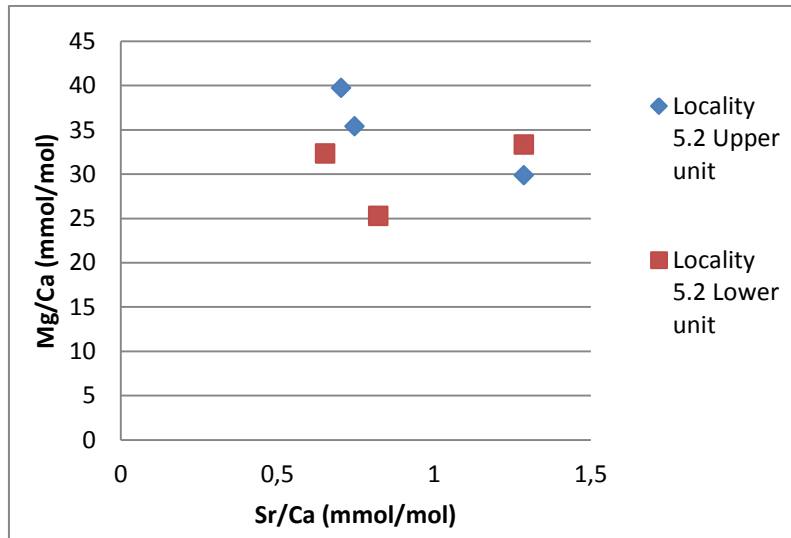
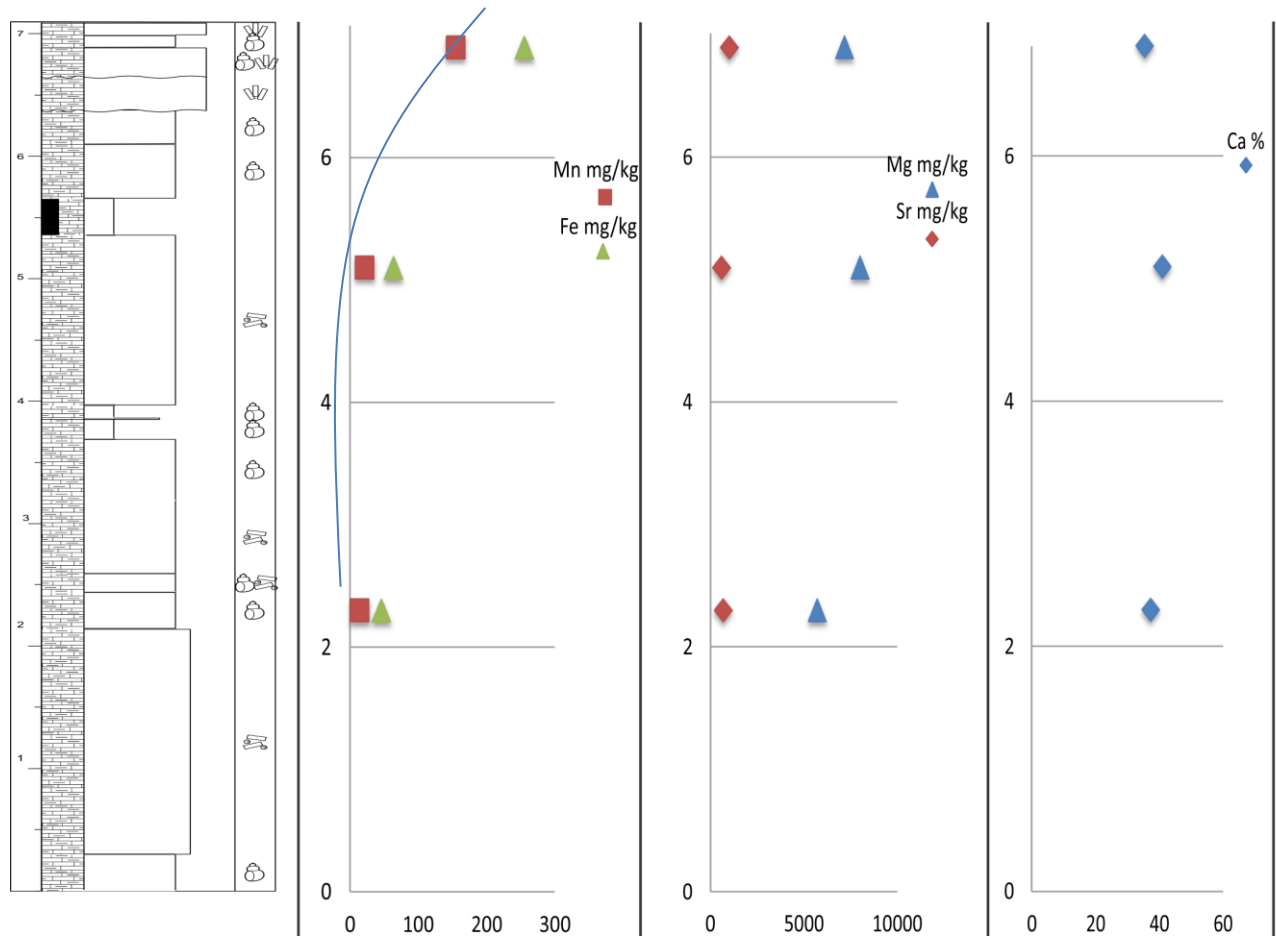
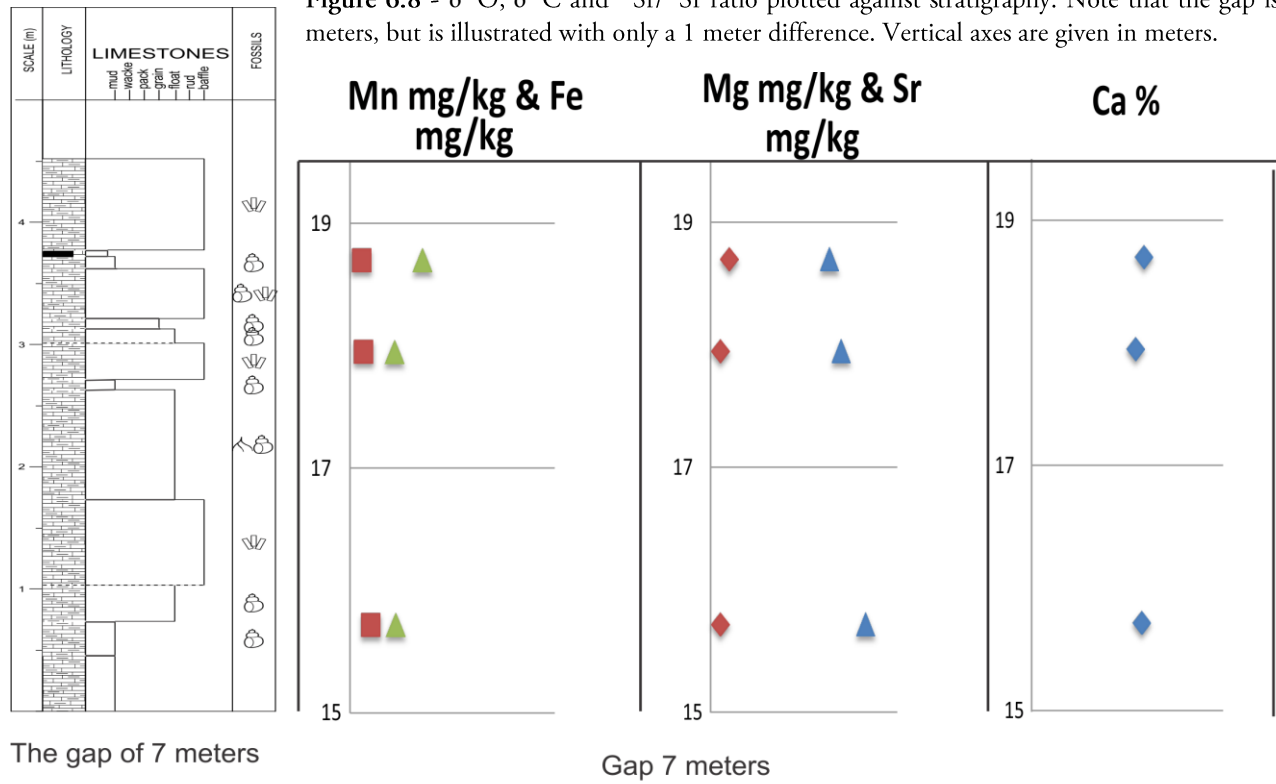


Figure 6.7 – Mg/Ca ratio plotted against Sr/Ca ratio. No sign of trends.

Figure 6.7 shows no trends between the upper and lower unit. In the next figure (figure 6.8) the trace element are plotted with stratigraphy, to see any changes in stratigraphy. One sample at 7 meters in the lower unit stands out with a slightly higher level of iron and manganese. The other samples show no trends or significant differences in values



**Figure 6.8** -  $\delta^{18}\text{O}$ ,  $\delta^{13}\text{C}$  and  $^{87}\text{Sr}/^{86}\text{Sr}$  ratio plotted against stratigraphy. Note that the gap is 7 meters, but is illustrated with only a 1 meter difference. Vertical axes are given in meters.



## 7. Discussion

This chapter discusses the results presented in chapters 5 and 6. Firstly, the reason why Pistarda formation is interpreted to have been formed in a lake setting is discussed. Then, the facies distribution in the Pistarda formation is discussed along with what it could indicate. The third and fourth subchapters discuss the lake depth and geometry, and how the Pistarda formation initiated and terminated. The fifth subchapter presents the formation in the Megara Basin. The sixth subchapter discusses the geochemical data with respect to the facies and the depositional environment of the upper and lower unit of the Pistarda formation. Finally, a suggestion for further work in the Pistarda formation is proposed.

### 7.1 The Pistarda formation – lake

The Pistarda formation is interpreted to be a lake for a number of reasons. Firstly, all of the gastropods that are found are interpreted to be freshwater species. Secondly, the sedimentology interpretation indicates a lake, because facies 4 is interpreted to be a turbidity current which is only formed in water and also that facies 2 has reeds that are known to only grow near water level. Thirdly, no evidence was found in the field of evaporation minerals, suggesting that it was an open lake. Also in the thin sections it is possible to see ostracodes, which are deep-water dwelling animals.

There were two different gastropods found in the formation. One is the *M. g proteus*, which was found in locality 5.2 in the upper unit. The sample was taken 1 meter above the base in the upper unit. The other, *M. g aegaea*, was found in locality 9 at the middle of the sequence. Willmann (1985) meant that the *M. g aegaea* evolved into *M. g proteus*. This could indicate that locality 9 has older sediments than 5.2, but there is not enough data to confirm this. The reason is that this information was found after the fieldwork, so only a few samples of gastropods were collected from these two localities. It would be interesting to see what types of gastropods are in the lower unit at locality 5.2 and if *M. g aegaea* is among them.

## 7.2 Facies distribution in the Pistarda formation – vertical and distribution

Much of the sediments found in Pistarda formation are interpreted to be deposited in shallow water, especially all of the facies that are deposited as *in situ*. Locality 5.2 gives a good indication of the depth, based on what facies are found in each of the units. The lower unit has more reworked layer, like slumps (facies 3) and turbidity (facies 4), also with coquina layers (facies 6). In the upper unit, much more reeds (facies 2) are found as well as interlayering micritic layers with gastropods (facies 7) and one paleosol layer (facies 1). This indicates that it started as deeper lake and gradually becomes shallower at this locality. The other localities are interpreted to be from shallow water, because of the many *in situ* reeds layers found there. In addition, most of them show no evidence of material deposits in deeper waters. The only exceptions are locality 9 and 10, which are thought to be deeper waters because of more hemipelagic/pelagic mud with fewer reeds layers. Also, in locality 10, there is evidence of reeds *in situ*. In the Pistarda formation, no evidence of common algae, Charophyta, was found in the sediments. This algae is very common in these types of lakes (García, 1994). Glover and Robertson (2003) interpreted that lakes without Charophyta have had periodical drying and were also very shallow, keeping the higher plants and algal species (e.g. Chara) from establishing in the lake.

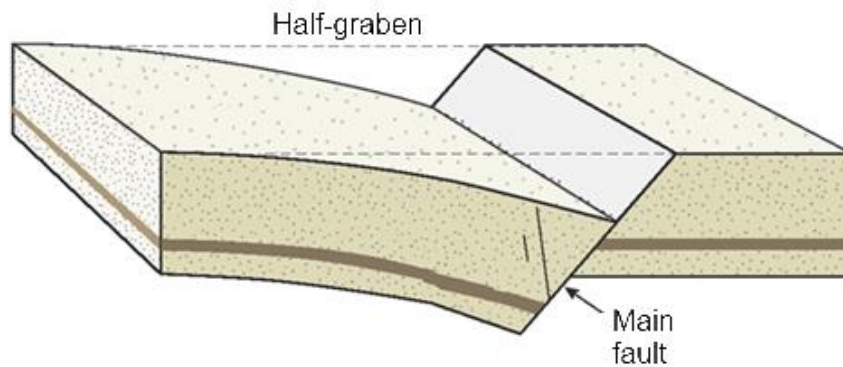
## 7.3 Lake geometry and lake depth

The Pistarda formation has a large distribution and the length from locality 1 to 10 is around 12 km. When looking at the Pistarda formation from an overview point, it is possible to see the geometry of the formation. It consists mostly of sub-horizontally bedded layers with a low gradient from 5-15 degrees inclination. By comparing the Pistarda formation to the different models from Platt and Wright (1991), it is interpreted that the Pistarda formation represents a ramp margin of a low energy system (figure 3.4, page 15). No clinoforms that indicate steep gradients are observed.

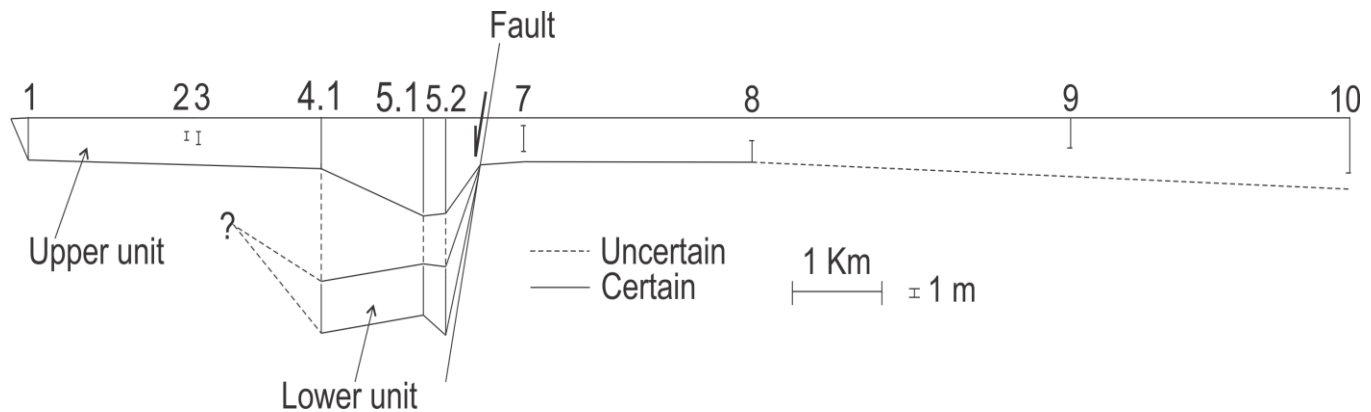
From the correlation panel (Appendix III), localities 5.1 and 5.2 as well as locality 4.1, have much thicker sequences than the other localities. The difference between locality 5.2 and locality 3 and 7 are especially significant. Locality 5 lies southwest of the Toumpaniari fault which is interpreted to have been active during the formation of the Pistarda (Bentham et al., 1991). Also from the figures 2.4 and 2.5 (pages 9 and 10) it is possible to see that there is a fault on both sides

of the Toumpaniari fault. They may have been active during the deposition of the Pistarda formation, providing the subsidence associated with these faults and creating some of the accumulation space necessary to deposit the thickness of the Pistarda formation. These faults could also be the source of water coming into the lake via springs.

It is interpreted that an unmarked fault between localities 4, 5, 6 and locality 7 (Figure 2.4, page 9), is the main reason why it was possible to create the accumulation space needed to develop the over 20 meters thick sequence of the Pistarda formation. Locality 7 lies around 250 meters above sea level and localities 5 and 6 lie around 200 meters above sea level, so the offset is about 50 meters. Therefore, it is interpreted that the footwall sank down and provided the accumulation space needed for localities 4, 5, 6, creating a half-graben where locality 7 is on top of the hanging wall (figure 7.1). This must have been a small fault bounded by others faults, since the other localities do not show signs of two units. On the left side of the fault it is interpreted that the upper unit is found in the locality 1, 2 and 3. But on the other side of the fault it is difficult to say what unit they compose (figure 7.2).



**Figure 7.1** – A model of how the fault gives rise to the increase accumulation space due to creation of a half-graben. This is further interpreted as the reason why the Pistarda formation has a thicker sequence close to the fault, with decreasing thickness to the northwest Modified from Fossen (2010)



**Figure 7.2** – A simple sketch of how the thickness varies due to the fault. The logs are aligned with the top, if the true top is known, and the same applies for the base. For the left side of the fault the lower and upper unit is clearly defined. On the right side it is not so clear what unit it may be composed of. The same difference between the locations (marked by number) is used here as in the correlation panel in appendix III.

#### 7.4 The formation of the Pistarda formation - Climate

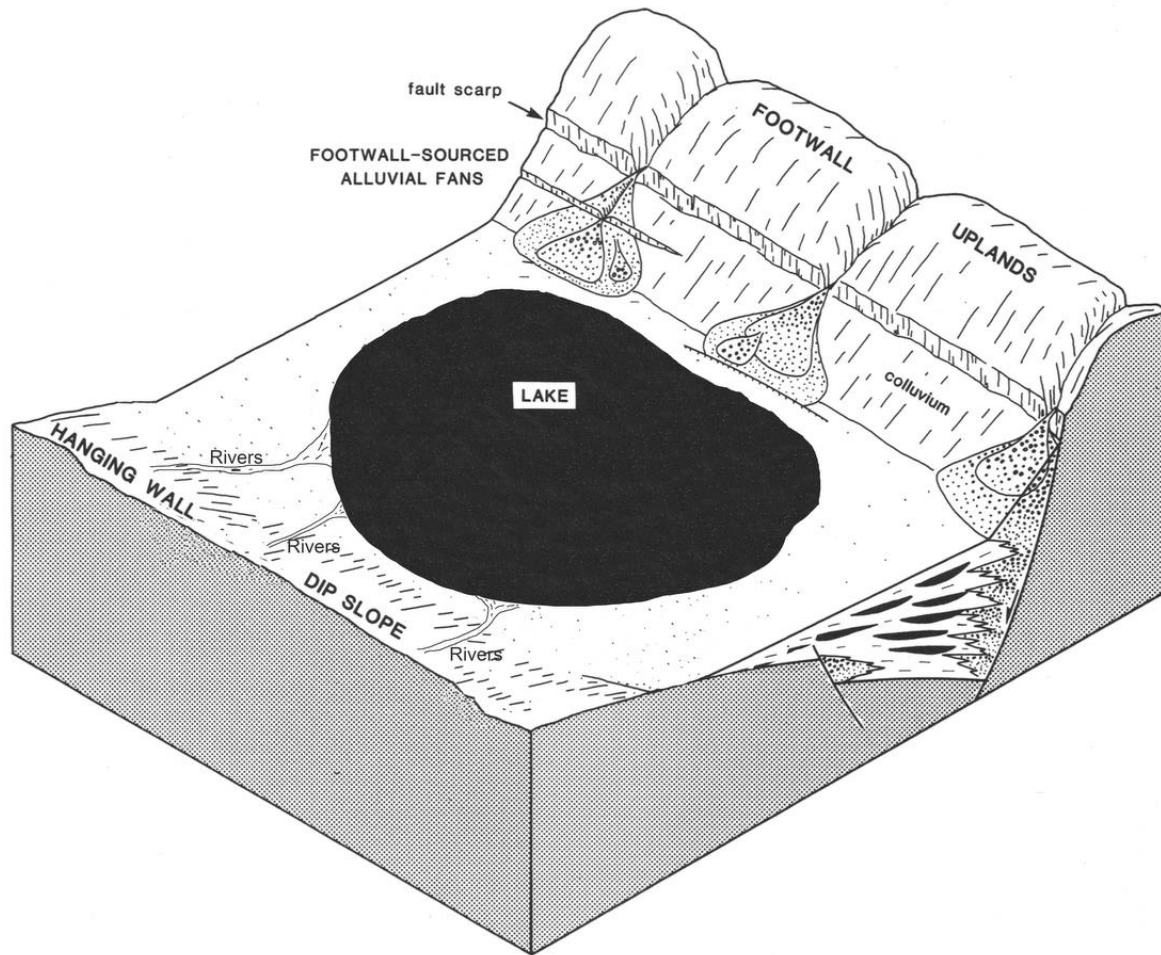
As mentioned in chapter two, below the Pistarda formation is the Toumpaniari formation and below that is the Kremida formation. The last formation is interpreted by Bentham et al. (1991) to be formed by a delta that was filling an ancient lake, called Lake Megara. The Toumpaniari formation is a fluvial system that deposited gravel sheets by braided streams that flooded down the hanging wall dip slope (Bentham et al., 1991). These pebbly sandstones are found at the base of the Pistarda formation in some localities. Deposition continued to fill the basin, before a quiet period where the deposition of the Pistarda formation started. Afterward, the deposition of fluvial sediments in the Harbour Ridges formation started. In some localities the Harbour Ridges formation is exposed above the Pistarda formation. This indicates that the sediments were first part of a fluvial system, and then the Pistarda formation was deposited in a lacustrine environment before it stopped and new sediments were deposited from a fluvial system. An important remark is that the accumulation space left in the basin must have been very low, meaning it must have been a shallow lacustrine environment. The reason why it shifted into a lacustrine environment is interpreted to be due to climatic changes (Leeder et al., 1998). When the lower formations were deposited the climate was drier, leading to a higher input of siliciclastic material because the sparse vegetation couldn't hold it in place. During the Pistarda formation the climate became wet, which gave rise to more vegetation keeping the siliciclastic material from entering the Megara Basin. Similar interpretations of climatic shifts are made for much younger tufa deposits in Greece during the MIS 5 (Brasier et al., 2010). The same

interpretation is thought for the end of the Pistarda, i.e. that the climate became drier and a fluvial environment replaced the lacustrine settings. When the vegetation disappears the siliciclastic material starts again to be transported out into basin. There is little evidence found of rivers in the Pistarda formation, which is quite different than for example the Antalya tufa, Turkey (Glover and Robertson, 1998). This indicates that the Pistarda was flooding over the area and had a permanent lake.

### 7.5 Pistarda formation in the Megara Basin

The Megara Basin is bounded by two main faults, one on each side of the basin at the Pateras Mountains and at the Gerania Mountains. The whole basin is a half-graben dipping towards the Pateras in the north-northeast (figure 2.4, page 9). The Pistarda formation was measured to have a dip of 5-15 degrees towards the Pateras Mountains in the northeast. The Pistarda formation localities only consist of exposures closer to the fault by the Gerania Mountains. Since the layers are dipping, the dip-extent of the lake is more difficult to reconstruct from outcrop data when no subsurface data (e.g. wells or seismic) is available. Therefore, it is very difficult to interpret how large the lake was in the Megara Basin, but since the gradient is towards the mountain it should have been much larger. What we can now see of the Pistarda formation is interpreted to be only the margin of the lake. This is also concluded due to all the *in situ* facies. It is difficult to say how the Pistarda formation looks throughout the Megara Basin, but it must have been a shallow lake with a low gradient in half-graben setting. Figure 7.3 illustrates how the lake may have been in the Megara Basin. There rivers was running down the hanging wall into a permanent lake, with a low gradient. On the other side, in the northeast, alluvial fan was coming into the lake from the Pateras Mountains.





**Figure 7.3** –This is a simple model of how the lake in the Megara Basin may have looked, with rivers coming down the hanging wall dip slope feeding into a permanent lake. The lake was shallow, with a low gradient and an abundance of reeds growing in the margin. On the north side, alluvial fans come down from the Pateras Mountains. Modified from (Leeder and Gawthorpe, 1987)

## 7.6 Geochemistry - locality 5.2 lower unit and upper unit

The geochemistry from locality 5.2 gave many different signals and in this section the interpretation of these trends will be discussed. They will also be linked up to the sedimentology in the Megara Basin and the Pistarda formation.

### 7.6.1 $\delta^{13}\text{C}$ and $\delta^{18}\text{O}$

In figure 6.4 (page 64) the  $\delta^{13}\text{C}$  value is plotted against  $\delta^{18}\text{O}$  and a clear difference between the units is visible. The major difference between these units, is that the lower unit has a significantly more positive  $\delta^{13}\text{C}$  than the upper unit, but the  $\delta^{18}\text{O}$  is similar to and typical of

meteoric water at mid-latitudes (Arthur et al., 1983). This is interpreted to mean that the lake had a shifting in drainage area from the lower to the upper unit. Based on the geological map of the area from Bentham et al. (1991), the mountains around the basin consist of marine limestone from the Cretaceous age. This type of limestone generally has positive values throughout the period (Jarvis et al., 2006). From this it is understood that during the depositing of the lower unit the lake must have been supplied by rivers that drained the marine Cretaceous limestone, thus providing the lake with  $^{13}\text{C}$  enriched water (e.g. Bade et al. (2004) with a DIC source from the mountains. The upper unit is believed to come from a shallower lake which had isotopically lighter DIC from oxidation of organic matter during frequent lake overturns, as well as lighter DIC from erosion of soils during lake lowstand (e.g. Bade et al. (2004).

In figure 6.1 (page 61), where the stratigraphy is plotted against  $\delta^{13}\text{C}$ , it is clear that carbon in the lower unit has a near vertical trend, indicating an overall stable input of isotopically heavier carbon from dissolution of marine limestone of the Cretaceous age. The graph also indicates that the lake had no significant thermocline and chemocline for a prolonged period of time, because  $\delta^{13}\text{C}$  changes little upward in the stratigraphy. In the upper unit,  $\delta^{13}\text{C}$  shifts from a positive trend and then back to a negative trend. This is suggested to come from frequent upwelling of isotopically lighter DIC.

The  $\delta^{18}\text{O}$  value in the lower unit shows a somewhat higher level of evaporation from the lake towards the top of the stratigraphy. For the upper unit the same interpretation is made, indicating a shallowing of the lake. A trend towards more positive values indicates enrichment of the heavier isotopes. This is interpreted as increasing amounts of evaporating water, taking the lighter  $^{16}\text{O}$  with it.

In the upper unit (figure 6.1), around 11 meters from the base, a clearly different sample has a higher  $\delta^{18}\text{O}$  and lower  $\delta^{13}\text{C}$  when compared to the other samples. The sample is taken from a layer which is interpreted to be a paleosol layer. Paleosol will have relatively low  $\delta^{13}\text{C}$  values (Cerling, 1984). The  $\delta^{18}\text{O}$  is probably signaling the relative enrichment of  $^{16}\text{O}$  in water evaporating from the soil (Allan and Matthews, 1982).

### 7.6.2 $^{87}\text{Sr}/^{86}\text{Sr}$

The strontium ratio is significantly different between the two units. The lower unit has a lower strontium ratio than the upper unit, indicating that it had a varying drainage pattern. The interpretation is that the lower unit was deposited by a larger lake, which flooded over a siliciclastic hinterland. The drainage was mainly through marine Cretaceous limestones which gave it a lower  $^{87}\text{Sr}/^{86}\text{Sr}$  ratio. When the lake became smaller and shallower the water then eroded through more siliciclastic rocks, either this gave it a higher strontium ratio. This happened as the upper unit was deposited.

The strontium ratio in the lower unit in the stratigraphy shows a deepening trend with a more Cretaceous limestones signature, which means that the lake is becoming larger. In the upper unit a similar trend is showing, with decreasing signs of erosion of siliciclastic rocks, as the lakes are increasing in size. Cretaceous limestone contains a relatively lower value of  $^{87}\text{Sr}/^{86}\text{Sr}$  ratio through time, varying from 0,7078 to 0,7072 (McArthur et al., 2001). The less radioactive strontium-isotopes in the lower unit probably reflect an increase in the lake area (as well as increasing depth), and a relatively higher contribution of strontium from eroded limestones.

### 7.6.3 Summary

The geochemical data indicates that the lower unit was formed by an increasingly larger and deeper lake. This is also reflected in an abundance of reworked sediments in the lower unit, and in the composition of the facies. Less *in situ* reeds are found in the lower unit than in the upper unit, which almost only consists of layers that are interpreted as *in situ* and material that is formed in shallow water and on land, paleosol. Thus, the upper unit is concluded to be formed by a relatively smaller and shallower lake than the lower unit or it had a lower input of strontium with marine Cretaceous limestones signal.

As for the other localities, no clear evidence is found of them either belonging to the lower or the upper unit on both side of the fault. Specifically, in figures 6.2 and 6.3 (pages 63), locality 1 is plotted between the units from locality 5.2. If the strontium ratio was similar for some of the localities it could be possible to say that they were formed from the same water.

## 7.7 Further studies

The Megara Basin is well described in the literature, although more work is necessary to fully understand the depositional system in the area in order to get a better understanding of the Pistarda formation. One suggestion for future work is to try to find more of the paleosol layers, as they could be a useful to correlate layers within the Pistarda formation. Also, a more complete geochemical analysis with more samples might contribute to a broader understanding of how the outcrop develops. An interesting idea is to check what the middle unit consists of, as it looks like sandstones from a distance. This could indicate that the Pistarda was formed in two events. From an observation point it also appears like the Pistarda formation has a minor deposition below the lower unit as well.

## 8. Summary and conclusion

The main objective of this study is to establish detailed facies models of the Pistarda formation and to understand the formation of the tufa deposits, both from fieldwork and geochemical analysis. The formation was traced all over the Megara basin, where 10 localities were found. Some of them were impossible to reach. 9 sections were logged and taken samples of. Along with the geochemical analysis the main conclusions of the study are summarized in these pullet points.

- The Pistarda formation consists of two units, lower and upper unit, which can be traced over a relatively long distance, but they are only found in localities 4, 5, and 6. Both of them had significant difference in strontium ratio.
- The lower unit consists of more reworked material, like mass transport sedimentation and turbidity. Also reworked gastropods are found in the lower unit, indicating a deeper a lake.
- The upper unit consists of more *in situ* material, for example reeds *in situ*, paleosol and organic matter, interpreted to be a shallow lake. The sedimentology in most of the localities is similar to the upper unit.
- The relatively thicker sediments on localities 4, 5 and 6 are related to fault controlled accumulation space. This is interpreted to be the reason why the Pistarda formation could develop more than one unit and a thickness of over 20 meters.
- The geochemical analysis confirms that the Pistarda formation consist of two distinctive units with their respective signals. The strontium ratio in the lower unit has a signal interpreted to be from the surrounding marine Cretaceous limestones. From this it is understood that the lake that formed the Pistarda formation must have been flooding a larger part of the basin, which would give it a mainly marine signal. In the upper unit the lake level sinks, giving rise to a higher strontium ratio from erosion of more siliciclastic rocks. This is also seen with the  $\delta^{13}\text{C}$  value. The marine limestones enriched in  $^{13}\text{C}$  are



found in the lower unit, and the upper unit has negative values indicating less input from marine carbonates. The strontium ratio,  $\delta^{13}\text{C}$  value and sediments in the lower unit indicate that it was formed by a deeper and larger lake. The opposite is found for the upper unit, indicating that it was formed by a shallower and smaller lake.

- From the studies on the Pistarda formation it is understood that it was formed by a lacustrine environment which has fluvial deposits below and above. The reason why it changes is due to climatic changes from a drier to a wetter climate and back again. In a wetter climate, more vegetation could develop and holding back siliciclastic material, preventing it from entering the lake.

## 9. Bibliography

- Allaby, A. & Allaby, M. 2008. *A dictionary of earth sciences*, Oxford University Press.
- Allan, J. & Matthews, R. 1982. Isotope signatures associated with early meteoric diagenesis. *Sedimentology*, 29, 797-817.
- Armijo, R., Meyer, B., Hubert, A. & Barka, A. 1999. Westward propagation of the North Anatolian fault into the northern Aegean: Timing and kinematics. *Geology*, 27, 267-270.
- Arthur, M. A., Anderson, T. F., Kaplan, I. R., Veizer, J. & Land, L. S. 1983. Stable isotopes in sedimentary geology. *SEPM Short Course Notes*, 10.
- Bade, D. L., Carpenter, S. R., Cole, J. J., Hanson, P. C. & Hesslein, R. H. 2004. Controls of  $\delta^{13}\text{C}$ -DIC in lakes: Geochemistry, lake metabolism, and morphometry. *Limnol. Oceanogr.*, 49, 1160-1172.
- Bell, R., McNeill, L., Bull, J., Henstock, T., Collier, R. & Leeder, M. 2009. Fault architecture, basin structure and evolution of the Gulf of Corinth Rift, central Greece. *Basin Research*, 21, 824-855.
- Bell, R. E., McNeill, L. C., Bull, J. M. & Henstock, T. J. 2008. Evolution of the offshore western Gulf of Corinth. *Geological Society of America Bulletin*, 120.
- Bentham, P., Collier, R., Gawthorpe, R., Leeder, R. & Stark, C. 1991. Tectono-sedimentary development of an extensional basin: the Neogene Megara Basin, Greece. *Journal of the Geological Society*, 148, 923-934.
- Berner, R. A. 1980. *Early diagenesis: A theoretical approach*, Princeton University Press.
- Blatt, H., Middleton, G. & Murray, R. 1980. *Origin of sedimentary rocks*: Prince-Hall. Inc., New Jersey, 782.
- Boggs, S. 1995. *Principles of sedimentology and stratigraphy*, Prentice Hall New Jersey.
- Bouma, A. H., Kuenen, P. H. & Shepard, F. P. 1962. *Sedimentology of some flysch deposits: a graphic approach to facies interpretation*, Elsevier Amsterdam.
- Boyer, B. W. 1982. Green River laminites: Does the playa-lake model really invalidate the stratified-lake model? *Geology*, 10, 321-324.
- Brand, U. & Veizer, J. 1980. Chemical diagenesis of a multicomponent carbonate system--1: Trace elements. *Journal of Sedimentary Research*, 50.
- Brasier, A., Andrews, J., Marca-Bell, A. & Dennis, P. 2010. Depositional continuity of seasonally laminated tufas: Implications for  $\delta^{18}\text{O}$  based palaeotemperatures. *Global and Planetary Change*, 71, 160-167.
- Briole, P., Rigo, A., Lyon-Caen, H., Ruegg, J., Papazissi, K., Mitsakaki, C., Balodimou, A., Veis, G., Hatzfeld, D. & Deschamps, A. 2000. Active deformation of the Corinth rift, Greece: results from repeated Global Positioning System surveys between 1990 and 1995. *Journal of Geophysical Research: Solid Earth (1978–2012)*, 105, 25605-25625.
- Cerling, T. E. 1984. The stable isotopic composition of modern soil carbonate and its relationship to climate. *Earth and Planetary science letters*, 71, 229-240.
- Chafetz, H. S. & Guidry, S. A. 1999. Bacterial shrubs, crystal shrubs, and ray-crystal shrubs: bacterial vs. abiotic precipitation. *Sedimentary Geology*, 126, 57-74.
- Cohen, A. S. 2003. *Paleolimnology: the history and evolution of lake systems*, Oxford University Press, USA.
- Cohen, A. S., Soreghan, M. J. & Scholz, C. A. 1993. Estimating the age of formation of lakes: an example from Lake Tanganyika, East African Rift system. *Geology*, 21, 511-514.
- Cohen, A. S. & Thouin, C. 1987. Nearshore carbonate deposits in Lake Tanganyika. *Geology*, 15, 414-418.
- Craig, H. 1954. Carbon 13 in plants and the relationships between carbon 13 and carbon 14 variations in nature. *The journal of geology*, 115-149.

- De Deckker, P. 1988. Biological and sedimentary facies of Australian salt lakes. *Palaeogeography, Palaeoclimatology, Palaeoecology*, 62, 237-270.
- Dean, W. E. & Fouch, T. 1983. Lacustrine environment. *Carbonate Depositional Environments* (Scholle, PA; Bebout, DG; Moore, CH, 97-130.
- Demets, C., Gordon, R. G., Argus, D. & Stein, S. 1990. Current plate motions. *Geophysical journal international*, 101, 425-478.
- Dewey, J. F. & Sengor, A. M. C. 1979. AEGEAN AND SURROUNDING REGIONS - COMPLEX MULTI-PLATE AND CONTINUUM TECTONICS IN A CONVERGENT ZONE. *Geological Society of America Bulletin*, 90, 84-92.
- Donovan, R. N. 1975. Devonian lacustrine limestones at the margin of the Orcadian Basin, Scotland. *Journal of the Geological Society*, 131, 489-510.
- Doutsos, T. & Kokkalas, S. 2001. Stress and deformation patterns in the Aegean region. *Journal of Structural Geology*, 23, 455-472.
- Doutsos, T., Kontopoulos, N. & Poulimenos, G. 1988. The Corinth-Patras rift as the initial stage of continental fragmentation behind an active island arc (Greece). *Basin Research*, 1, 177-190.
- Dravis, J. J. & Yurewicz, D. A. 1985. Enhanced carbonate petrography using fluorescence microscopy. *Journal of Sedimentary Research*, 55.
- Dunham, R. J. 1962. Classification of carbonate rocks according to depositional texture.
- Eardley, A. J. 1938. Sediments of Great Salt Lake, Utah. *AAPG Bulletin*, 22, 1305-1411.
- Eggins, S., Woodhead, J., Kinsley, L., Mortimer, G., Sylvester, P., Mcculloch, M., Hergt, J. & Handler, M. 1997. A simple method for the precise determination of  $\geq 40$  trace elements in geological samples by ICPMS using enriched isotope internal standardisation. *Chemical Geology*, 134, 311-326.
- Elderfield, H. 1986. Strontium isotope stratigraphy. *Palaeogeography, Palaeoclimatology, Palaeoecology*, 57, 71-90.
- Embry, A. F. & Klovan, J. E. 1971. A Late Devonian reef tract on northeastern Banks Island, NWT. *Bulletin of Canadian Petroleum Geology*, 19, 730-781.
- Eyles, N. & Lagoe, M. B. 1989. Sedimentology of shell-rich deposits (coquinas) in the glaciomarine upper Cenozoic Yakataga Formation, Middleton Island, Alaska. *Geological Society of America Bulletin*, 101, 129-142.
- Fairchild, I. J. 1983. Chemical controls of cathodoluminescence of natural dolomites and calcites: new data and review. *Sedimentology*, 30, 579-583.
- Ferguson, J. & Ibe, A. 1982. SOME ASPECTS OF THE OCCURRENCE OF PROTO-KEROGEN IN RECENT OOLITES. *Journal of Petroleum Geology*, 4, 267-285.
- Folk, R. L. 1959. Practical petrographic classification of limestones. *AAPG Bulletin*, 43, 1-38.
- Folk, R. L. 1962. Spectral subdivision of limestone types.
- Ford, M., Rohais, S., Williams, E. A., Bourlange, S., Jousset, D., Backert, N. & Malartre, F. 2012. Tectono-sedimentary evolution of the western Corinth rift (Central Greece). *Basin Research*, n/a-n/a.
- Fossen, H. 2010. *Structural geology*, Cambridge University Press.
- Galat, D. & Jacobsen, R. 1985. Recurrent aragonite precipitation in saline-alkaline Pyramid Lake, Nevada. *Archiv für Hydrobiologie*, 105, 137-159.
- García, A. 1994. Charophyta: their use in paleolimnology. *Journal of Paleolimnology*, 10, 43-52.
- Garlick, G. 1969. The stable isotopes of oxygen. *Handbook of geochemistry*, 2, 1.
- Gierlowski-Kordesch, E. H. 2010. Lacustrine carbonates. *Developments in Sedimentology*, 61, 1-101.
- Glover, C. & Robertson, A. H. 2003. Origin of tufa (cool-water carbonate) and related terraces in the Antalya area, SW Turkey. *Geological journal*, 38, 329-358.
- Glover, C. P. & Robertson, A. H. 1998. Role of regional extension and uplift in the Plio-Pleistocene evolution of the Aksu Basin, SW Turkey. *Journal of the Geological Society*, 155, 365-387.

- Heimann, A. & Sass, E. 1989. Travertines in the northern Hula Valley, Israel. *Sedimentology*, 36, 95-108.
- Jackson, J., Gagnepain, J., Houseman, G., King, G., Papadimitriou, P., Soufleris, C. & Virieux, J. 1982. Seismicity, normal faulting, and the geomorphological development of the Gulf of Corinth (Greece): The Corinth earthquakes of February and March 1981. *Earth and Planetary Science Letters*, 57, 377-397.
- Jackson, J. & Mckenzie, D. 1984. Active tectonics of the Alpine—Himalayan Belt between western Turkey and Pakistan. *Geophysical Journal International*, 77, 185-264.
- Jackson, J. A. & Mckenzie, D. P. 1988. Rates of active deformation in the Aegean Sea and surrounding areas. *Basin research*, 1, 121-128.
- Jacobson, R. L. & Langmuir, D. 1970. The Chemical History of Some Spring Waters in Carbonate Rocks. *Groundwater*, 8, 5-9.
- James, N. P. & Choquette, P. W. 1984. Diagenesis 9. Limestones-the meteoric diagenetic environment. *Geoscience Canada*, 11.
- Jarvis, I., Gale, A. S., Jenkyns, H. C. & Pearce, M. A. 2006. Secular variation in Late Cretaceous carbon isotopes: a new  $\delta^{13}\text{C}$  carbonate reference curve for the Cenomanian–Campanian (99.6–70.6 Ma). *Geological Magazine*, 143, 561-608.
- Jenner, G., Longerich, H., Jackson, S. & Fryer, B. 1990. ICP-MS—a powerful tool for high-precision trace-element analysis in earth sciences: evidence from analysis of selected USGS reference samples. *Chemical Geology*, 83, 133-148.
- Jolivet, L. 2001. A comparison of geodetic and finite strain pattern in the Aegean, geodynamic implications. *Earth and Planetary Science Letters*, 187, 95-104.
- Jolivet, L., Brun, J.-P., Gautier, P., Lallemand, S. & Patriat, M. 1994. 3D-kinematics of extension in the Aegean region from the early Miocene to the present; insights from the ductile crust. *Bulletin de la Société géologique de France*, 165, 195-209.
- Kahle, H.-G., Straub, C., Reilinger, R., McClusky, S., King, R., Hurst, K., Veis, G., Kastens, K. & Cross, P. 1998. The strain rate field in the eastern Mediterranean region, estimated by repeated GPS measurements. *Tectonophysics*, 294, 237-252.
- Kidwell, S. M. 1986. Models for fossil concentrations: Paleobiologic implications. *Paleobiology*, 12, 6-24.
- Kinsman, D. J. 1969. Interpretation of  $\text{Sr}^{+2}$  concentrations in carbonate minerals and rocks. *Journal of Sedimentary Research*, 39.
- Kneller, B. & Buckee, C. 2000. The structure and fluid mechanics of turbidity currents: a review of some recent studies and their geological implications. *Sedimentology*, 47, 62-94.
- Królikowska, J. 1997. Eutrophication processes in a shallow, macrophyte dominated lake-species differentiation, biomass and the distribution of submerged macrophytes in Lake Łuknajno (Poland). *Hydrobiologia*, 342, 411-416.
- Langmuir, D. 1971. The geochemistry of some carbonate ground waters in central Pennsylvania. *Geochimica et Cosmochimica Acta*, 35, 1023-1045.
- Leeder, M. & Gawthorpe, R. 1987. Sedimentary models for extensional tilt-block/half-graben basins. *Geological Society, London, Special Publications*, 28, 139-152.
- Leeder, M., Mack, G., Brasier, A., Parrish, R., McIntosh, W., Andrews, J. & Duermeijer, C. 2008. Late-Pliocene timing of Corinth (Greece) rift-margin fault migration. *Earth and Planetary Science Letters*, 274, 132-141.
- Leeder, M. R., Harris, T. & Kirkby, M. J. 1998. Sediment supply and climate change: implications for basin stratigraphy. *Basin Research*, 10, 7-18.
- Leeder, M. R. & Mack, G. H. 2009. Basin-Fill Incision, Rio Grande and Gulf of Corinth Rifts: Convergent Response to Climatic and Tectonic Drivers. *Sedimentary Processes, Environments and Basins: A Tribute to Peter Friend (Special Publication 38 of the IAS)*, 22, 9.

- Lorah, M. M. & Herman, J. S. 1988. The chemical evolution of a travertine-depositing stream: Geochemical processes and mass transfer reactions. *Water Resources Research*, 24, 1541-1552.
- Lowe, D. R. 1982. Sediment gravity flows: II Depositional models with special reference to the deposits of high-density turbidity currents. *Journal of Sedimentary Research*, 52.
- Mcarthur, J. 1994. Recent trends in strontium isotope stratigraphy. *Terra nova*, 6, 331-358.
- Mcarthur, J., Howarth, R. & Bailey, T. 2001. Strontium isotope stratigraphy: LOWESS version 3: best fit to the marine Sr-isotope curve for 0–509 Ma and accompanying look-up table for deriving numerical age. *The Journal of Geology*, 109, 155-170.
- Mcclusky, S., Balassanian, S., Barka, A., Demir, C., Ergintav, S., Georgiev, I., Gurkan, O., Hamburger, M., Hurst, K. & Kahle, H. 2000. Global Positioning System constraints on plate kinematics and dynamics in the eastern Mediterranean and Caucasus. *Journal of Geophysical Research: Solid Earth (1978–2012)*, 105, 5695-5719.
- Mckenzie, D. 1970. Plate tectonics of the Mediterranean region. *Nature*, 226, 239-243.
- Merlivat, L. & Jouzel, J. 1979. Global climatic interpretation of the deuterium-oxygen 18 relationship for precipitation. *Journal of Geophysical Research: Oceans (1978–2012)*, 84, 5029-5033.
- Meulenkamp, J. E. 1985. Aspects of the Late Cenozoic evolution of the Aegean region. *Geological evolution of the Mediterranean basin*. Springer.
- Meyers, W. J. 1974. Carbonate cement stratigraphy of the Lake Valley Formation (Mississippian) Sacramento Mountains, New Mexico. *Journal of Sedimentary Research*, 44.
- Mills, P. C. 1983. Genesis and diagnostic value of soft-sediment deformation structures—a review. *Sedimentary Geology*, 35, 83-104.
- Morgenstern, N. 1967. Submarine slumping and the initiation of turbidity currents. *Marine geotechnique*, 189-220.
- Müller, J. & Milliman, J. D. 1973. Relict carbonate-rich sediments on southwestern Grand Bank, Newfoundland. *Canadian Journal of Earth Sciences*, 10, 1744-1750.
- Nielsen, A. E. 1964. *Kinetics of precipitation*, Pergamon Press; [distributed in the Western Hemisphere by Macmillan, New York].
- O'leary, M. H. 1988. Carbon isotopes in photosynthesis. *Bioscience*, 328-336.
- Papazachos, B. & Comninakis, P. 1971. Geophysical and tectonic features of the Aegean arc. *Journal of Geophysical Research*, 76, 8517-8533.
- Pierson, B. J. 1981. The control of cathodoluminescence in dolomite by iron and manganese. *Sedimentology*, 28, 601-610.
- Pin, C., Briot, D., Bassin, C. & Poitrasson, F. 1994. Concomitant separation of strontium and samarium-neodymium for isotopic analysis in silicate samples, based on specific extraction chromatography. *Analytica Chimica Acta*, 298, 209-217.
- Platt, N. & Wright, V. P. 1991. Lacustrine carbonate: facies models, facies distributions and hydrocarbon aspects. *Anadón P, Cabrera L, Kelts K, Lacustrine facies analysis. Special publication*, 57-74.
- Platt, N. H. 1989. Climatic and tectonic controls on sedimentation of a Mesozoic lacustrine sequence: the Purbeck of the western Cameros Basin, northern Spain. *Palaeogeography, palaeoclimatology, palaeoecology*, 70, 187-197.
- Reading, H. G. 2009. *Sedimentary environments: processes, facies and stratigraphy*, John Wiley & Sons.
- Rhodes, M. K., Carroll, A. R., Pietras, J. T., Beard, B. L. & Johnson, C. M. 2002. Strontium isotope record of paleohydrology and continental weathering, Eocene Green River Formation, Wyoming. *Geology*, 30, 167-170.
- Robbins, L. & Blackwelder, P. 1992. Biochemical and ultrastructural evidence for the origin of whittings: a biologically induced calcium carbonate precipitation mechanism. *Geology*, 20, 464-468.



- Rohais, S., Eschard, R., Ford, M., Guillocheau, F. & Moretti, I. 2007. Stratigraphic architecture of the Plio-Pleistocene infill of the Corinth Rift: Implications for its structural evolution. *Tectonophysics*, 440, 5-28.
- Sandberg, P. A. 1975. New interpretations of Great Salt Lake ooids and of ancient non-skeletal carbonate mineralogy. *Sedimentology*, 22, 497-537.
- Şengör, A. C. 1984. The Cimmeride orogenic system and the tectonics of Eurasia. *Geological Society of America Special Papers*, 195, 1-74.
- Shackleton, N. J. & Opdyke, N. D. 1973. Oxygen isotope and palaeomagnetic stratigraphy of Equatorial Pacific core V28-238: Oxygen isotope temperatures and ice volumes on a 10<sup>5</sup> year and 10<sup>6</sup> year scale. *Quaternary research*, 3, 39-55.
- Shepard, F. P. 1955. Delta-front valleys bordering the Mississippi distributaries. *Geological Society of America Bulletin*, 66, 1489-1498.
- Stabel, H. 1986. Calcite precipitation in Lake Constance: Chemical equilibrium sedimentation, and nucleation by algae. *Limnology and Oceanography*, 31, 1081-1093.
- Stumm, W. & Morgan, J. 1981. Aquatic chemistry. Wiley, New York.
- Theodoropoulos, D. 1968. Stratigraphic und Tectonik des Isthmus von Megara. *Erlanger Geol. Abh*, 73.
- Thompson, J. B., Schultze-Lam, S., Beveridge, T. J. & Des Marais, D. J. 1997. Whiting events: biogenic origin due to the photosynthetic activity of cyanobacterial picoplankton. *Limnology and oceanography*, 42, 133-141.
- Tucker, M. E. & Wright, V. P. 1990. Carbonate Sedimentology. *Carbonate Sedimentology*, 101-227.
- Veizer, J., Ala, D., Azmy, K., Bruckschen, P., Buhl, D., Bruhn, F., Carden, G. A., Diener, A., Ebner, S. & Godderis, Y. 1999. <sup>87</sup>Sr/<sup>86</sup>Sr,  $\delta^{13}\text{C}$  and  $\delta^{18}\text{O}$  evolution of Phanerozoic seawater. *Chemical Geology*, 161, 59-88.
- Verrecchia, E. P. 2007. Lacustrine and palustrine geochemical sediments. *Geochemical Sediments and Landscapes*, 298-329.
- Wetzel, R. 1983. Limnology. Saunders College Publishing, Philadelphia.
- Wilcox, D. A., Thompson, T. A., Booth, R. K. & Nicholas, J. 2007. *Lake-level variability and water availability in the Great Lakes*, US Geological Survey.
- Williamson, C. R. & Picard, M. D. 1974. Petrology of carbonate rocks of the Green River Formation (Eocene). *Journal of Sedimentary Research*, 44.
- Willmann, R. 1985. Responses of the Plio-Pleistocene freshwater gastropods of Kos (Greece, Aegean Sea) to environmental changes. *Sedimentary and evolutionary cycles*, 295-321.

## Appendix I – Results of geochemistry analysis

Table A - Geochemistry results of samples from the Pistarda formation with an estimate of microbial shrubs.

Locality	Sample	Mean $\delta^{13}\text{C}$	Mean $\delta^{18}\text{O}$	Ca (%)	Mg (mg/kg)	Mn (mg/kg)	Fe (mg/kg)	Sr (mg/kg)	$^{87}\text{Sr}/^{86}\text{Sr}$	Microbial shrubs (%)
Loc 1	1.1a	-7,06	-1,72						0,707934	0
	1.1b	-6,97	-1,90						0,707937	0
	1.2a	-5,74	-4,80							10
	1.2b	-6,42	-3,50							10
	1.3a	-6,83	-2,08							10
	1.3b	-6,76	-2,22							10
	1.4a	-6,95	-3,35						0,707932	10
	1.4a	-6,88	-3,32							10
	1.4b	-7,10	-3,89						0,707936	10
	1.5a	-7,63	-0,78							
	1.5b	-7,36	-0,83							
	1.6a	-7,89	0,04						0,707903	10
	1.6b	-7,70	-0,01						0,707917	10
Loc 4.1	4.1-1.5a	-6,81	-0,55						0,707923	30
	4.1-1.7a	-7,47	-2,22						0,707937	20
	4.1-1.10a	-6,93	-0,32						0,708223	20
Loc 4.1	4.1-2.1a	-5,90	-1,49						0,707925	10
	4.1-2.2a	-6,26	-0,96						0,707903	50
	4.1-2.3a	-6,60	-0,49						0,707895	
Loc 5.2 Upper	5.2-1.1a	-6,72	-4,86							
	5.2-	-6,58	-4,49							

<b>unit</b>	1.1b									
	5.2-1.2a	-7,76	-1,77	35,1	6357	16,7	106	987.1	0,707966	
	5.2-1.2b	-7,17	-2,10						0,707950	
	5.2-1.3a	-7,65	0,13	32,5	6976	19,6	64,7	530,5	0,707981	
	5.2-1.3b	-7,56	-0,62						0,707981	
	5.2-1.4a	-8,03	0,07							10
	5.2-1.4b	-7,97	0,23							10
	5.2-1.5a	-6,07	-6,11							30
	5.2-1.5b	-6,28	-6,27							30
	5.2-1.Reed A	-7,11	-0,39							
	5.2-1.Reed B	-7,08	-1,05							
	5.2-1.6a	-8,71	-2,01	34,4	8290	30,4	66,6	528,7	0,707998	
	5.2-1.6b	-8,53	-1,86						0,708012	
<b>Loc 5.2 Lower unit</b>	5.2-2.1a	-6,96	-2,46							
	5.2-2.1b	-7,14	-2,72							
	5.2-2.2a	-5,73	-0,14	35,4	7159	154,6	253,3	995,5	0,707867	20
	5.2-2.2b	-5,57	0,10						0,707864	20
	5.2-2.4a	-6,06	-1,11							20

	5.2-2.4b	-5,88	-1,11							20
	5.2-2.6a	-6,07	-0,01							
	5.2-2.6b	-6,00	0,00							
	5.2-2.7a	-7,02	1,01	40,8	7998	21,5	63,3	581,5	0,707888	
	5.2-2.7b	-6,98	1,10						0,707876	
	5.2-2.8a	-7,50	0,11							10
	5.2-2.8b	-7,28	0,15							10
	5.2-2.9a	-6,74	0,60							
	5.2-2.9b	-7,61	0,96							
	5.2-2.10a	-7,15	-0,16							
	5.2-2.10b	-6,79	0,18							
	5.2-2.11a	-6,22	0,73	37,2	5702	14,1	45,5	668,1	0,707890	30
	5.2-2.11b	-7,03	0,72						0,707885	30
	5.2-2.12a	-7,29	1,29							
	5.2-2.12b	-7,41	1,54							
<b>Loc 7</b>	7.2a	-6,64	-2,59						0,707901	10
	7.3a	-6,51	-0,32						0,707881	10
	7.5a	-7,85	1,20						0,707879	0

<b>Loc 8</b>	8.2Reed	-4,78	1,66						0,708215	
	8.4a	-5,83	-4,48						0,707971	40
	8.5a	-5,10	-5,33						0,707999	50
<b>Loc 9</b>	9.1a	-6,47	-0,34						0,707772	10
	9.3a	-6,09	-0,93						0,707835	0
	9.4a	-6,67	1,53						0,707953	0
<b>Loc 10</b>	10.1a	-6,36	1,05						0,707968	30
	10.5a	-5,25	0,80						0,708259	50
	10.16a	-6,95	-2,79						0,707823	70

**Table B** - Table of the strontium isotope ratio results from the first round of analysis.

Lab#	Sample	$^{87/86}\text{Sr}$	2S error	$^{87/86}\text{Sr}$ corrected	
gs 6914	1.1.1a	0,707943	0,000008	0,707934	a
gs 6915	1.1.4a	0,707941	0,000009	0,707932	a
gs 6916	1.1.6a	0,707912	0,000008	0,707903	a
gs 6917	1.1.1b	0,707946	0,000009	0,707937	a
gs 6918	1.1.4b	0,707945	0,000009	0,707936	a
gs 6919	1.1.6b	0,707908	0,000009	0,707917	b
gs 6920	5.2-1.2a	0,707957	0,000009	0,707966	b
gs 6921	5.2-1.3a	0,707972	0,000009	0,707981	b
gs 6922	5.2-1.6a	0,708016	0,000008	0,707998	c
gs 6923	5.2-1.2b	0,707968	0,000008	0,707950	c
gs 6924	5.2-1.3b	0,707982	0,000008	0,707981	d
gs 6925	5.2-1.6b	0,708013	0,000009	0,708012	d
gs 6926	5.2-2.2a	0,707868	0,000008	0,707867	d
gs 6927	5.2-2.7a	0,707889	0,000009	0,707888	d
gs 6928	5.2-2.11a	0,707891	0,000008	0,707890	d
gs 6929	5.2-2.2b	0,707865	0,000008	0,707864	d
gs 6930	5.2-2.7b	0,70788	0,000008	0,707876	e
gs 6931	5.2-2.11b	0,707889	0,000006	0,707885	e
SRM 987		0,710240		$^{84/86}\text{Sr}$	
SRM 987	41557	0,710249	0,000008		a
SRM 987	41558	0,710231	0,000008		b
SRM 987	41561	0,710258	0,000007		c
SRM	41562	0,710241	0,000007		d



987

SRM	41563	0,710244	0,000008	0,056502	e
-----	-------	----------	----------	----------	---

987

Table C - Table of the strontium isotope ratio results from the second round of analysis.

Lab#	Sample	$^{87/86}\text{Sr}$	2S error	$^{87/86}\text{Sr}$ corrected	
gs 7171	4.1.10a	0,708216	0,000009	0,708223	a
gs 7172	4.1.5a	0,707916	0,000008	0,707923	a
gs 7173	4.1.7a	0,70793	0,000009	0,707937	a
gs 7174	4.1.1a	0,707918	0,000009	0,707925	a
gs 7175	4.2.2a	0,707896	0,000008	0,707903	a
gs 7176	4.2.3a	0,707901	0,000008	0,707895	b
gs 7177	7.2	0,707907	0,000009	0,707901	b
gs 7178	7.3	0,707887	0,000007	0,707881	b
gs 7179	7.5	0,707885	0,000007	0,707879	b
gs 7180	8.2R	0,708216	0,000008	0,708215	c
gs 7181	8.4	0,707972	0,000009	0,707971	c
gs 7182	8.5	0,708000	0,000009	0,707999	c
gs 7183	9.1	0,707773	0,000009	0,707772	c
gs 7184	9.3	0,707836	0,000009	0,707835	c
gs 7185	9.4	0,707954	0,000009	0,707953	c
gs 7186	10.1a	0,707976	0,000009	0,707968	d
gs 7187	10.5	0,708267	0,000009	0,708259	d
gs 7188	10.16	0,707831	0,000008	0,707823	d
	Spike wt.(mantle)	$^{84/86}\text{Sr}$ spike			
Blank	0,0263	21,64			
SRM 987		0,710240		$^{84/86}\text{Sr}$	
SRM 987	41731	0,710233	0,000008		a
SRM 987	41732	0,710246	0,000008		b

SRM 987	41733	0,710241	0,000008		c
SRM 987	41736	0,710248	0,000008	0,056480	d

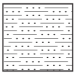

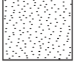
















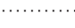

**Table D** - The table shows the internal uncertainty of the analyzed trace elements

Sample ID	Sample	Ca3179	Mg24	Mn55	Fe57	Sr88
		%RSD	%RSD	%RSD	%RSD	%RSD
3152*	5.2-2.7a	0,53	3,5	5,3	8,6	6,2
3153*	5.2-2.11a	0,16	8,4	3,0	5,6	7,5
3154*	5.2-1.2a	0,45	2,6	5,6	7,5	9,2
3155*	5.2-1.3a	0,28	3,5	5,1	5,5	6,2
3156*	5.2-1.6a	0,46	6,6	9,4	10,3	5,0

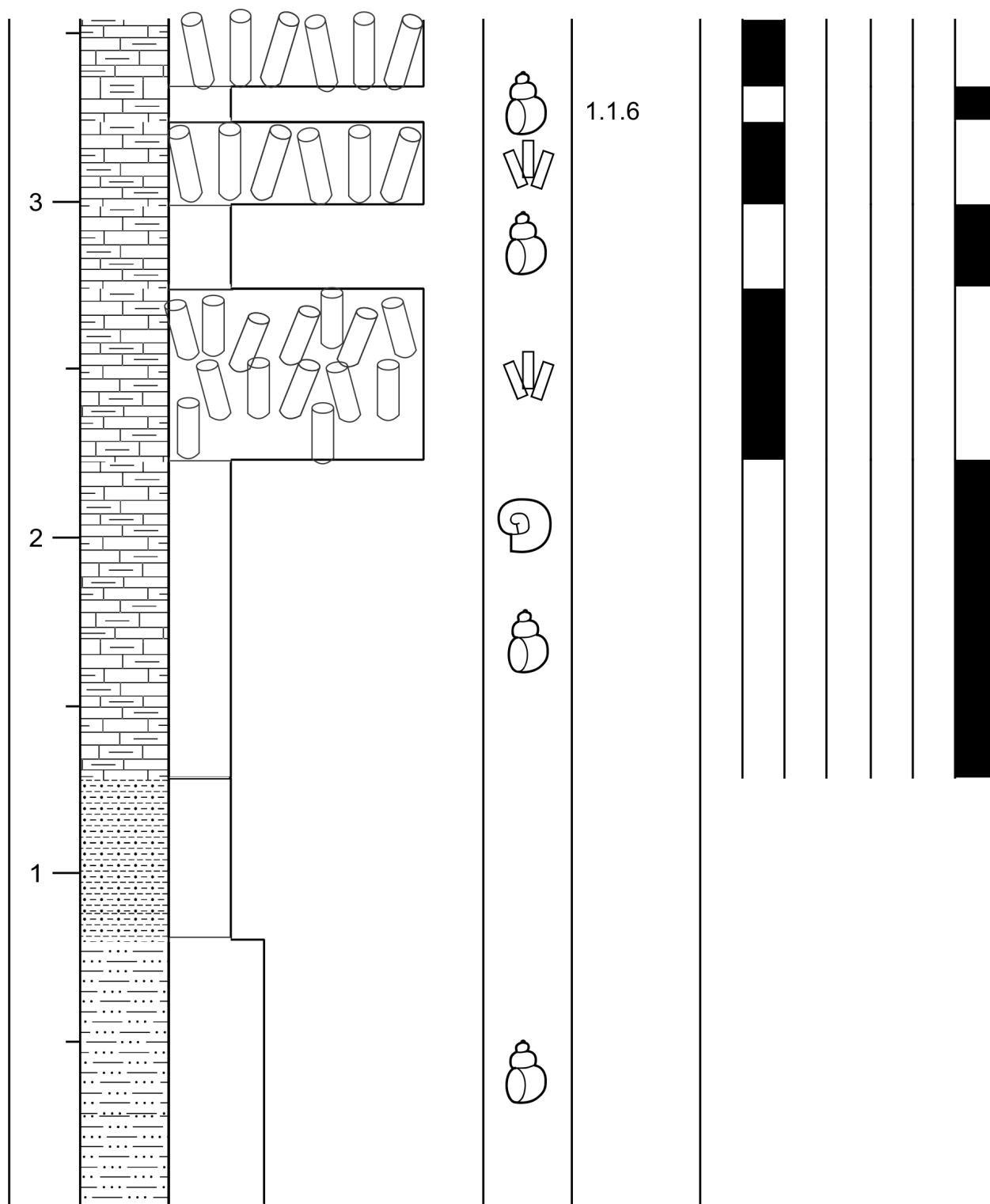
\*Samples with visible precipitation after centrifugation. Analyses were performed on dissolved fraction. The standard derivation for the ICP-MS shows greater values than expected, due to instrumental influence.

## Appendix II – Logs

## Legend

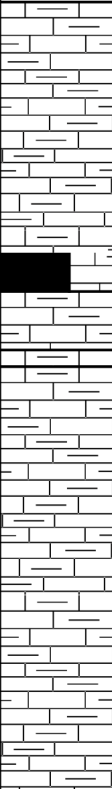
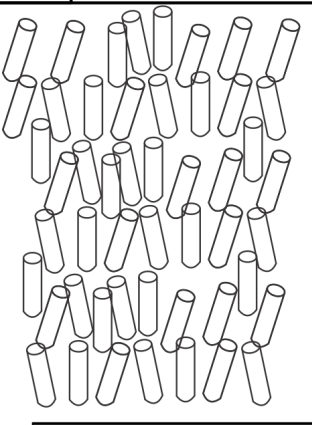



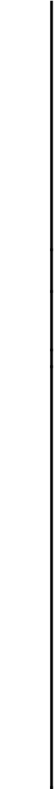
Lithology	Fossils
 Mudstone  Siltstone  Sandstone  Pebbly sandstone  Limestone	 Gastropods  Broken gastropods  Dissolved gastropods  Bivalve  Viviparus viviparus  Reeds <i>in-situ</i>  Reeds reworked  Roots  Algal mat
Sedimentary structures	
 Laminated  Planar cross bedding  Alternation  Concretions	Base boundaries
	 Sharp  Gradational  Erosion

Locality 1 - East N38° 4.852' E23° 11.680'																								
SCALE (m)	LITHOLOGY	LIMESTONES						FOSSILS	SAMPLES	FACIES														
		mud	wacke	pack	grain	float	rud			baffle	1	2	3	4	5	6	7							
6									1.1.1															
5																								
4									1.1.5															

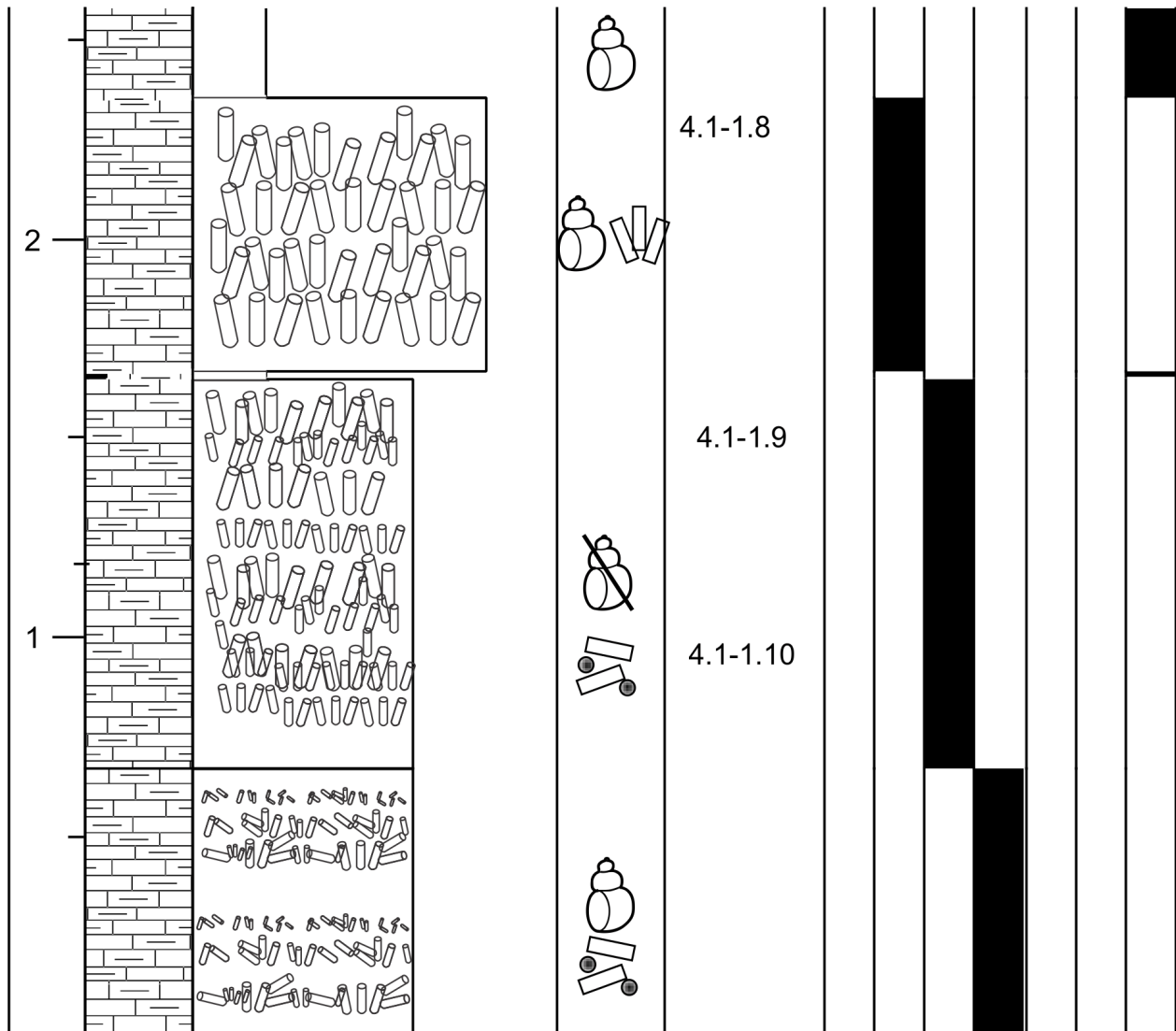


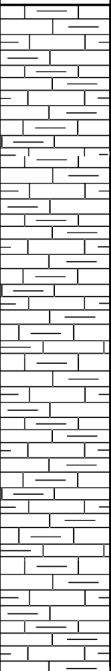
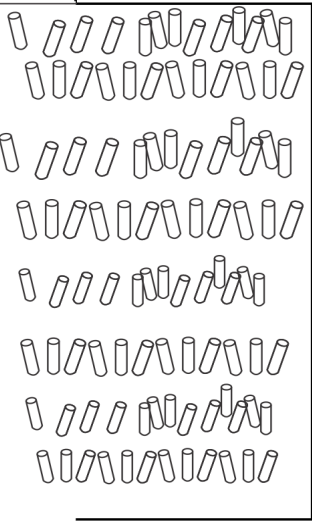




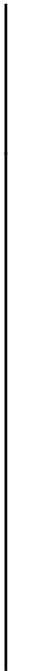

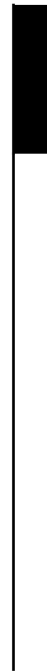

Locality 2 - N38°04,055 E023°11,315						
SCALE (m)	LITHOLOGY	LIMESTONES				
		mud	wacke	pack	grain	float
						rud
						baffle
				FOSSILS	SAMPLES	FACIES
						1 2 3 4 5 6 7
1				2.1		
				2.2		
				2.3		
				2.4		

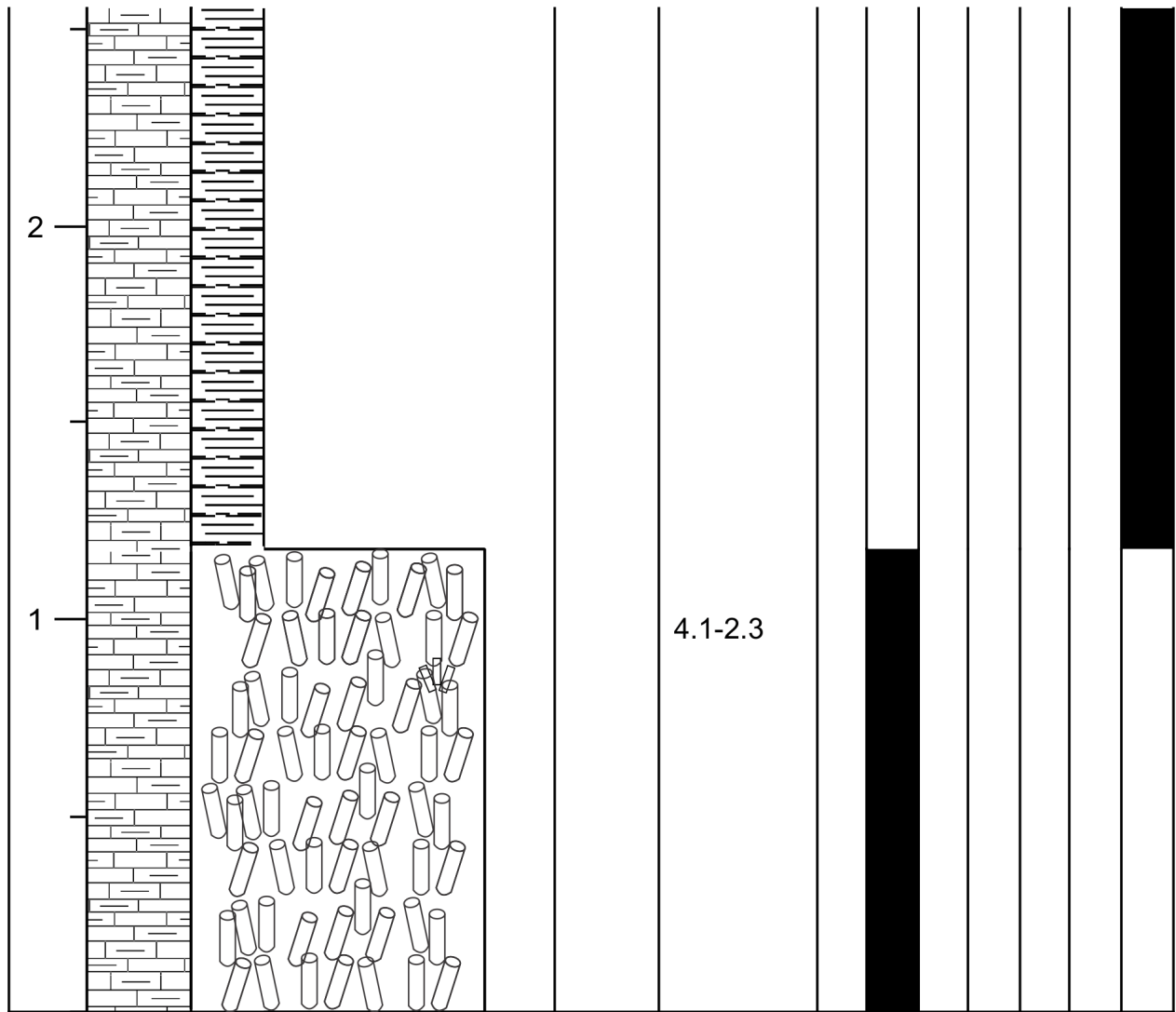


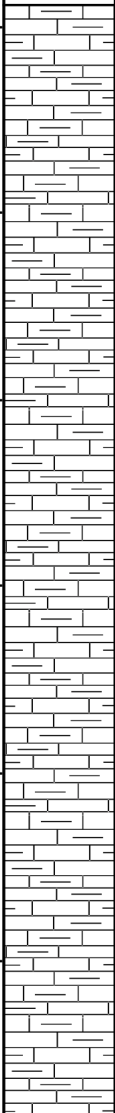
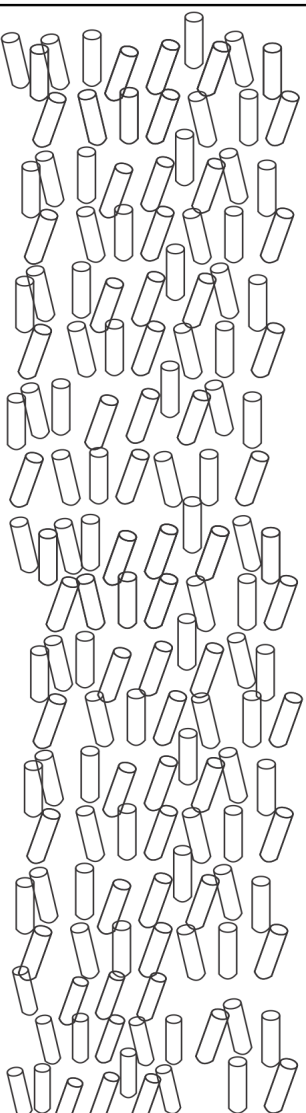

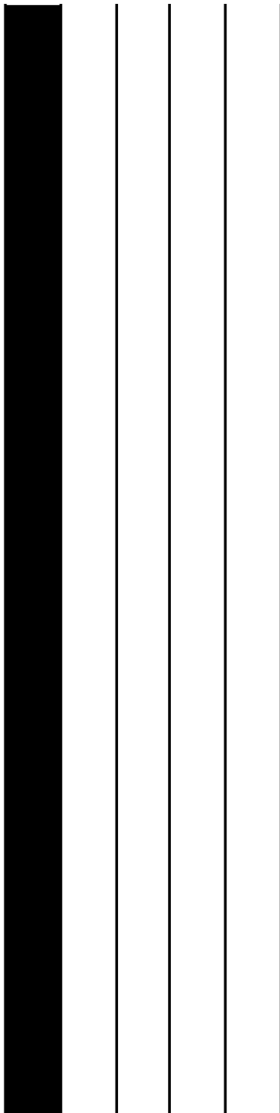
Locality 3 - N38°03,967 E023°11,274							
SCALE (m)	LITHOLOGY	LIMESTONES	FOSSILS	SAMPLES	FACIES		
		mud wacke pack grain float rud baffle			1	2	3
1							

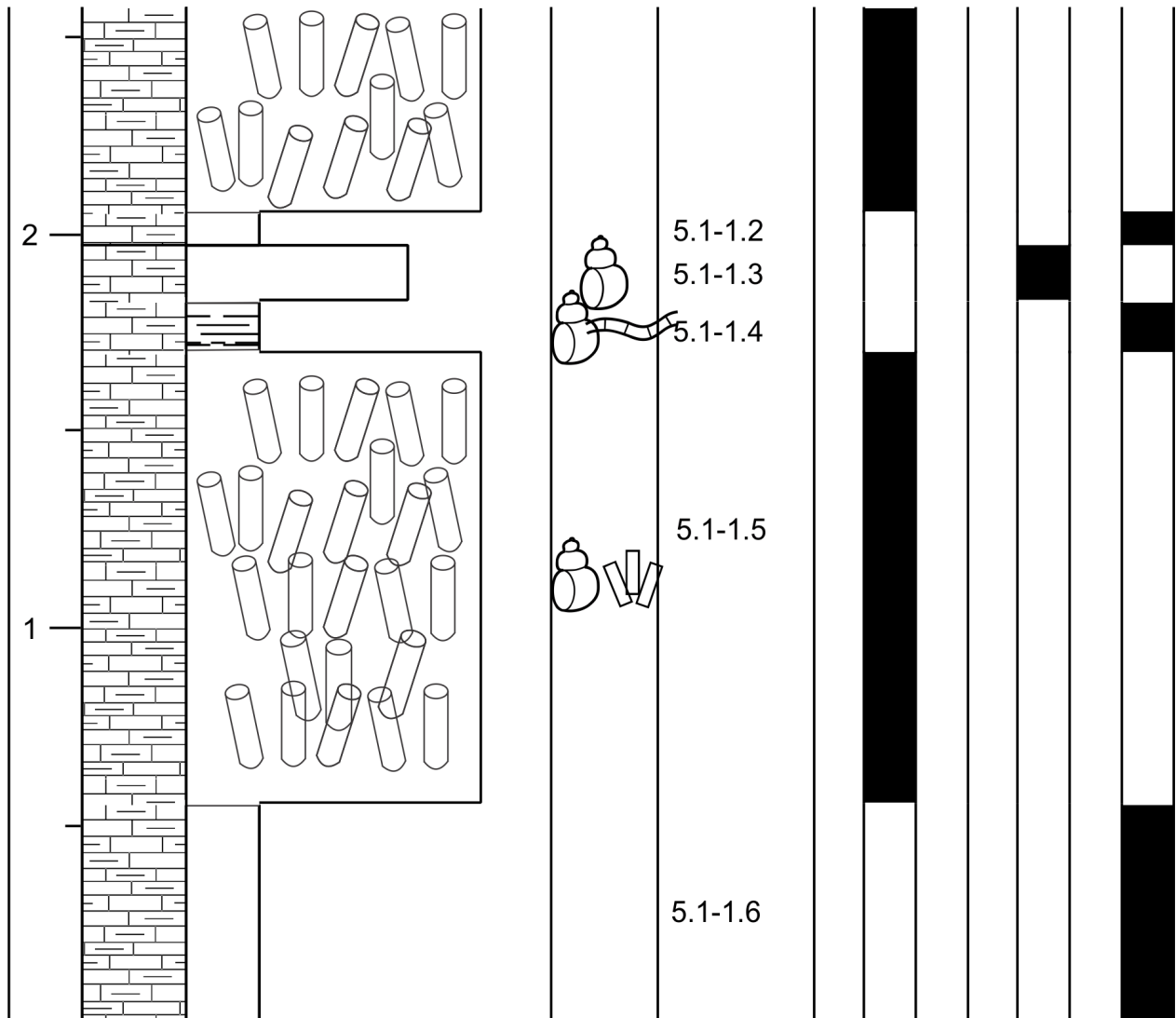
Locality 4.1 Upper Unit - N38°03.398' E023°11.958 '																	
SCALE (m)	LITHOLOGY	LIMESTONES						FOSSILS	SAMPLES	FACIES							
		mud	wacke	pack	grain	float	rud			baffle	1	2	3	4	5	6	7
5										4.1-1.1							
										4.1-1.2							
										4.1-1.3							
4										4.1-1.4							
										4.1-1.5							
										4.1-1.6							
3										4.1-1.7							
										4.1-1.8							



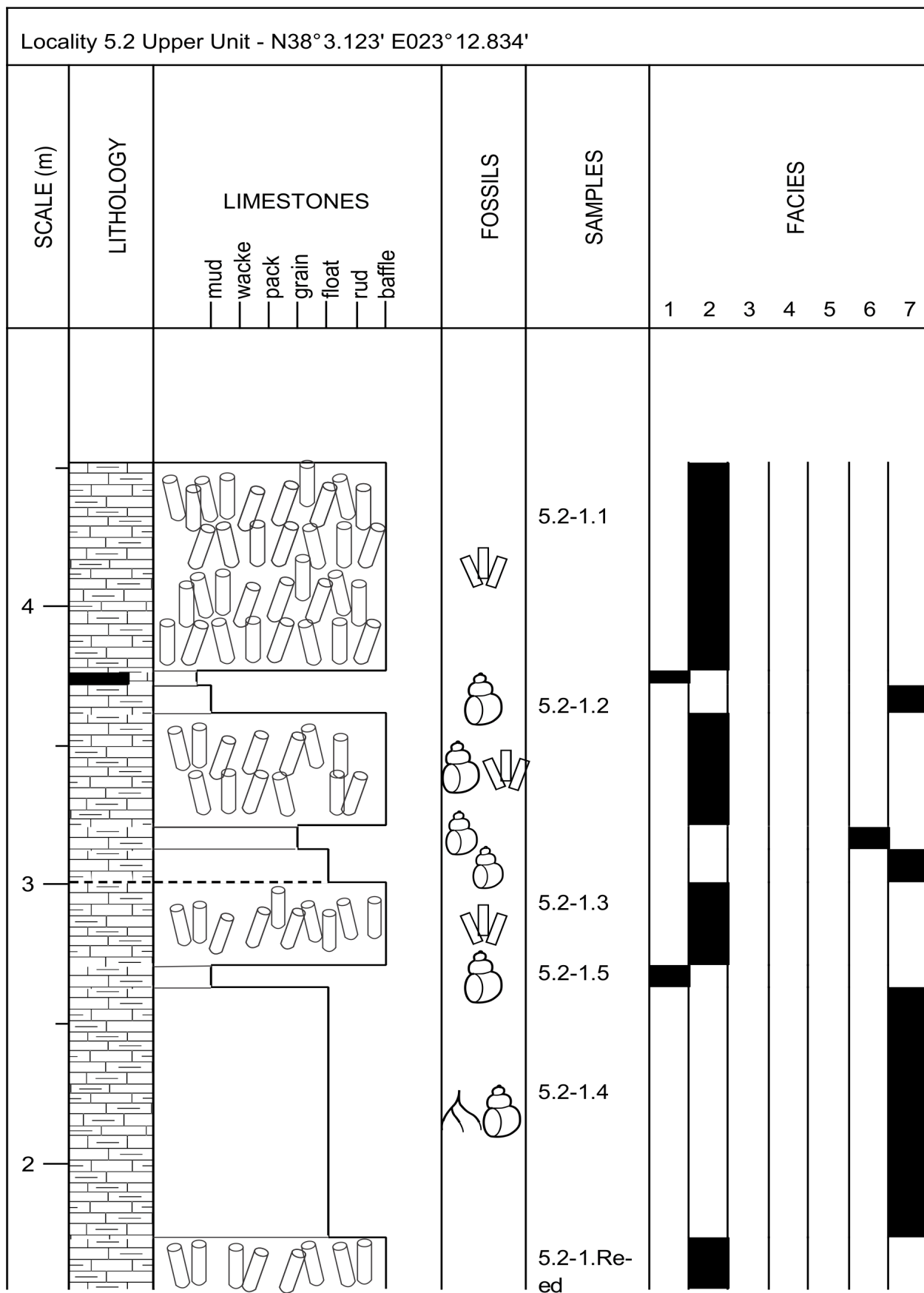
Locality 4.1 Lower Unit - N38°03.398' E023°11.958 '																			
SCALE (m)	LITHOLOGY	LIMESTONES						FOSSILS	SAMPLES	FACIES									
		mud	wacke	pack	grain	float	rud			baffle	1	2	3	4	5	6	7		
5									4.1-2.1										
4																	3		
3									4.1-2.2										

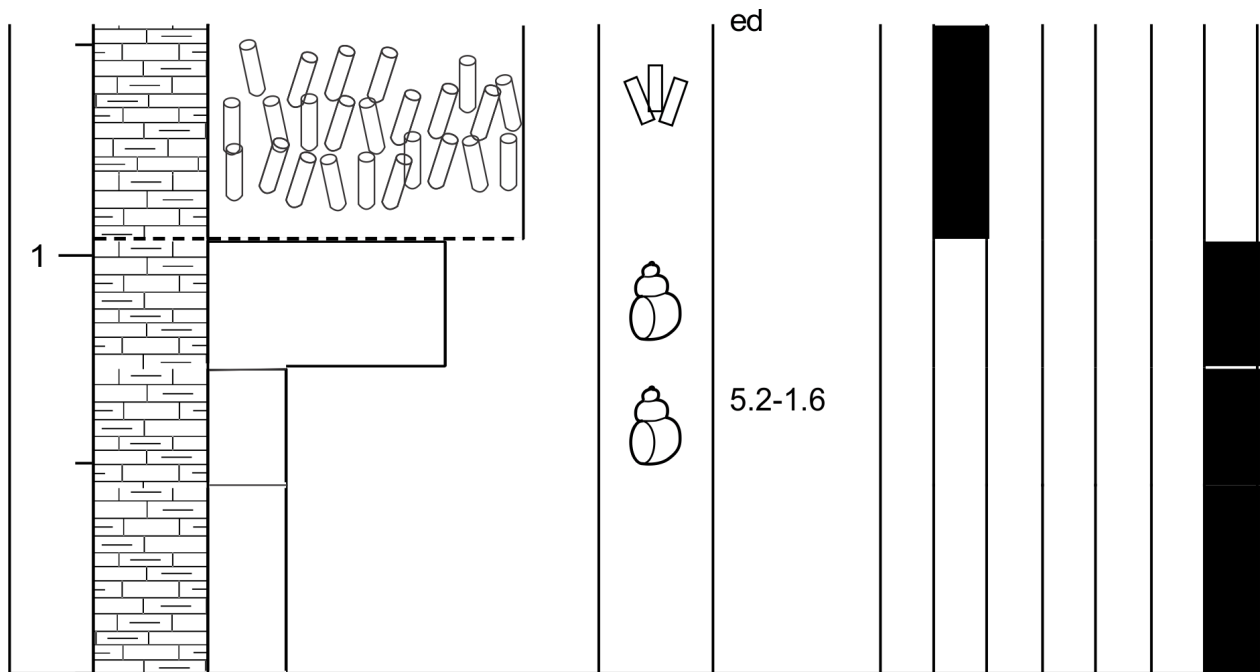


Locality 5.1 - N38°3.194' E023°12.701'																
SCALE (m)	LITHOLOGY	LIMESTONES						FOSSILS	SAMPLES	FACIES						
		mud	wacke	pack	grain	float	rud			baffle	1	2	3	4	5	6
5									5.1-1.1							
4																
3																

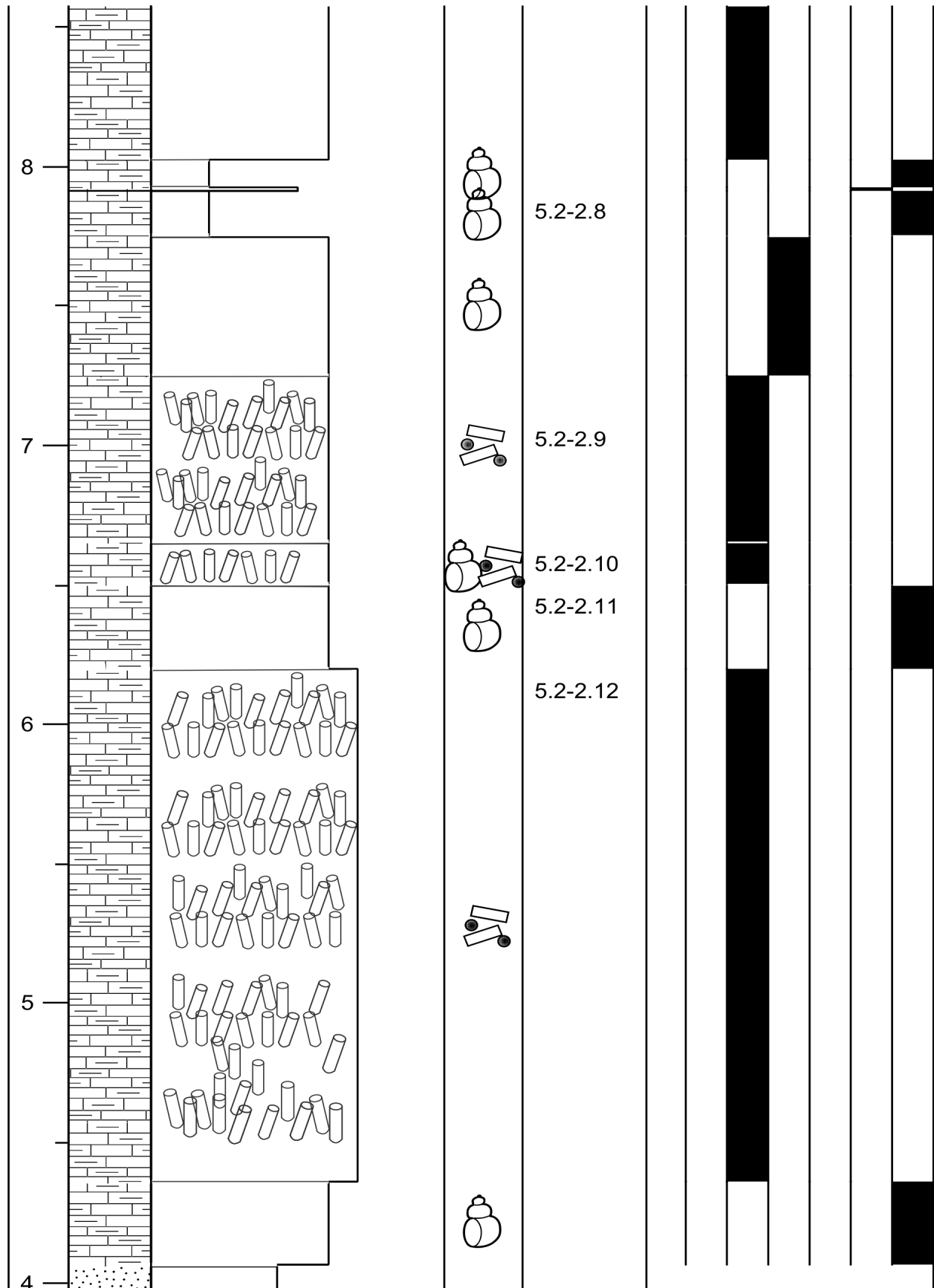


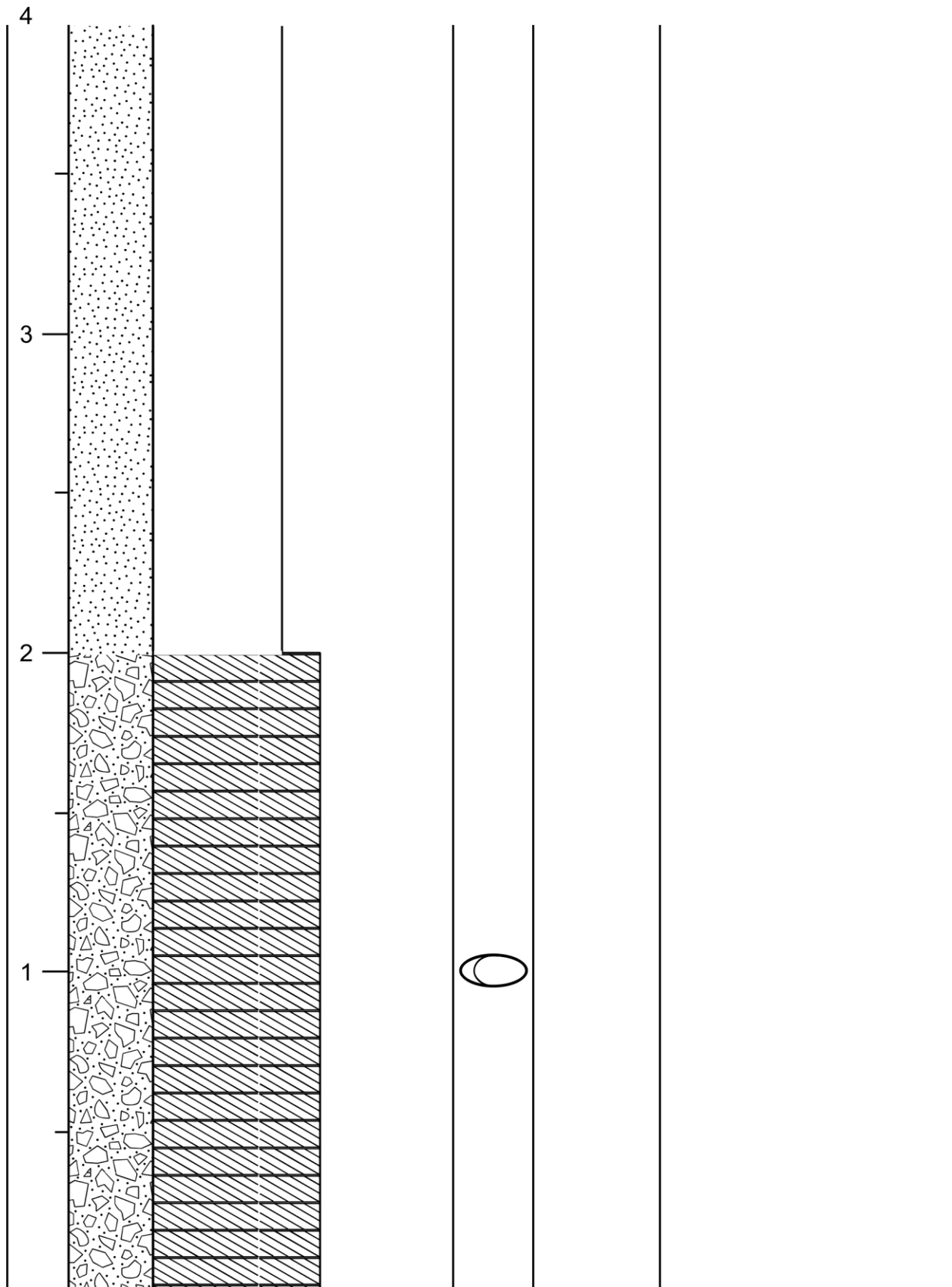




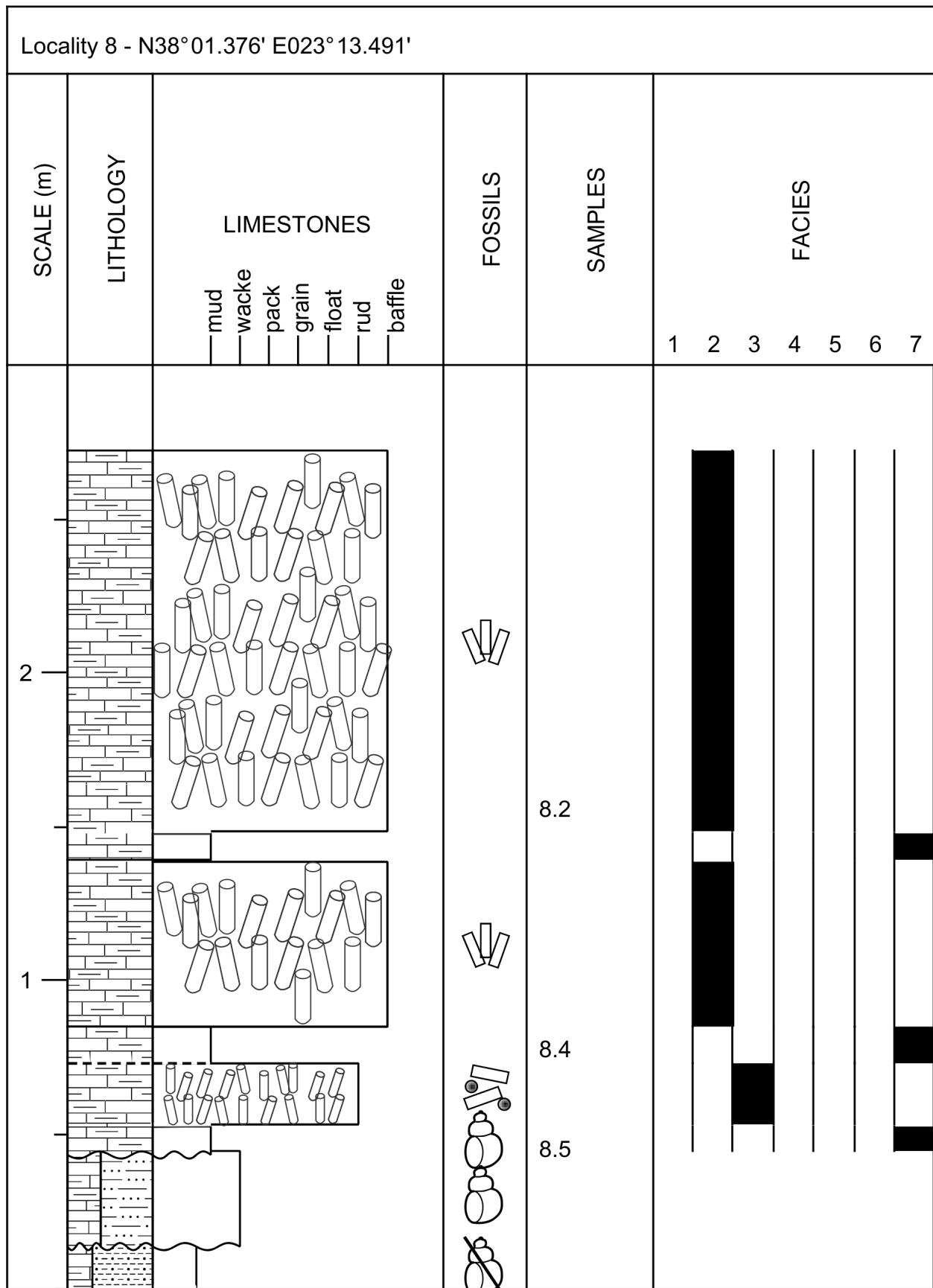


Locality 5.2 Lower Unit - N38° 3.123' E023° 12.834'																
SCALE (m)	LITHOLOGY	Limestones						FOSSILS	SAMPLES	FACIES						
		mud	wacke	pack	grain	float	rud			baffle	1	2	3	4	5	6
11									5.2-2.1							
									5.2-2.2							
									5.2-2.3							
									5.2-2.4							
									5.2-2.5							
10									5.2-2.6							
									5.2-2.7							

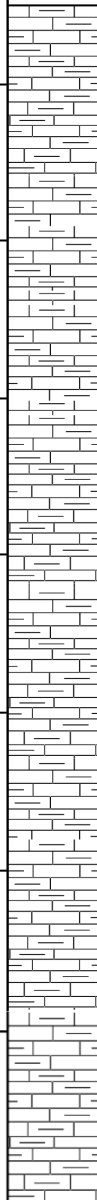


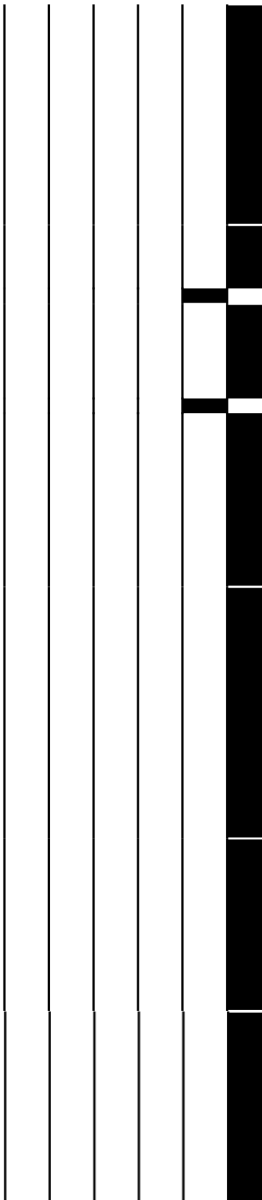


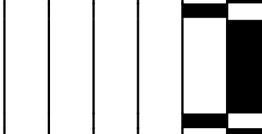


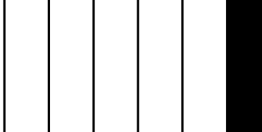
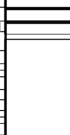

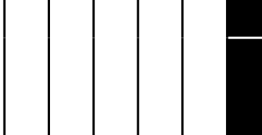


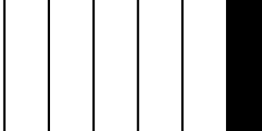


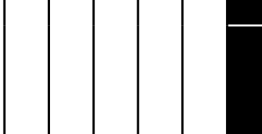
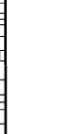

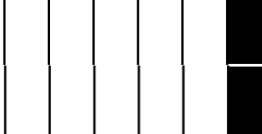




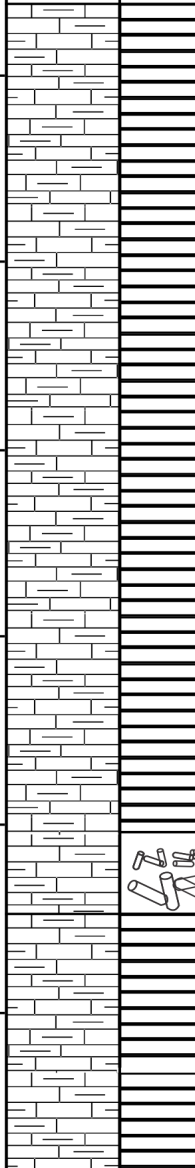


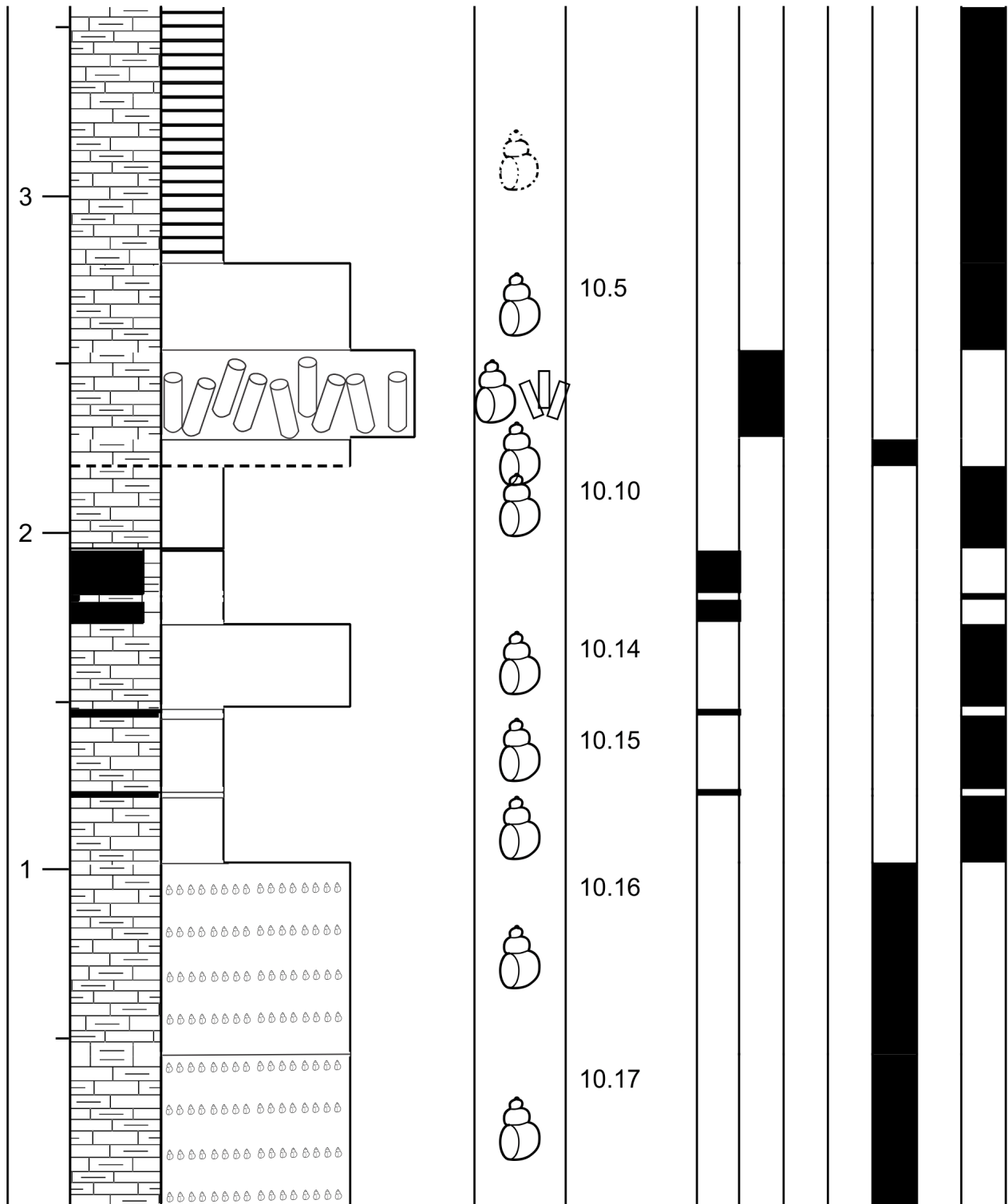
Locality 7 - N38°02,646 E023°12,774											
SCALE (m)	LITHOLOGY	LIMESTONES	FOSSILS	SAMPLES	FACIES						
		mud wacke pack grain float rud baffle			1	2	3	4	5	6	7
3				7.1							
2											
1											
				7.2							
				7.3							
				7.5							





Locality 9 - N38°01.675' E023° 15.929'																	
SCALE (m)	LITHOLOGY	LIMESTONES						FOSSILS	SAMPLES	FACIES							
		mud	wacke	pack	grain	float	rud			baffle	1	2	3	4	5	6	7
3									9.1								
							9.3										
								9.4									
										9.5							
							9.5										
2									9.6								
1								9.7									
									9.8								

Locality 10 - N38°00.517' E023°17.459'																			
SCALE (m)	LITHOLOGY	LIMESTONES						FOSSILS	SAMPLES	FACIES									
		mud	wacke	pack	grain	float	rud			baffle	1	2	3	4	5	6	7		
6																			
5																			
4																			



## **Appendix III – Correlation panel**

